SISSA - SCUOLA
INTERNAZIONALE
SUPERIORE
DI STUDI AVANZATI
TRIESTE
Strada Costiera 11

ISAS - INTERNATIONAL SCHOOL FOR ADVANCED STUDIES

July 1985.

NUMERICAL METHODS IN GENERAL RELATIVITY

Thesis submitted for the degree

of

Master of Philosophy

CANDIDATE:
Mark R. Dubal

SUPERVISOR:
Dr. Patrick Mann

TRIESTE

ISAS - INTERNATIONAL SCHOOL FOR ADVANCED STUDIES

July 1985.

NUMERICAL METHODS IN GENERAL RELATIVITY

Thesis submitted for the degree

of

Master of Philosophy

CANDIDATE:
Mark R. Dubal

SUPERVISOR:
Dr. Patrick Mann

ABSTRACT

This thesis is concerned with the numerical solution of Einstein's equations. In particular we look at computer generated solutions to the astrophysical problem of the collapse of self gravitating fluid bodies. General Relativity predicts significant deviations from the Newtonian picture when velocities and densities become large.

Chapter one reviews results from past collapse computer codes for spherically symmetric and axi-symmetric bodies.

Chapter two details the methods and techniques used to obtain the results discussed in chapter one. The ADM (3+1) and the [(2+1)+1] formulations of General Relativity are briefly described, and we then systematically review the all important choice of gauge conditions. York's conformal approach to the initial value problem is outlined, and the chapter ends with some numerical considerations.

Chapter three introduces an old but little used formulation of General Relativity known as Regge Calculus. After a review of previous work in this area we present Regge Calculus in a (3+1) form. In chapter four the formalism is extended to include a perfect fluid and we then go on to apply it to the relativistic collapse of spherically symmetric bodies. The Regge Calculus equivalent of the Tolman - Oppenheimer - Volkov equations describing fluid spheres in hydrostatic equilibrium are solved. The results are found to be in excellent agreement with those produced by other numerical methods. A static equilibrium configuration is then evolved using a Regge Calculus collapse code. This exhibits numerical instability in the central regions but work is in progress to overcome this problem.

ACKNOWLEDGEMENTS

It is a pleasure to thank my supervisor, Dr. Patrick Mann, for all the help and advice he has given me concerning this work.

I would also like to thank Coral - Leigh Mann for the typing and for encouragement to get this thesis finished.

CONTENTS

1. NUMERICAL RELATIVITY

1.1 Introduction:

Numerical Relativity is a quite recent field of study which has experienced rapid growth in the past ten years [1] - [3]. This is no doubt, partly due to the equally rapid growth of computer technology on which the subject is so dependent. However the development of formalisms of General Relativity (GR) suitable for computer implementation and the deeper understanding of crucial issues such as the initial value problem are the major factors governing this growth.

The usefulness of Numerical Relativity in the calculation of space-time generated by strong field (Newtonian gravitational potential $\phi \sim c^2$ where c = light speed), high velocity ($v \sim c$) sources is clear. Perturbation methods [4]- [6] depend on the existance of a small expansion parameter which is physical and characteristic of the problem (such as the ratio of the masses for a test particle falling into a black hole [6]). For strong field, highly non-linear problems all natural expansion parameters are large and one must use numerical methods, which depend on unphysical expansion parameters. There are many interesting astrophysical problems which fall into this category, a particular one being the catastrophic collapse of self-gravitating fluid bodies [7],[8].

At the endpoint of thermonuclear burning stars of mass $M \gtrsim 8M_\odot$ tend to produce cores of iron group elements with a central density of $\rho \sim 3.7 \times 10^9$ g cm^{-3} and a mass of around $1.4M_\odot$ [9] - [11]. As the core cools electron degeneracy pressure supports it against gravitational forces, but, as first suggested by Landau [12] and shown in detail by Chandrasekhar [13], there is a maximum stable mass for such cold, degenerate configurations of

$$M_{max} = 5.76 \langle Y_e^2 \rangle M_\odot \qquad (1.1)$$

where Y_e is the number of electrons per nucleon = 0.41 - 0.43. This assumes no rotation and observations [14] indicate that this is probably a good approximation. Any core exceeding this maximum mass necessarily undergoes gravitational collapse until it reaches nuclear densities of $\rho \sim 10^{14}$ g cm^{-3}. At this point the hardcore repulsion of the neutrons cause the core to bounce producing an outward moving shockwave. The strength of the shockwave depends sensitively on details such as the equation of state and the degree of neutrino trapping (neutrinoes are produced via neutronization ie. the capture of free electrons onto protons). In some cases the shockwave is able to eject matter from the star. The core is now a relativistic, degenerate neutron star.

Such a scenario may describe the general features of type II supernova explosions [15] - [17]. The high densities and large fluid velocities reached particularly at neutron star formation, means that GR should be used.

Further gravitational collapse of the neutron star can occur if, either

i) it accretes matter from an infalling stellar envelope and thereby exceeds the maximum stable mass for a relativistic, degenerate configuration (thought to be around $1.3M_\odot$ - $2.7M_\odot$ and almost certainly less than $5M_\odot$ [9]),

or, ii) it has a composition such that the average adiabatic index $\Gamma = \frac{d\ln p}{d\ln \rho}$ satisfies

$$\Gamma < \Gamma_{crit} = \frac{4}{3} + O\left(\frac{GM}{c^2 R}\right) \qquad (1.2)$$

where M is the mass and R is the radius of the star. The last term is a GR correction to the Newtonian picture. This collapse criterion is very general.

At higher densities there are no stable configurations. GR predicts the formation of a black hole provided that the ratio of specific angular

momentum to mass satisfies $\frac{a}{M} < 1$ ($c = G = 1$) [18].

Numerical simulations of gravitational collapse to neutron stars and black holes can provide quantitative details of the scenarios described above. We would hope to obtain information on such fundamental issues as the conditions necessary for supernova explosions, the quantity and nature of gravitational waves emitted during collapse, and the final fate of collapsing configurations with $\frac{a}{M} > 1$.

The plan of this thesis is as follows; in the first chapter we review the results of fully relativistic numerical simulations of spherically symmetric and axi-symmetric gravitational collapse. All of these use a simple equation of state and do not treat the detailed microphysics. Present computer power limits one to spherical symmetry if realistic equations of state and nuclear reaction energetics are to be considered. However we are concerned only with the role of numerical relativity and do not discuss such codes [19] - [21].

Chapter two begins with a description of the ADM (3+1) formulation of GR on which most modern numerical relativity codes are based. This treats the gravitational field as a dynamical entity evolving from conditions prescribed on an initial spatial hypersurface. A modification of the (3+1) approach particularly suitable for axi-symmetric rotating collapse, known as the [(2+1)+1] formalism, is then outlined. Gauge conditions for spherical and axi-symmetric spacetimes are reviewed, York's conformal approach to the initial value problem is outlined, and the chapter ends with a discussion of some numerical points including differencing of equations and shock handling.

Chapters three and four form the main part of this thesis. We introduce a little used formulation of GR known as Regge Calculus. This differs significantly from other formulations used in numerical relativity in that the Einstein field equations are derived in a discrete form ready for implementation on the computer. After an introduction to the method and a review

of previous work in the area we describe Regge Calculus in a form which has many similarities with the ADM (3+1) approach. These similarities are pointed out as they appear. The construction of a Regge Calculus collapse code for spherical bodies is the subject of chapter four.

The notation used in this thesis mainly follows that of [22], except for chapters three and four. We refer the reader to Appendix I for the notation used in these chapters. Geometrized units (c = G = 1) and a metric with signature (-,+,+,+) are always used unless explicitly stated otherwise.

1.2 Spherically Symmetric Collapse:

Analytic expressions are available for the dynamic collapse of homogeneous [23] and inhomogeneous [24] dust (zero pressure) spheres within the framework of GR. However when pressure is included a numerical approach is necessary. May and White [25], [26] were the first to make an extensive study of the relativistic collapse of self-gravitating polytropic spheres using numerical methods.

May and White use a Lagrangian co-ordinate system, ie. each fluid element has constant spatial co-ordinates along its world line. In this case only the time component of the fluid 4-velocity is non-zero. Also simplification of the Einstein equations is acheived by using a diagonal metric in the form [27],

$$ds^2 = -a^2 dt^2 + b^2 d\mu^2 + R^2 d\Omega^2 \qquad (1.3)$$

where a, b and R are functions of t and μ, and $d\Omega^2 = d\theta^2 + \sin^2\theta\, d\phi^2$. We note that this combination of Lagrangian co-ordinates and a diagonal metric is

possible only for spherical collapse.

The matter is divided into a series of concentric spheres of proper area $4\pi R^2(\mu,t)$ each enclosing a fixed rest mass μ. During the collapse these spheres 'expand and contract' to ensure μ remains constant, thus μ is a Lagrangian radial co-ordinate. A perfect fluid with isentropic flow is assumed and shocks are handled using an artificial viscosity of the von Neumann and Richtmyer type [28] (see chapter two). In the Lagrangian frame the stress-energy tensor is

$$T^0_0 = -\rho_0(1+\Pi) \quad , \quad T^1_1 = T^2_2 = T^3_3 = p \tag{1.4}$$

where p is the pressure, ρ_0 is the rest mass density and Π is the specific internal energy. All other components of T^ν_μ are zero. We define relativistic specific enthalpy as

$$w = 1 + \Pi + \frac{p}{\rho_0} \quad , \tag{1.5}$$

the 4-velocity normalization is

$$g_{\mu\nu}u^\mu u^\nu = -1 \tag{1.6}$$

so that in the co-moving frame we have,

$$u^\nu = \left(\frac{1}{\alpha}, 0, 0, 0\right) \tag{1.7}$$

then from the Einstein equations, baryon conservation and energy and momentum conservation we may obtain [26], [29] the dynamical equations

$$\frac{1}{a}\frac{\partial u}{\partial t} = -\left[4\pi R^2 \frac{\Gamma}{w}\frac{\partial p}{\partial \mu} + \frac{m}{R^2} + 4\pi p R\right] \tag{1.8}$$

$$\frac{1}{a}\frac{\partial R}{\partial t} = u \tag{1.9}$$

$$\frac{1}{a}\frac{1}{\rho_0 R^2}\frac{\partial(\rho_0 R^2)}{\partial t} = -\frac{\left(\frac{\partial u}{\partial \mu}\right)}{\left(\frac{\partial R}{\partial \mu}\right)} \tag{1.10}$$

$$\frac{\partial \Pi}{\partial t} = -p\frac{\partial}{\partial t}\left(\frac{1}{\rho_0}\right) \tag{1.11}$$

for u, R, ρ_0 and Π, where we have the definitions

$$m = 4\pi\int_0^{\mu} \rho_0 (1+\Pi) R^2 \frac{\partial R}{\partial \mu}\, d\mu \tag{1.12}$$

$$\Gamma = 4\pi\rho_0 R^2 \frac{\partial R}{\partial \mu} = \left(1 + u^2 - \frac{2m}{R}\right)^{1/2} \tag{1.13}$$

$$p = p(\Pi, \rho_0). \tag{1.14}$$

(1.12) is the mass interior to radial co-ordinate μ, (1.13) is a generalization of the special relativistic factor $\gamma = (1-v^2)^{-1/2}$ and (1.14) is the equation of state. The metric component a is then found using

$$\frac{\partial a}{\partial \mu} = -\frac{a}{\rho_0 w}\frac{\partial p}{\partial \mu} \tag{1.15}$$

From eq. (1.9) we interpret u as the 3-velocity of the fluid in a gauge using

R as the radial co-ordinate.

May and White integrated this system of equations using a two step finite difference scheme ([26] gives the full details). We present results from two runs of their code.

First we consider the collapse of a $1.1M_\odot$ sphere of constant density $\rho_0 = 10^{13}$ g cm^{-3} starting from rest. The equation of state is that of a polytrope

$$P = K\rho_0^{\gamma} \tag{1.16}$$

where in this case the adiabatic index $\gamma = 5/3$ and K = constant = 1.06. Figs. 1.1 - 1.4 show the values of velocity u, radius R, density ρ_0 and metric function a verses Lagrangian co-ordinate μ at various times during the collapse. There are a number of noteworthy features. The build up of central pressure was sufficient to halt the collapse causing the inner regions to bounce. A shockwave then propagated outwards, and in this example some mass was ejected. The final system is an equilibrium core with an expanding shell of matter. For high central densities, $\rho_0 > 5\times10^{14}$ g cm^{-3}, the adiabatic index was changed to $\gamma = 2$. this represents a hardcore equation of state and enhances the bounce.

Fig. 1.5 shows the same set of results for a $21M_\odot$ sphere of constant density $\rho_0 = 10^{7}$ g cm^{-3} starting from rest. Again a polytropic equation of state with $\gamma = 5/3$ is used, but this time K = constant = 0.05. We expect pressure to play a less significant role in this case. The pressure gradient is never large and continued collapse occurs. At a certain point Γ becomes negative so that the pressure accelerates the inward flow; this is seen from eq. (1.8). Qualitatively the results are similar to the dust results of Oppenheimer and Snyder [23]. The value of K separating those models which bounced or underwent continued collapse was found to lie between K = 1 - 2 for $\gamma = 5/3$ for a wide variety

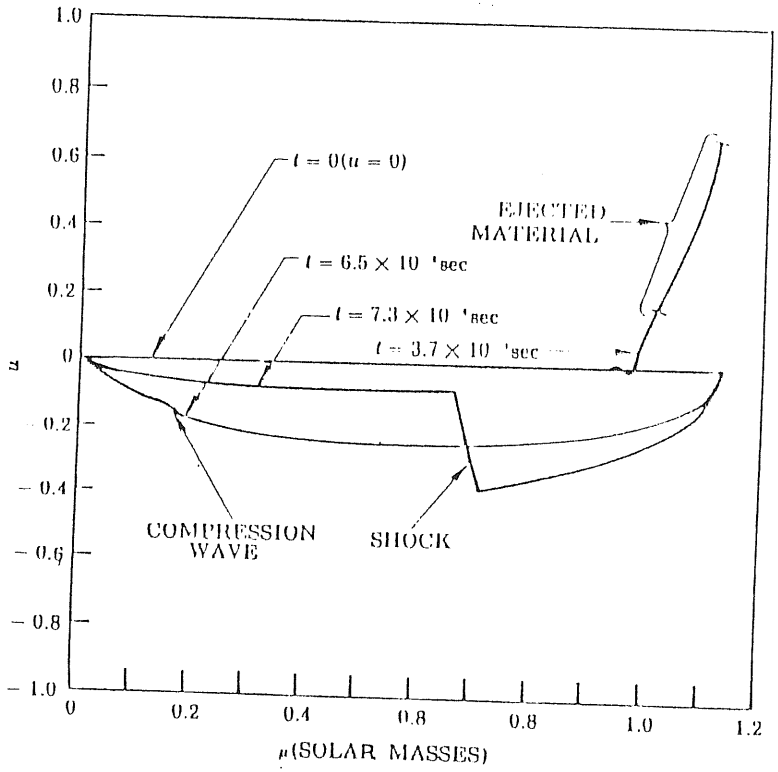

Fig. 1.1 u vs μ at several times during the collapse and bounce of a $1.1M_\odot$ sphere. Initial uniform density $\rho_o = 10^{13}\,gcm^{-3}$, $\gamma = 5/3$ and k = 1.06.

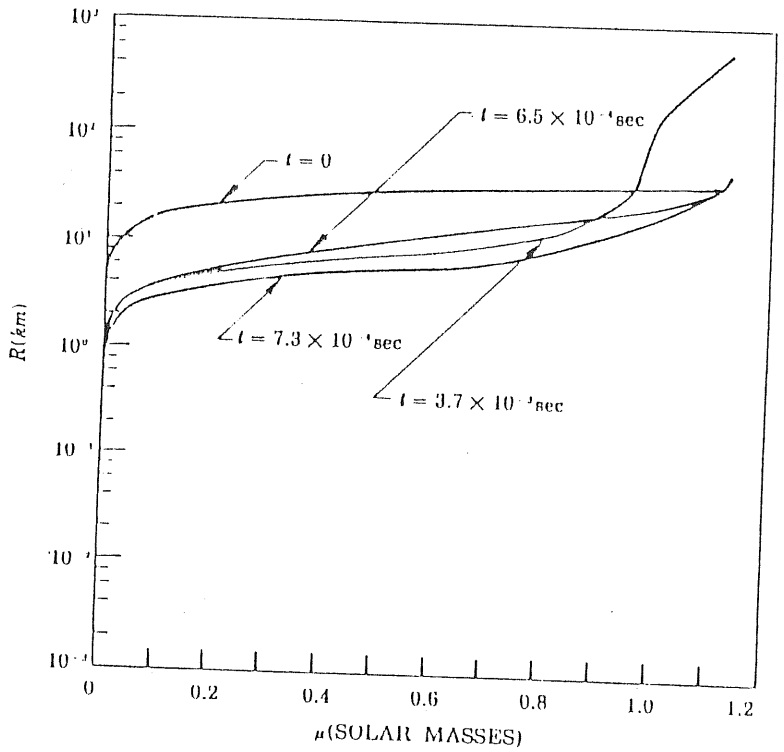

Fig. 1.2 R vs μ at several times during the collapse and bounce of a $1.1M_\odot$ sphere.

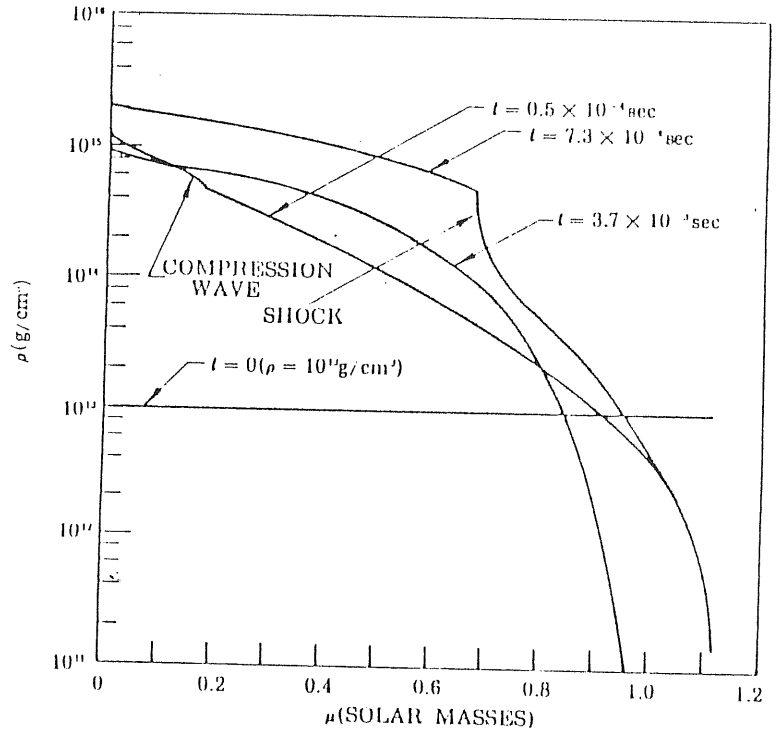

Fig. 1.3 ρ vs μ at several times during the collapse and the bounce of a 1.1$M_\odot$ sphere.

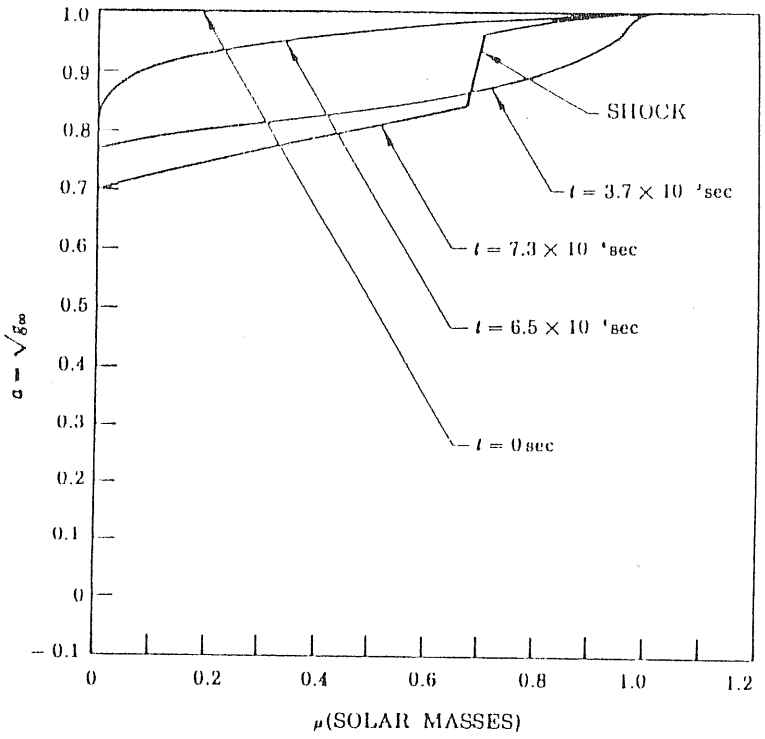

Fig. 1.4 a vs μ at several times during the collapse and bounce of a 1.1$M_\odot$ sphere.

of initial conditions.

Fig. 1.5 shows the start of black hole formation, however it was not possible to follow the evolution further because a singularity developed in the co-ordinate system. This can be seen from the R verses μ graph. R reaches zero at an intermediate zone in a finite co-ordinate time. A solution to the problem was given by Hernandez and Misner [30] who suggested the use of Lagrangian co-ordinates with a non-diagonal metric where the time co-ordinate is constant along null geodesics.

Writing

$$c\,du = a\,dt + b\,d\mu \tag{1.17}$$

we transform the metric (1.3) to

$$ds^2 = -c^2 du^2 - 2cb\,du\,d\mu + R^2 d\Omega^2 \tag{1.18}$$

where u is referred to as observer time. [30] lists the new equations for spherical hydrodynamics in this gauge. Since photons interior to the Schwarzschild radius R = 2m cannot escape, events inside this region, which produce the co-ordinate singularity of the previous gauge, occur at infinite observer time.

Miller [9], [31] presents collapse results using both the May and White and Hernandez and Misner co-ordinate systems. Figs. 1.6 and 1.7 show some of the results. They are not directly comparable with those of fig. 1.5 since the initial conditions are different. A relativistic polytrope with $\gamma = 5/3$ was first constructed by integrating the Tolman - Oppenheimer - Volkov (TOV) equations and was made unstable by reducing K. The collapse of a $2.1M_\odot$ configuration from rest is shown. We see that observer time successfully avoids

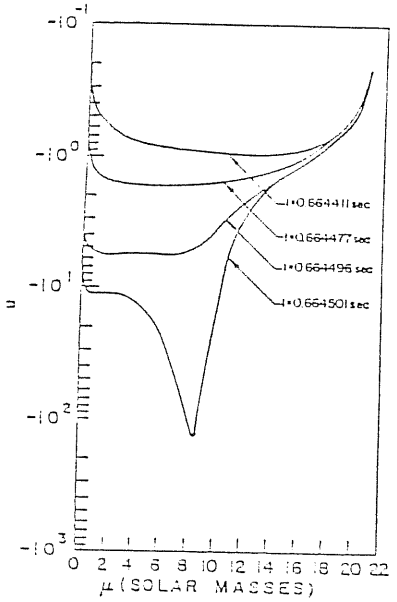

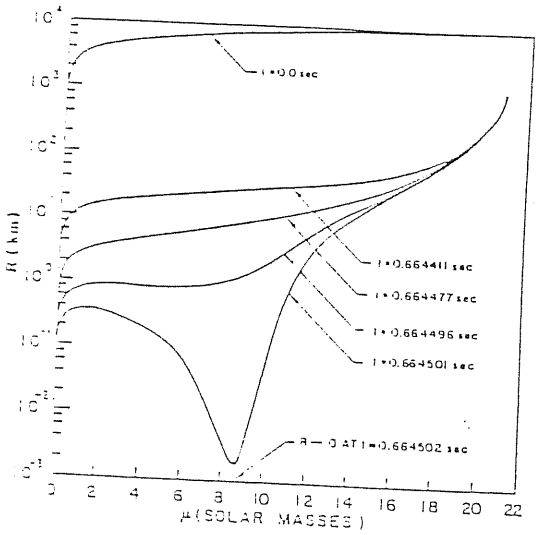

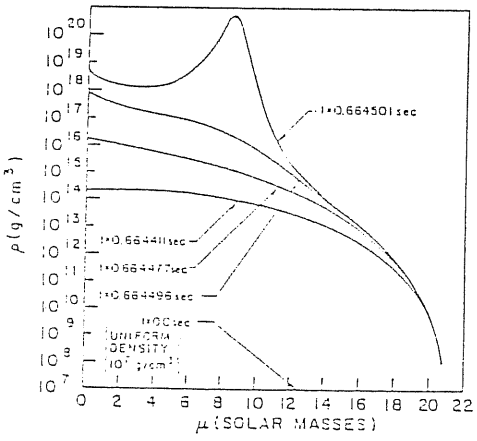

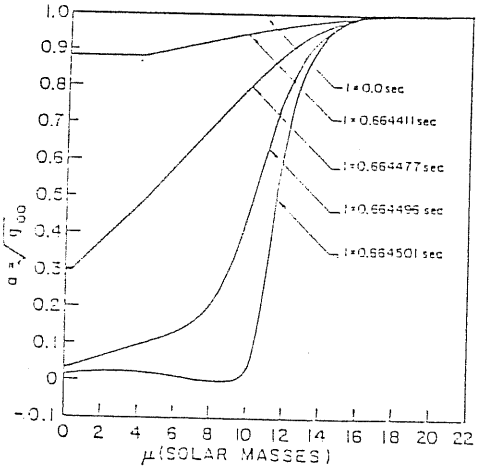

Fig. 1.5 The collapse of a $21M_\odot$ sphere. Initial uniform density $\rho_o = 10^7\,gcm^{-3}$, $\gamma = 5/3$ and $k = 0.05$. Note that R goes singular at a finite time and simultaneously the density becomes infinite.

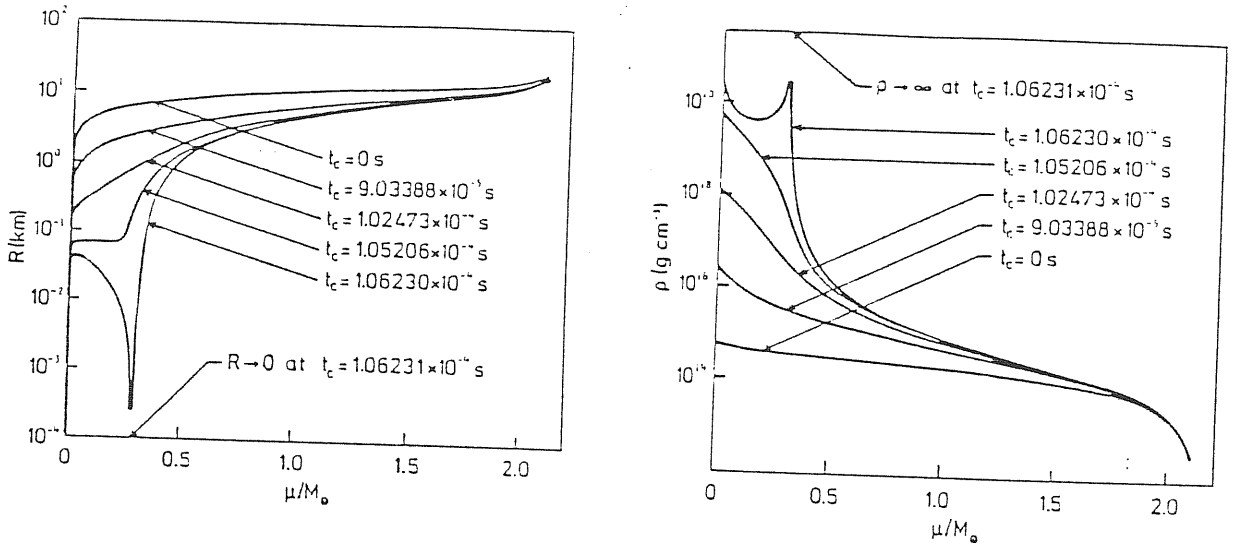

Fig. 1.6 Results from Miller. Initial coniguration is a TOV polytrope with $\gamma = 5/3$, collapse is initiated by reducing K. The collapse of a $2.1M_\odot$ sphere in the co-ordinate system of May and White is shown.

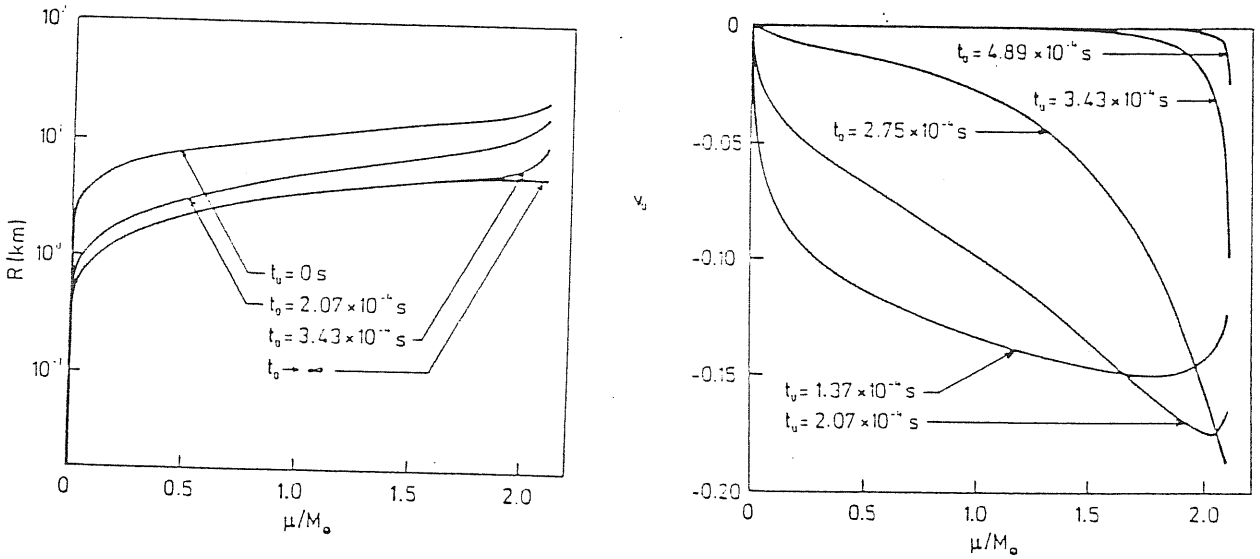

Fig. 1.7 The same collapse as above using the observer time co-ordinate of Hernandez and Misner. R never becomes singular. V_0 is the fluid velocity measured by a stationary observer at infinity.

the singularity in R.

Two modern spherical collapse codes are those of Smarr and Wilson [32], and Shapiro and Teukolsky [33], [34]. Both use the ADM (3+1) formulation of GR (see chapter two), and difference the hydrodynamic equations in an Eulerian form. A grid velocity which moves the grid nodes relative to the co-ordinate system was employed to ensure adequate coverage of the collapsing matter, and a von Neumann - Richtmyer artificial viscosity handled shocks.

A general picture emerged from the large number of initial conditions considered by Shapiro and Teukolsky. Equilibrium polytropic spheres with $\gamma = 2, \frac{5}{3}$ or $\frac{7}{5}$ were destabilized by reducing the pressure. Depending on the initial conditions one of three scenarios occured. If the pressure deficit is moderate and the mass $M < M_{max}$, where M_{max} is the maximum stable mass for the given γ (see [8]), then the star bounces homologously. For $M > M_{max}$ with moderate pressure deficits continued collapse to a black hole is the result. While if the pressure deficit is large a non-homologous bounce occurs, regardless of mass, with subsequent oscillations of the inner regions. The latter scenario may be explained by the fact that a large pressure reduction causes the inner regions to collapse much sooner than the overlying matter. Final collapse to a black hole probably occurs on a secular timescale as the outer regions fall through the shock. The three scenarios for a $\gamma = \frac{5}{3}$ equation of state are shown in fig. 1.8. R_5 is the radius of the star after pressure reduction; the curves represent the motion of Lagrangian matter tracers each labeled by a fixed fraction of rest mass interior to it. By using a maximal time slicing condition singularities were avoided (see chapter two) and it was possible to evolve the system for many hundreds or thousands of M.

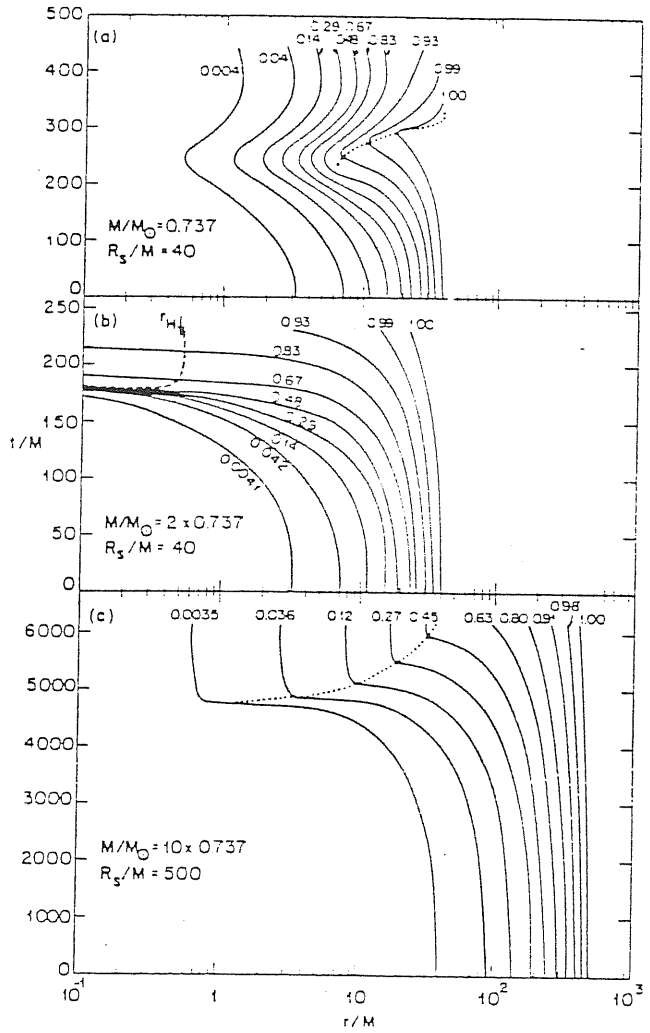

Fig. 1.8 (a) homologous bounce, dotted line denotes the shock front.

(b) continued collapse to a black hole, dashed line represents the event horizon.

(c) non-homologous bounce, dotted line denotes the shock front.

1.3 Axi-symmetric Collapse:

Spherical symmetry represents a great simplification of the true nature of gravitational collapse. Only non-spherical systems allow gravitational radiation to be emitted and thus only then does the whole of spacetime become dynamical. Also the effects of rotation should be included. There are several axi-symmetric codes which solve the Einstein equations coupled to a perfect fluid [35] - [38]. We concentrate on two of them.

Firstly we consider the work of Nakamura [38] - [42] who used a [(2+1)+1] formulation of GR [43] to construct a computer code simulating the collapse of relativistic, rotating, super massive ($M = 10^8 M_\odot$) stars. Although axi-symmetry with rotation allows both polarizations of gravitational radiation to be present no results regarding wave emission were obtained. There are several reasons for this absence:

i) The use of cylindrical co-ordinates (r, ϕ, z) combined with a choice of zero shift vector produced a gauge which did not isolate the gravitational degrees of freedom. This makes interpretation of the wave content difficult.

ii) Their spatial grid of 28 x 28 nodes in the (r,z) direction cannot resolve deformations of the body to the accuracy required for estimates of wave emission. The outermost grid points were at a distance of 25M (where M = mass of the body) which is not sufficiently distant since typical gravitational waves have a wavelength of $\sim 15M$. Computer resource limitations governed the size of the grid. The choice of zero shift vector meant no simplification of the Einstien equations and all six spatial metric components needed to be evolved.

iii) A difference scheme with a large, implicit numerical viscosity was used to approximate the equations. Thus any waves or oscillations were damped.

The code was used to study the hydrodynamical aspects of axi-symmetric collapse for a wide variety of initial conditions. A polytropic equation of

state with $\gamma = 4/3$ was assumed. The Einstein constraint equations were solved using York's conformal approach (see section 2.4) with the assumption of a conformally flat metric and the trace and transverse-traceless parts of the extrinsic curvature set to zero. Two rotation laws were considered,

$$J_\phi \propto e^{-\left(\frac{C_\phi}{r_0^2} r^2\right)} \tag{1.19}$$

where J_ϕ is the specific angular momentum, r_0 is the initial radius of the star = 14.5 in all the models shown, and C_ϕ is a constant which took two values,

a) rotation law A; $C_\phi = 2$ (almost rigidly rotating)

b) rotation law B; $C_\phi = 10$ (strongly differential rotation).

Input parameters are the polytropic index K, $J = \frac{E_{rot}}{|E_{grav}|}$ and $U = \frac{E_{int}}{|E_{grav}|}$ where E_{rot} is the rotational kinetic energy, E_{int} the internal energy and E_{grav} the gravitational energy of the star. We note that for a rotating polytrope in equilibrium J satisfies the inequality $0 < J < 0.5$ as a consequence of the Virial theorem [46].

Fig. 1.9 lists the initial conditions and final outcome of several runs. Models are characterized by the rotation law and Kerr parameter $q = \frac{a}{m}$, max denotes maximal time slicing while hyper denotes hypergeometric time slicing, (see section 2.3).

For a slowly rotating model, q = 0.5, with rigid rotation (A) the deviation from spherical symmetry is slight and collapse to a Kerr black hole is the result. In the differentially rotating case (B) the final result is the same but the inner regions are deformed more strongly due to the faster rotation. The most interesting results are for rapid rotation. A collapsing configuration with an initial $q > 1$ cannot form a stationary black hole unless q is somehow reduced to < 1 by eg mass shedding [47] or emission of gravitational radiation [48]. All models with $q > 1$ failed to form a black hole producing instead either a vertical jet (for rigid rotation) or an expanding horizontal

disk (for differential rotation). In run A146 (see fig. 1.10) the centre matter first falls vertically along the z - axis and outflow in the radial direction occurs. The central regions then bounce producing a shockwave which reverses the infall. At this point the core has a value of $q \sim 1$ and thus it is possible for the final outcome to be a black hole with a jet.

Differential rotation gives a different picture. In run B143 (see fig. 1.11) there is a strong outflow in the radial direction and a disk forms. The thin shell of matter left behind eventually falls vertically onto the disk producing a weak shock. At late times the radial velocity of the central regions decreases while that of the outer parts remain large. Mass shedding is the result.

It seems that the final fate of rapidly rotating configurations is very dependent upon the initial conditions. For slow rotation, $q \lesssim 1$, a black hole is the end product.

Stark and Piran [37] have recently constructed an axi-symmetric code which is capable of following the hydrodynamical evolutions and estimating the gravitational wave emissions from rotating stellar collapse. Its success is a result of carefully chosen gauge conditions.

The ADM (3+1) approach is adopted. Isolation of the gravitational degrees of freedom is achieved by employing the radial gauge which in spherical polar co-ordinates (r, θ, ϕ) has the interval

$$ds^2 = -(\alpha^2 - \beta^i \beta_i)\,dt^2 - 2\beta_i\,dx^i\,dt + g_{rr}\,dr^2 + \frac{r^2 d\theta^2}{(1+\gamma)} + r^2(1+\gamma)(\sin\theta\,d\phi + \xi\,d\theta)^2 \qquad (1.20)$$

where α is the lapse function and β^i is the shift vector. For asymptotically flat spacetimes this becomes a transverse - traceless gauge at $r \to \infty$ with the metric components ξ and γ representing the $h_\times$ and h_+ modes of the

Model	Case	q	U	J	Time Slice	Horizon?[1]	Remarks
A146	A	1.46	0.94	0.77	Max	NO	jet
A122	A	1.22	0.86	0.51	Max	NO	jet
A105	A	1.05	0.84	0.37	Max	YES	——
A93	A	0.93	0.82	0.29	Max	YES	——
A75	A	0.75	0.82	0.19	Max	YES	——
A50	A	0.50	0.81	0.08	Max	YES	——
B143	B	1.43	1.01	1.20	Max	NO	expanding disk
B121	B	1.21	0.88	0.76	Max	NO	"
B104	B	1.04	0.84	0.54	Max	NO	"
B92	B	0.92	0.82	0.42	Max/Hyper	YES	——
B74	B	0.74	0.81	0.27	Max/Hyper	YES	——
B51	B	0.51	0.81	0.12	Max	YES	——

Fig. 1.9 Table of initial conditions and final outcome of axi-symmetric rotating collapse. The presence or absence of an apparent horizon is indicated. An apparent horizon always lies inside, or coincides with, the event horizon. (see [43] for details of how to numerically locate apparent horizons in the [(2+1)+1] formalism).

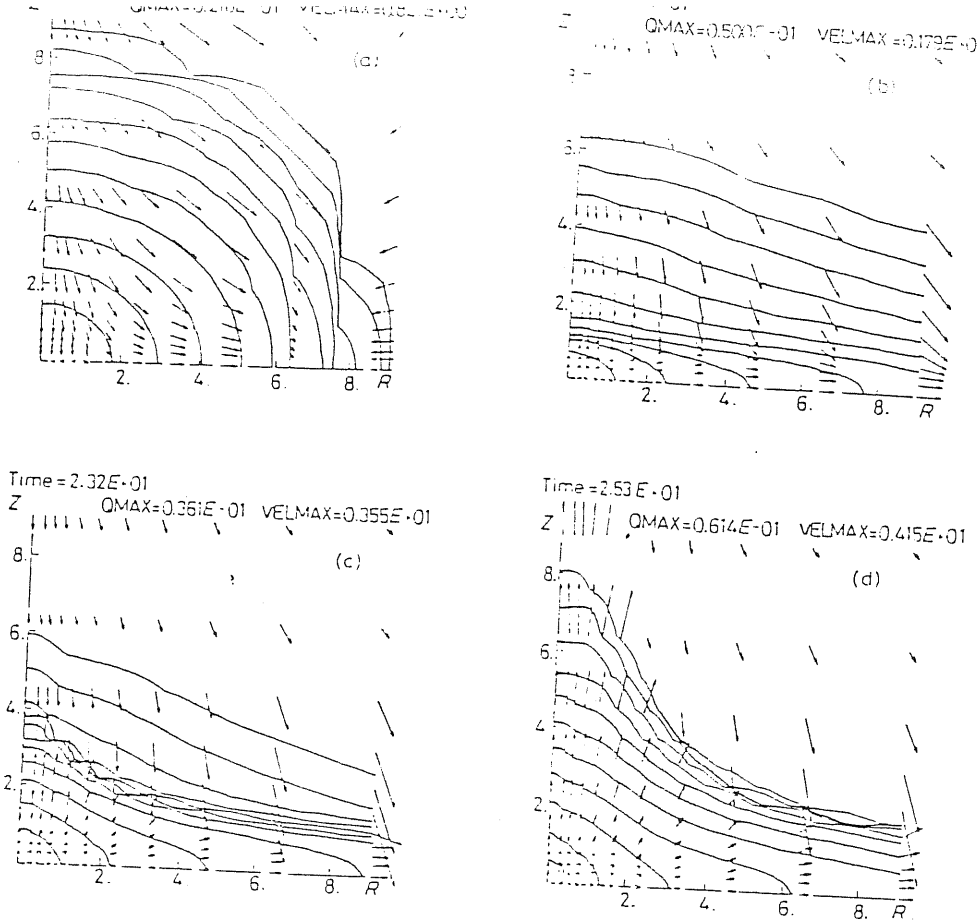

Fig. 1.10 Isodensity contours for the collapse of model A146 (see text). Length of arrows is proportional to the matter velocity.

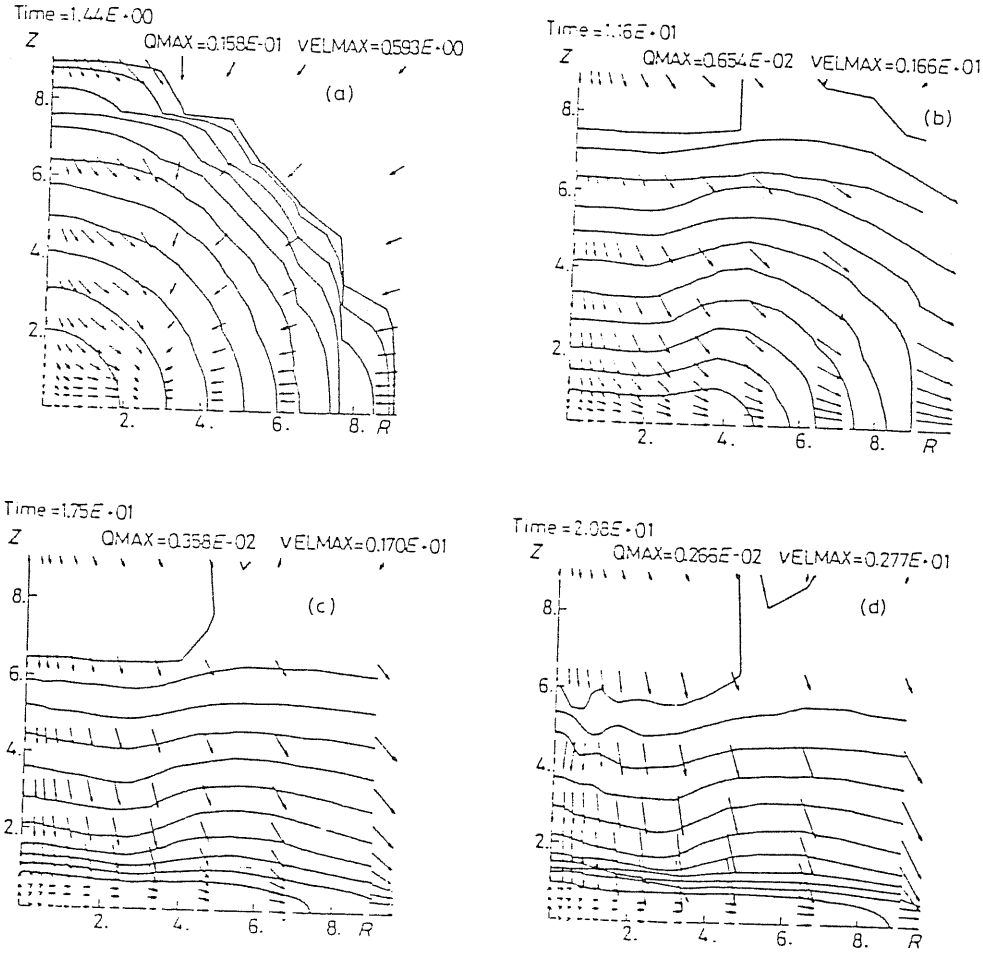

Fig. 1.11 Isodensity contours for the collapse of model B143.

gravitational radiation respectively. To minimise numerical errors ξ and η were evolved directly. The grid has some 100 x 8 nodes in the radial/angular directions with the outer nodes at a distance of 50M. Singularities due to black hole formation were avoided by using the polar hypersurface slicing condition. When combined with the radial gauge no event horizons are allowed to form. The presence of a black hole is inferred from an exponential decrease in the lapse function. This allows continuous evolution for times of many M which is necessary if the full gravitational wave content is to be estimated

The initial conditions were as follows; a static, equilibrium polytropic sphere with adiabatic index $\gamma = 2$, mass M and radius R = 6M is pressure reduced to either 1% or 40% of its equilibrium pressure. Simultaneously the star is given a rigid body rotation with the total angular momentum J measured by the parameter $a = \frac{J}{M^2}$ (a = q = Kerr parameter). The Einstein constraint equations are not used to provide initial data.

The nature of the collapse is determined by the value of a. For $a < 0.5$ continued collapse to a black hole is the result, with little deviation from spherical symmetry. If $0.5 < a < a_{crit}$ (where $a_{crit} = 1.2 \pm 0.2$ for a pressure reduction to 1% and $a_{crit} = 0.80 \pm 0.05$ for reduction to 40%) the effects of rotation are significant. An oblate spheroid forms but the final result is again a black hole. The time for black hole formation increases with a. These results are in qualitative agreement with those of Nakamura.

In the case of $a > a_{crit}$ a black hole never forms. Material near the pole flows along the rotation axis towards the equator while radial expansion occurs. The picture is qualitatively similar to that of fig. 1.10(b). The star then bounces and reverses the motions. The final result is oscillation about a flattened equilibrium structure. No jet is formed. Because of the large pressure reductions strong shocks do not occur. This may explain the difference.

The qualitative features of the gravitational radiation emitted during collapse are independent of the initial conditions. Fig. 1.12 shows the amplitudes of the h_x and h_+ modes for various values of parameter a. The amplitude increases as a increases. Wavelengths are in the range 12 - 28M. Perturbation results for a test particle falling into a black hole give a similar waveform [6]. Its shape is characteristic of the normal mode oscillations of a black hole [58] which are excited when particles fall in on a dynamical timescale. The oscillations are subsequently damped by gravitational wave emission. In this case the amplitude is decreased since phase cancellation effects occur. The total energy ΔE transformed into gravitational waves is very small. It increases with a approximately as $\frac{\Delta E}{M} \propto a^4$ with a maximum value of 7×10^{-4}. This indicates gravitational collapse is a poor source if axisymmetry is maintained.

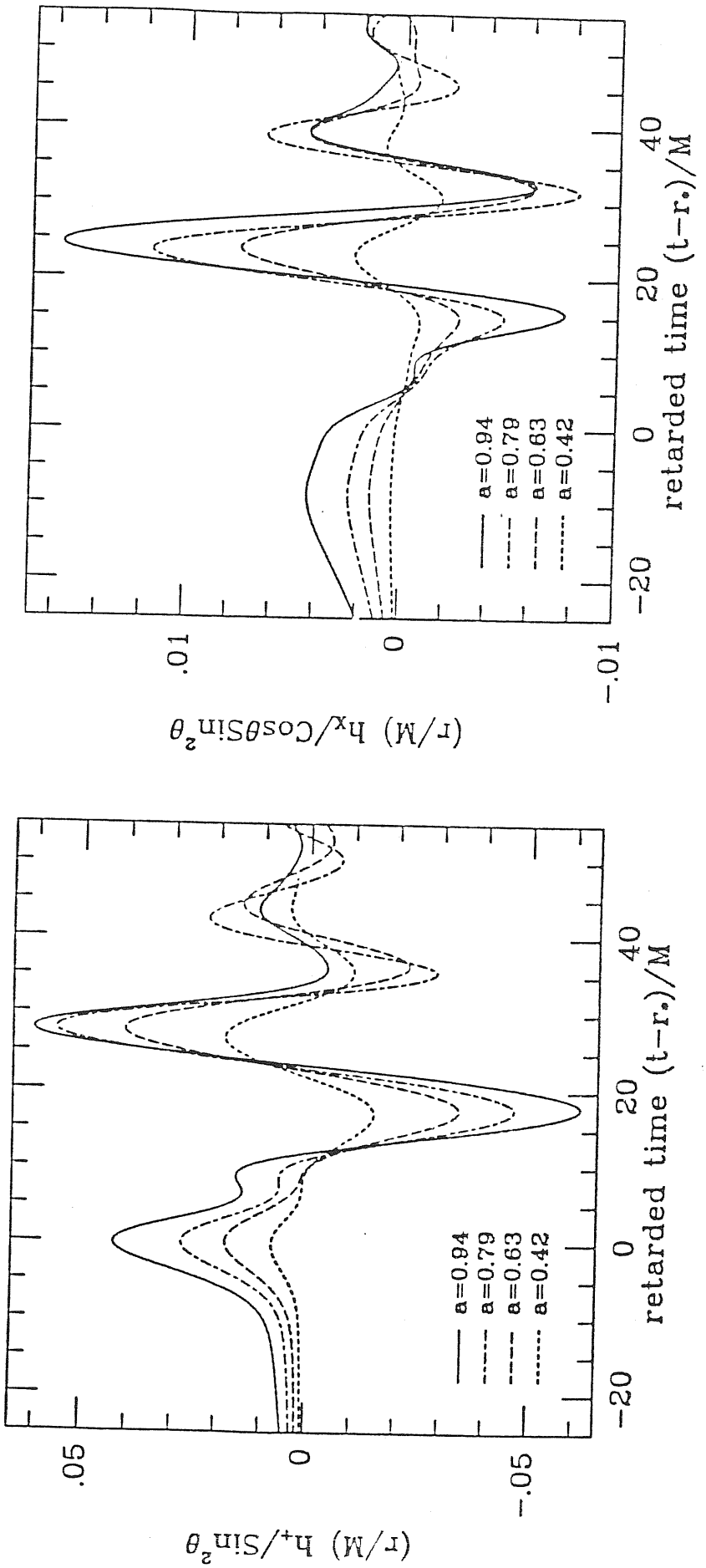

Fig. 1.12 The amplitudes of the h_+ and $h_\times$ polarization modes of Gravitational Radiation produced during axi-symmetric rotating collapse. The degree of rotation is governed by the Kerr parameter a.

2. METHODS AND TECHNIQUES

2.1 The ADM (3+1) Formalism:

The ADM (3+1) formulation of GR [53] has been reviewed many times [35], [54]. We will summerise the essential features.

Since there are no preferred observers for a general spacetime we must arbitrarily choose a congruence of world lines orthogonal to a family of spatial hypersurfaces and define Eulerian observers in terms of these. For local observers at rest in these hypersurfaces the spacetime metric is divided into the induced metric γ_{ij}, a lapse function α and a shift vector β^i. The latter two quantities depend on the subsequent motion of the observer; α determines the choice of the next hypersurface while β^i is a motion of the spatial co-ordinates (with repect to Eulerian observers). Thus constant time slices are distinguished and we write the metric in the form

$$ds^2 = -(\alpha^2 - \beta^i\beta_i)dt^2 + 2\beta_i dx^i dt + \gamma_{ij} dx^i dx^j \qquad (2.1)$$

where γ_{ij} is the spatial metric of the t = constant hypersurface, the lapse function $\alpha = (-g^{00})^{-\frac{1}{2}}$ and the shift vector $\beta^i = \gamma^{ij}\beta_j$, $\beta_j = g_{0j}$.

If n^μ is the unit normal to the hypersurface then

$$t^\mu = \alpha n^\mu + \beta^\mu \qquad (2.2)$$

where αdt is the orthogonal proper time separation of hypersurfaces t and t+dt, and $n^\mu = (\frac{1}{\alpha}, -\frac{\beta^i}{\alpha})$ is the 4-velocity of the Eulerian observers who measure the velocity of the spatial co-ordinates to be $\frac{\beta^i}{\alpha}$ (see fig. 2.1). The rate of change of the spatial metric with respect to local orthogonal proper time

(Eulerian observers) is given by the extrinsic curvature

$$K_{\mu\nu} = -\tfrac{1}{2} \pounds_{\bar{n}} \gamma_{\mu\nu} \tag{2.3}$$

where £ denotes the Lie derivative. Equivalently we define the extrinsic curvature by

$$K_{\mu\nu} = -\gamma_{\mu}^{\lambda} \nabla_{\lambda} n_{\nu} \tag{2.4}$$

where $n_{\nu} = (-\alpha, 0, 0, 0)$ is the 1-form dual to n^{ν} and $\gamma_{\mu}^{\lambda} = g_{\mu}^{\lambda} + n_{\mu} n^{\lambda}$ is a spatial projection operator. Note that the extrinsic curvature is a purely spatial quantity, $K_{\mu\nu}\, n^{\mu} = K_{\mu\nu}\, n^{\nu} = 0$. From (2.2) - (2.4) we write

$$K_{ij} = -\frac{1}{2\alpha}\left[\frac{\partial \gamma_{ij}}{\partial t} - D_i \beta_j - D_j \beta_i \right] \tag{2.5}$$

where $D_i \beta_j = \gamma_i^{\mu} \nabla_{\mu} \beta_j$ defines the covariant derivative D_i compatable with γ_{ij}.

We can now write the Einstein equations in a (3+1) form. If they are first written as

$$G_{\mu\nu} = 8\pi T_{\mu\nu} \tag{2.6}$$

where

$$G_{\mu\nu} = R_{\mu\nu} - \tfrac{1}{2} g_{\mu\nu} R \tag{2.7}$$

we obtain, by projection

i) the Hamiltonian constraint

$$G_{\mu\nu} n^{\mu} n^{\nu} = \tfrac{1}{2}\left({}^{(3)}R + K^2 - K_{ij} K^{ij} \right) = 8\pi \rho \tag{2.8}$$

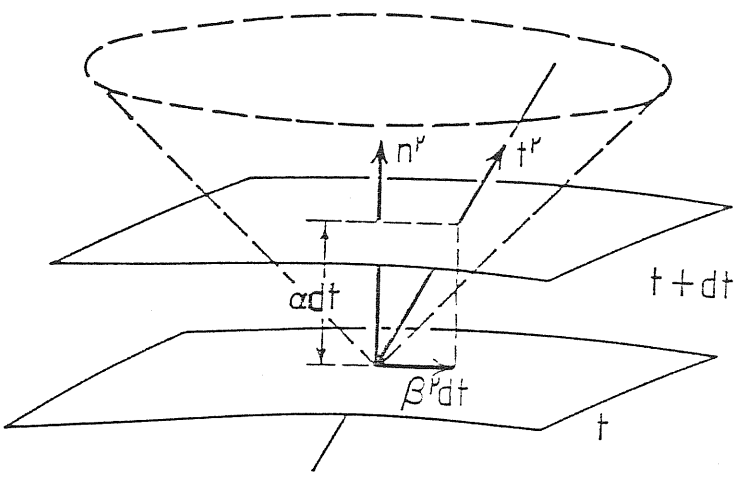

Fig. 2.1 Illustrated are parts of two nearly spatial hypersurfaces. The time vector is $t^\nu = \alpha n^\nu + \beta^\nu$ where α is the lapse function, β^ν is the shift vector and n^ν is the unit normal. The dashed figure represents a local light cone.

ii) the Momentum constraints

$$-\gamma^{i}_{\mu} G^{\mu}_{\nu} n^{\nu} = D_j (K^{ij} - \gamma^{ij} K) = 8\pi j^{i} \tag{2.9}$$

where the projections of the stress-energy tensor $T_{\mu\nu}$ are

$$\begin{aligned} T_{\mu\nu} n^{\mu} n^{\nu} &= \rho \\ -\gamma^{i}_{\mu} T^{\mu}_{\nu} n^{\nu} &= j^{i} , \end{aligned} \tag{2.10}$$

K denotes K^{i}_{i} and ${}^{(3)}R$ is the scalar curvature intrinsic to the spatial hypersurface. Use has been made of the Gauss - Codacci relations [56]

$$\gamma^{\mu}_{i} \gamma^{\nu}_{j} \gamma^{\sigma}_{\kappa} \gamma^{l}_{\lambda} R_{\mu\nu\sigma}{}^{\lambda} = {}^{(3)}R_{ijk}{}^{l} + K_{ik} K^{l}_{j} - K_{jk} K^{l}_{i} \tag{2.11}$$

$$\gamma^{\mu}_{i} R_{\mu\nu} n^{\nu} = D_j K^{j}_{i} - D_i K . \tag{2.12}$$

The dynamical Einstein equations are obtained by writing

$$R_{\mu\nu} = 8\pi \left(T_{\mu\nu} - \tfrac{1}{2} g_{\mu\nu} g^{\lambda\sigma} T_{\lambda\sigma} \right) \tag{2.13}$$

and projecting using the operator $\gamma^{\mu}_{i} \gamma^{\nu}_{j}$, to give

$$\begin{aligned} &\tfrac{1}{\alpha} \frac{\partial K_{ij}}{\partial t} - \tfrac{1}{\alpha} \pounds_{\vec{\beta}} K_{ij} + \tfrac{1}{\alpha} D_i D_j \alpha - {}^{(3)}R + 2 K_{ik} K^{k}_{j} \\ &\qquad - K_{ij} K = -8\pi \left(S_{ij} - \tfrac{1}{2} \gamma_{ij} S + \tfrac{1}{2} \rho \gamma_{ij} \right) \end{aligned} \tag{2.14}$$

where

$$\begin{aligned} \gamma^{\mu}_{i} \gamma^{\nu}_{j} T_{\mu\nu} &= S_{ij} \\ S &= S^{i}_{i} . \end{aligned} \tag{2.15}$$

The spacetime is then the time history of two spatial tensor fields K_{ij} and γ_{ij} evolved via equations (2.14) and (2.5) respectively. The initial data (γ_{ij}, K_{ij}) on the t = 0 hypersurface is subject to the constraints (2.8) and (2.9), which are satisfied at all times as a consequence of the Bianchi identities. The consistent specification of this initial data is outlined in section 2.4. We note that the equations cannot determine α or β^i. These must be specified arbitrarily on each hypersurface, and it is this which gives the (3+1) formalism its power. The choice of α and β^i determines the observers who record the data set (γ_{ij}, K_{ij}) which describes the spacetime. A good choice of these kinematic variables is crucial for the success of any numerical code. We review some of the many options in section 2.3.

2.2 The [(2+1)+1] Formalism:

For spacetimes possessing a Killing vector field ξ^μ Geroch has shown [57] that it is possible to divide out the Killing direction to reduce the four dimensional manifold M with metric $g_{\mu\nu}$ to a three dimensional quotient space S (called the orbit space of ξ^μ, ie. the orbits of ξ^μ are represented as points in S) with a scalar field $\lambda = \xi^\mu \xi_\mu$, a vector field $\omega_\mu = \varepsilon_{\mu\nu\sigma\lambda}\xi^\nu \nabla^\sigma \xi^\lambda$ and metric $h_{\mu\nu} = g_{\mu\nu} - \frac{1}{\lambda^2}\xi_\mu\xi_\nu$. $\varepsilon_{\mu\nu\sigma\lambda}$ is the totally anti-symmetric Levi - Civita tensor.

The next stage is to write the Einstein equations on S, with additional equations obtained for λ and ω_μ ;

$$R_{\mu\nu}(S) = \frac{1}{2\lambda^4}\left(\omega_\mu\omega_\nu - h_{\mu\nu}\omega_\rho\omega^\rho\right) + \frac{1}{\lambda}D_\mu D_\nu\lambda + h_\mu^\rho h_\nu^\sigma R_{\rho\sigma} \qquad (2.16)$$

$$D_\mu D^\mu\lambda = -\frac{1}{2\lambda^3}\omega_\rho\omega^\rho - \frac{1}{\lambda}R_{\mu\nu}(M)\xi^\mu\xi^\nu \qquad (2.17)$$

$$D_{[\mu}\omega_{\nu]} = \varepsilon_{\mu\nu\rho\sigma}\,\xi^{\sigma} R^{\rho}_{\lambda}(M)\,\xi^{\lambda}$$

$$D^{\rho}\left(\frac{1}{\lambda^{3}}\,\omega_{\rho}\right) = 0 \qquad (2.18)$$

where D_μ is the covariant derivative compatable with the metric $h_{\mu\nu}$. If ξ^μ is spacelike then S is a three dimensional spacetime and we may apply the (3+1) approach described earlier to obtain a (2+1) decomposition. The invariant interval in the orbit space S is written as

$$ds^2 = h_{\mu\nu}\,dx^\mu dx^\nu = -(\alpha^2 - \eta^A\eta_A)\,dt^2 + 2\eta_A\,dx^A\,dt + H_{AB}\,dx^A dx^B \qquad (2.19)$$

where H_{AB} is the metric of the two dimensional spatial surfaces, α is the lapse function and η^A is the shift vector. The indices A, B take values 1 - 3 excluding the value corresponding to the Killing direction. One of the advantages of this formalism is already apparent; there are only two shift vector components rather than the usual three. In some cases this can significantly simplify the choice of gauge.

Nakamura used this formalism to construct computer codes simulating the collapse of axi-symmetric, rotating stars, the results of which were reviewed in chapter one. Such a spacetime possesses the Killing vector field $\xi^\mu \frac{\partial}{\partial x^\mu} = \frac{\partial}{\partial \phi}$ so the β^ϕ shift vector component need not be considered. [41] and [44] list the [(2+1)+1] Einstein equations for this system. A remarkable feature which appears is the close similarity of some of the equations with those describing electromagnetic fields in curved spacetime. The formalism is easily extended to include a real electromagnetic field, and this has been done in [45].

Obviously a spacetime with the necessary symmetry requirement is needed to utilize this method. It cannot be applied to three dimensional stellar collapse.

2.3 Gauge Conditions:

There are several motivations for choosing a paticular gauge. We would like to avoid both co-ordinate and physical singularities. The latter are avoided by slowing down the evolution of the spatial region near the singularity as it is approached. This is controlled by the lapse function. Also one would like to make the Einstein equations as simple as possible so that a numerical solution is not unduly complicated. A good choice of shift vector can zero several components of the spatial metric and thus considerably reduce the number of calculations, particularly for quantities such as the 3-Ricci tensor ${}^{(3)}R_{ij}$. However there are other considerations governing the choice of shift. We may like the co-ordinate congruence to follow the matter world lines, or wish to globally minimise the distortion in the co-ordinate grid as the space-time evolves. Since the quantity of gravitational radiation in a spacetime is usually small (see chapter one) the gravitational degrees of freedom should be isolated as much as possible. If the difference of two large metric components gives the gravitational wave content then numerical rounding error can easily swamp the solution. We begin with the choice of lapse.

i) Geodesic slicing;

Set $\alpha = 1$, and if this is combined with shift $\beta^i = 0$ we use Eulerian observers who are freely falling so that spatial hypersurfaces are geodesically parallel. If a physical singularity forms the geodesics focus towards it and the calculation halts after a finite time. This slicing is singularity seeking [59] and is thus useless for collapse calculations where a black hole may form.

ii) Lagrangian slicing;

In spherical symmetry we may use a diagonal metric, $\beta^i = 0$, and the slicing condition $\alpha U^o = 1$ where U^o is the time component of the matter 4-velocity. This means $U^i = 0$ and the fluid world lines are orthogonal to the spatial hyper-

surfaces (possible because there is no vorticity). Since the shift is zero the co-ordinates follow the matter. This gauge was used by May and White for their collapse calculations (see chapter one) which were halted at the start of black hole formation. The fluid world lines focus towards any singularity producing singularities in both matter and co-ordinate variables after a finite time. Again this is not a useful gauge for collapse calculations.

iii) Maximal slicing;

We can avoid the focusing effect of world lines towards singularities by choosing α in such a way that the trace of the extrinsic curvature, K, remains zero on each time slice if it is zero on the initial one [60]. Physically K measures the expansion of a congruence of world lines normal to the spatial hypersurfaces. Setting K = 0 produces an 'incompressible fluid of observers'.

Since the Eulerian observers then have zero convergence their local volume element $\sqrt{\gamma}\, d^3x$, where $\gamma = \det \gamma_{ij}$, is time independent. The proper spatial volume V of any region Ω of the t = constant hypersurface is

$$V = \int_{\Omega} \sqrt{\gamma}\, d^3x \tag{2.20}$$

which may be maximised by the variational principle $\delta V = 0$. This leads directly to the condition K = 0, [61]. Substituting into the Einstein evolution equations (2.14) the conditions $K = 0, \frac{\partial K}{\partial t} = 0$ gives

$$\frac{1}{\alpha} \gamma^{ij} D_i D_j \alpha - {}^{(3)}R = 4\pi (S - 3\rho) \tag{2.21}$$

which is an elliptic equation for α to be solved on each slice.

The maximal slicing of Kruskal space [62] shows that α drops exponentially in the region of a singularity, although the time slices do penetrate

the event horizon. Motion within r = 1.5M, where M is the mass of the black hole, is effectively frozen so that the Schwarzschild throat stretches with time, becoming topologically a cylinder. As a consequence the co-ordinate grid is sucked down the black hole to cover the ever increasing proper length of the cylinder. This problem was encountered by Shapiro and Teukolsky who used maximal slicing for spherical collapse (see chapter one). In principle the problem may be solved by using a non-zero shift vector to push the co-ordinates out.

Maximal slicing has other drawbacks. Solving the elliptic equation requires several sweeps of the numerical grid which is time consuming. Also, at the moment, it is not clear whether general hyperbolic spacetimes admit maximal hypersurfaces. Despite all this the singularity avoiding feature and the fact that it simplifies the constraint equations has made it a popular choice for codes constructing asymptotically flat spacetimes with possible black hole formation.

iv) Constant mean curvature slicing;

The slicing condition is K = C(t) where C is a function constant on each hypersurface. This includes maximal slicing as a special case. It is a generalization of the natural time co-ordinate in homogeneous cosmologies and as such has been used extensively for cosmological problems [63].

v) Algebraic and hypergeometric slicing;

The slicing conditions

$$\frac{1}{r^2}\frac{d}{dr}\left(r^2\frac{d}{dr}\right)\alpha = V_0\,\mathrm{sech}^2(mr)\,\alpha \qquad (2.22)$$

can be made to simulate the singularity avoiding feature of maximal slicing without the need to solve an elliptic equation on each hypersurface. In fact with the boundary conditions $\alpha \to 1$ at $r \to \infty$ and $\frac{d\alpha}{dr} = 0$ at r = 0 it is possible

to express α directly in terms of hypergeometric functions. Also the free parameters V_0 and m give some latitude for adjustment and experimentation. This slicing condition was successfully used by Nakamura [41] for rotating axi-symmetric collapse. It does not simplify the Einstein equations in any way but offers other advantages. In particular it was found that for disk-like configurations hypergeometric slicing is superior to maximal slicing.

vi) Polar slicing;

In sphereical polar co-ordinates (r, θ, ϕ) we may express this slicing condition as $K = K^r_r$. Substituting into the Einstein equations yields a parabolic equation for α which can be integrated inwards with one sweep of the grid. The single boundary condition is $\alpha = 1$ at $r = \infty$. This means a significant saving of computer time in comparison with maximal slicing. When combined with the radial gauge the singularity avoiding feature is strong, the slices never cross the event horizon.

Unfortunately the slicing condition is irregular at r = 0 so it must be smoothly joined to some other type of slice at finite radius. Stark and Piran used mixed maximal and polar hypersurfaces for their rotating stellar collapse.

We direct the reader to the references [65] - [67] for a complete description of the powerful combination of polar slicing with the radial gauge and its application to stellar collapse.

The choice of shift vector is now considered.

i) Eulerian gauge;

We simply set $\beta^i = 0$ so that the co-ordinate congruence is normal to the spatial hypersurfaces. Early collapse codes [26], [31] used this gauge.

ii) Lagrangian gauge;

For spacetimes containing matter we can set $\beta^i = \frac{u^i}{u^0}$ where U^μ is the fluid 4-velocity. Thus the co-ordinate congruence coincides with the congruence

of fluid world lines. For one dimensional flows this is a convenient choice but in two and three dimensions where vorticity may be present the co-ordinate grid can become severely distorted leading to a loss of accuracy. Taub [68] gives the general formalism.

iii) Simplifying gauge;

A particular choice of β^i can considerably simplify the Einstein equations by zeroing certain components of the spatial metric. Three conditions on the shift vector enables three components to be eliminated giving, eg. a diagonal spatial metric

$$dl^2 = g_{xx}\, dx^2 + g_{yy}\, dy^2 + g_{zz}\, dz^2 \qquad (2.23)$$

Also the shift vector may be used to keep the spatial metric in a particular form, such as, eg; the isothermal gauge where $g_{r\theta} = g_{r\phi} = 0$ and $g^{rr} = g^{\theta\theta}$, or the radial gauge where $g_{r\theta} = g_{r\phi} = 0$ and $g_{\theta\theta} g_{\phi\phi} - g_{\theta\phi}^2 = r^4 \sin^2\theta$, and the three dimensional line element has the form

$$dl^2 = A^2 dr^2 + r^2 B^{-2} d\theta^2 + r^2 B^2 (\sin\theta\, d\phi + \xi\, d\theta)^2 \qquad (2.24)$$

where A, B and ξ are the metric functions to be determined. At $r \to \infty$ in asymptotically flat spacetime this gauge becomes transverse and traceless with $\xi = h_\times$ representing the x mode and $h_+ = B^2 - 1$ the + mode polarizations of gravitational radiation. Thus the gravitational wave content can be obtained directly from the computed metric components.

iv) Minimal distortion gauge;

Finally we mention the minimal distortion gauge [69] where the shift vector is found by imposing the condition $D_j\left(\frac{\partial \tilde{\gamma}^{ij}}{\partial t}\right) = 0$ where $\tilde{\gamma}_{ij} = \gamma_{ij}/\gamma^{1/3}$. In the linearized theory this reduces to a transverse-traceless gauge and also

eliminates non-physical gravitational waves due to co-ordinate effects. Thus it would be useful for studying gravitational wave emission. Unfortunately one must solve a complicated vector elliptic equation on each time slice to find the shift vector components. This combined with the fact that it offers no simplification of the Einstein equations restricts its practical use.

2.4 The Initial Value Problem:

By treating gravity as a dynamical theory one is restricted to globally hyperbolic spacetimes [70]. Also (3+1) numerical relativity can construct only those spacetimes which may be foliated with spatial hypersurfaces (however see [71]), although conversly Geroch has shown [72] that any hyperbolic spacetime has this property and so can be generated on the computer. A set of initial data consistent with the constraint equations (2.8) and (2.9) is required. One must decide which parts of (γ_{ij}, K_{ij}) are freely specifiable and which are to be determined from the satisfaction of the constraint equations. There may be no solution for arbitrary data. It is well known, however, that GR does possess a well posed initial value formulation [73], ie. that for a set of initial data satisfying the constraint equations there exists a unique spacetime which is a solution of Einstein's equations, is globally hyperbolic, contains the Cauchy initial data hypersurface and is such that the solution depends continuously on this data. The procedure for solving the constraint equations is then as follows:

We begin by writing the spatial metric of section 2.1 as [60]

$$\gamma_{ij} = \phi^4 \hat{\gamma}_{ij} \qquad (2.25)$$

where ϕ is a conformal factor to be determined and $\hat{\gamma}_{ij}$ is some given spatial metric (usually $\hat{\gamma}_{ij}$ is taken to be the flat space metric). The scalar curvature intrinsic to the spatial hypersurfaces transforms as

$$ {}^{(3)}R = {}^{(3)}\hat{R}\,\phi^{-4} - 8\phi^{-5}\hat{\gamma}^{ij}\hat{D}_i\hat{D}_j\phi \qquad (2.26) $$

where ${}^{(3)}\hat{R}$ is the scalar curvature associated with $\hat{\gamma}_{ij}$ and $\hat{D}_i$ is the compatable covariant derivative. For the extrinsic curvature we first decompose it into a trace and trace-free part,

$$ \text{trace} \qquad K = \gamma^{ij}K_{ij} \qquad (2.27) $$

$$ \text{trace-free} \qquad A^{ij} = k^{ij} - \tfrac{1}{3}\gamma^{ij}K \qquad (2.28) $$

and it is assumed that K will be specified. The trace-free part A^{ij} will be subject to a conformal transformation followed by decomposition into a sum of divergence free and trace-free parts. The ordering of these operations is ambiguous and can lead to different initial data sets (see [61]), we show one method.

By transforming A^{ij} as

$$ A^{ij} = \phi^{-10}\hat{A}^{ij} \qquad (2.29) $$

we find the desirable relations

$$ D_j A^{ij} = \phi^{-10}\hat{D}_j\hat{A}^{ij} \qquad (\text{for } \phi > 0) \qquad (2.30) $$

and

$$A = \hat{A} = 0 \tag{2.31}$$

where A and $\hat{A}$ are the trace of A^{ij} and $\hat{A}^{ij}$ respectively. Any traceless symmetric tensor can be split into two parts [74]

$$\hat{A}^{ij} = \hat{A}^{ij}_{*} + (lW)^{ij} \tag{2.32}$$

where

$$(lW)^{ij} = \hat{D}^{i} W^{j} + \hat{D}^{j} W^{i} - \tfrac{2}{3} \hat{\gamma}^{ij} \hat{D}_{k} W^{k} \tag{2.33}$$

$$\hat{D}_{j} \hat{A}^{ij}_{*} = \hat{A}_{*} = 0 \tag{2.34}$$

$$\hat{D}_{j} (lW)^{ij} = \hat{D}_{j} \hat{A}^{ij} = \hat{\gamma}^{kj} \hat{D}_{k} \hat{D}_{i} W^{i} + \tfrac{1}{3} \hat{D}^{i} \hat{D}_{j} W^{j} + \hat{R}^{i}_{j} W^{j} \tag{2.35}$$

W^{i} is a vector potential which is to be determined by the constraint equations along with the conformal factor ϕ. At this stage the initial data which is freely specified is $\hat{\gamma}_{ij}$, K and $\hat{A}^{ij}_{*}$. The matter terms should now be considered.

The detailed treatment of the ρ and j^{i} terms depends on the nature of the source [75], [76]. We assume $\hat{\rho}$ and $\hat{j}^{i}$ are given and write

$$\rho = \phi^{-8} \hat{\rho} \tag{2.36}$$

$$j^{i} = \phi^{-10} \hat{j}^{i} \tag{2.37}$$

so that the local 'dominant energy condition' [77]

$$\rho^2 - \gamma_{ij} j^i j^j \geq 0 \tag{2.38}$$

is satisfied for all $\phi > 0$. The constraint equations are now written as;

i) the Hamiltonian constraint

$$8\hat{\gamma}^{ij}\hat{D}_i D_j \phi - \hat{R}\phi + \hat{A}_{ij}\hat{A}^{ij}\phi^{-7} - \tfrac{2}{3}K^2\phi^{-5} + 16\pi\hat{\rho}\phi^{-3} = 0 \tag{2.39}$$

ii) the Momentum constraints

$$\hat{\gamma}^{kj}\hat{D}_k\hat{D}_j W^i + \tfrac{1}{3}\hat{D}^i\hat{D}_j W^j + \hat{R}^i_j W^j - \tfrac{2}{3}\phi^6\hat{D}^i K - 8\pi\hat{j}^i = 0 \tag{2.40}$$

which are solved for ϕ and W^i to give the initial data set

$$\begin{aligned} \gamma_{ij} &= \phi^4\hat{\gamma}_{ij} \\ K_{ij} &= \phi^{-2}[\hat{A}_{*ij} + (lW)_{ij}] + \tfrac{1}{3}\phi^4\hat{\gamma}_{ij}K \\ \rho &= \hat{\rho}\phi^{-8} \\ j^i &= \hat{j}^i\phi^{-10} \end{aligned} \tag{2.41}$$

There are no global existance and uniqueness theorems for this elliptic system of equations in its most general form, however the analysis has been done for some special cases (see [54]).

The equations are simplified considerably if we assume the initial data is time symmetric ($K_{ij} = 0$, $j^i = 0$) and conformally flat ($\gamma_{ij} = \phi^4 f_{ij}$), then (2.40) is an identity and (2.39) reduces to

$$\hat{\gamma}^{ij}\hat{D}_i\hat{D}_j\phi + 2\pi\hat{\rho}\phi^{-3} = 0. \tag{2.42}$$

This also has the effect of eliminating gravitational waves from the initial data [39].

Another simplifying condition, which is often used, is to set K = 0 on each slice, ie. maximal time slicing. Then ϕ decouples from (2.40) resulting in a linear, second order elliptic system for W^i.

York and Piran [78] give a method for the numerical solution of (2.39) in its general form. This is based on a successive over relaxation (SOR) iteration scheme. Obviously good boundary conditions for ϕ are required and the assumption of asymptotic flatness offers many advantages in this respect.

2.5 Numerical Considerations:

a) Differencing;

For implementation on the computer the partial differential Einstein equations (2.8), (2.9) and (2.14) need to be written in a discrete form. This is normally achieved using the method of finite differences [81], [82], although Mann [86], [87] has introduced the finite element method (FEM) [88] into GR.

The many ways to difference a given differential equation is the subject of a vast literature [81] - [85]. One is concerned with accuracy, stability, convergence and the efficient solution of the resulting large system of algebraic (possibly non-linear) equations. These are specialized fields and we direct the reader to the references cited for the details.

b) Shock handling;

The non-linearity of the fluid flow equations will ensure the formation of steep gradients in most cases even if the initial data is perfectly smooth and regular. Energy is transferred from long wavelength modes to ever decreasing wavelengths causing smooth waves to evolve naturally into steep gradients.

Mathematically the final result would be a discontinuity, however nature avoids this phenomenon by converting the kinetic energy into heat via viscous effects. There is an associated entropy production and the discontinuity is converted into a region where the fluid variables change rapidly but smoothly. Such a region is referred to as a shock.

On the numerical grid there is an upper limit to the wavelengths which may be represented. This is dictated by the spatial step length. Energy accumulates in this shortest wavelength and appears as a numerical oscillation which destroys the solution. The remedy is to follow nature and introduce viscous terms to spread the discontinuity over several grid nodes.

The addition of a scalar bulk viscosity $q = -\xi \nabla_\alpha u^\alpha$ to the pressure has proved to be very successful and popular. Here u^α is the 4-velocity of the fluid and ξ is a proportionality factor. A real bulk viscosity is linear in the term $\nabla_\alpha u^\alpha$ so that the thickness of the shock varies with shock strength (the weaker the shock the larger the transition region). To obtain shock widths independent of strength one makes ξ wavelength dependent. For Newtonian hydrodynamics in slab symmetry von Neumann and Richtmyer [28] proposed an artificial viscosity of the form

$$q = -K\rho\Delta x^2 \left|\frac{dv}{dx}\right| \frac{dv}{dx} \qquad (2.43)$$

where K is an arbitrary constant whose value is to be determined by experiment, ρ is the density, Δx is a spatial interval and v is the fluid velocity. This has a number of very desirable features:

i) The shock width is independent of shock strength as required. Its value in terms of Δx is determined by K.

ii) q is very small except in regions of large stress $\frac{dv}{dx}$. For expansions one normally sets q = 0.

iii) q is of the order of the kinetic energy. This allows thermal and kinetic energy to interchange.

iv) The addition of q to the pressure means the fluid flow equations automatically satisfy the internal boundary ('jump') conditions across the shock. These are the Rankine - Hugoniot relations and are necessary in addition to the hydrodynamic equations for a unique solution [82].

A relativistic form of (2.43) in spherical symmetry was used by May and White [26] to treat shocks in their stellar collapse code. Using the same notation as in section 1.2 their relativistic generalization is

$$q = K \Delta\mu^2 \rho_0 \left(\frac{\partial u}{\partial \mu}\right) \frac{1}{\Gamma} \qquad \text{if} \quad \frac{\partial \rho_0}{\partial t} > 0$$

$$q = 0 \qquad \text{if} \quad \frac{\partial \rho_0}{\partial t} \leq 0. \tag{2.44}$$

The term $\frac{1}{\Gamma}$ compensates for the fact that kinetic energy, $(\Gamma - 1)$, is of order u rather than u^2 at extreme relativistic energies, thus it keeps q ~ kinetic energy. For spherical symmetry (2.44) is

$$q = K \left(\frac{\Delta\mu}{R^2}\right) \rho_0 \left(\frac{\partial (R^2 u)}{\partial \mu}\right)^2 \frac{1}{\Gamma} \qquad \text{if} \quad \frac{\partial \rho_0}{\partial t} > 0$$

$$q = 0 \qquad \text{if} \quad \frac{\partial \rho_0}{\partial t} \leq 0. \tag{2.45}$$

In spherical collapse large but smooth velocity gradients can form and no shock appears. This can generate a q larger than the pressure which causes numerical instability. For this reason May and White also experimented with the artificial viscosity

$$q = -K^2 \rho_0 (1+\Pi) \frac{\Delta\mu^4}{(4\pi R^2)^2} \frac{1}{a} \frac{\partial}{\partial t}\left(\frac{1}{\rho_0}\right) \frac{\partial^2}{\partial \mu^2}\left[\frac{1}{a}\frac{\partial}{\partial t}\left(\frac{1}{\rho_0}\right)\right] \tag{2.46}$$

which is zero when the compression is large but uniform.

For two and three dimensional flows an artificial tensor viscosity could be used [81], however the satisfaction of the jump conditions is not guaranteed. It is simplest to always use one of the form $q = -\xi \nabla_\alpha u^\alpha$.

Other numerical techniques have been developed for dealing with shocks. If the equations are put in a conservation law form and differenced using the Lax - Wendroff scheme [82] then an implicit diffusive term is introduced. This has the same effect as an artificial viscosity.

Shock fitting [82], [90] involves following the shock front and implementing the jump conditions directly across it. The hydrodynamic equations are usually written in a characteristic form. Continuous monitoring of the fluid variables is required along with some criterion for the presence of a shock. The method can give high accuracy, but it is complicated and so seldom used.

A recent development which is becoming increasingly popular is the flux corrected transport (FCT) algorithm [91], [92] although it has not yet been applied to GR problems. Breifly, the technique consists of two stages. Stage one is transport by a difference scheme which has a large numerical diffusion. This is followed by an anti-diffusion stage which localizes the diffusion to those regions where unphysical, high frequency oscillations occur. This corrective diffusion is non-linear and varies with the solution from point to point. The overall scheme is conservative so that when a quantity of flux is subtracted from one point an equal amount is added somewhere else. Physically reasonable results have been obtained from shock tube calculations without using an artificial viscosity. For astrophysical applications of the method see [93], [94].

3. A REGGE CALCULUS APPROACH TO NUMERICAL RELATIVITY

3.1 Introduction:

Regge Calculus (RC) [95] provides a discrete formulation of GR based on a variational approach. It bears a close resemblence to the Ritz variational techniques used in finite elements, and in this sense RC is a natural finite element formulation of GR.

The basic idea is to approximate a smooth, differentiable, curved manifold by one which is continuous but piecewise flat. An elementary example in two dimensions (2 d) serves to illustrate this and at the same time we can define the important concept of a deficit angle.

Consider the smooth 2 d curved surface shown in fig. 3.1(a). This surface can be approximated by a polyhedron composed of a collection of flat plaquettes (triangles in this case) as shown in fig. 3.1(b). The curvature of this piecewise flat surface is evident. The triangles A, B, C, D meeting at some vertex cannot lie in a 2 d Euclidean plane and stay attached to each other; a gap must appear. We then define the deficit angle ε by

$$\varepsilon = 2\pi - \sum_{\substack{\text{triangles meeting} \\ \text{at a vertex}}} (\text{vertex angles of triangles}). \qquad (3.1)$$

So, although the geometry is Euclidean both inside each triangle and at the 1 d interfaces where two triangles join, there is curvature at the vertices. A vector parallel transported on a path from A through B, C, D and back to A so as to encircle the vertex undergoes a rotation equal to the deficit angle. If the vector returns to A without encircling the vertex then no rotation occurs. Thus we can say that the vertex 'carries the curvature'.

The above idea is extended to higher dimensions in a natural way. An

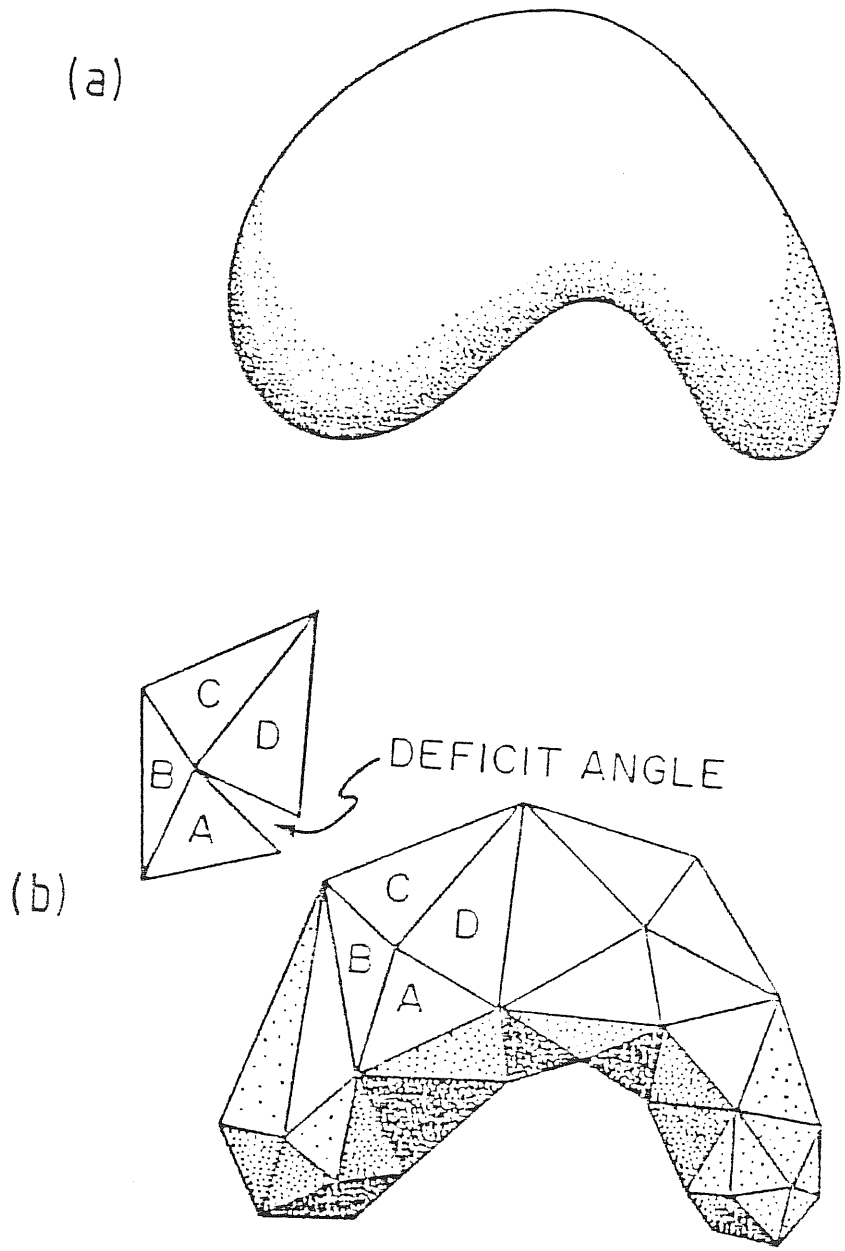

Fig. 3.1 A 2-geometry with continuously varying curvature can be approximated arbitrarily closely by a polyhedron built of triangles.

n d curved surface is approximated by a collection (lattice or net) of n d flat blocks (Regge blocks) which meet , or hinge, on the (n-2) d sub-blocks (bones) which carry the curvature.

That in general the curvature is carried by the (n-2) d bones is easily shown. Consider a 2 d Euclidean plane in polar co-ordinates. The metric is $ds^2 = dr^2 + r^2 d\theta^2$, and points of equal r but θ differing by 2π are identical. Now delete a wedge $2\pi - \varepsilon \leq \theta \leq 2\pi$ and thus obtain a manifold with the intrinsic geometry of a cone. This is the ε - cone. The origin r = 0 is a vertex with deficit ε while the rest of the ε - cone is Euclidean. If $\mathbb{R}$ is the real line we can consider the 3 d product topology $\mathbb{R} \times \varepsilon$ - cone which is Euclidean everywhere except at the straight line r = 0. For an n d topology we consider $\mathbb{R}^{n-2} \times \varepsilon$ - cone which is Euclidean everywhere outside of the (n-2) d subset r = 0. This is just the n d Regge block.

Regge [95] considered the approximation of the Hilbert action,

$$I_H = \frac{1}{16\pi} \int R \sqrt{-g}\, d^4x \qquad (3.2)$$

over a lattice composed of 4 d Regge blocks. Since the curvature R has support only on the 2 d bones (areas) we do not expect the 3 and 4 d blocks to contribute to the integral. The discrete analogue of (3.2) is found to be

$$I_R = \frac{1}{8\pi} \sum_n A_n \varepsilon_n \qquad (3.3)$$

where A_n is the magnitude of the area of a bone n, ε_n is the deficit angle associated with that bone, and the sum is over all bones n. An alternative derivation of (3.3) which considers it to be the limit of progressively 'more discrete' approximations of (3.2) is given in [96].

Since spacetime is described by a manifold with an indefinite metric we

require the Regge blocks to be Minkowskian, with Lorentz metric $\eta_{\mu\nu}$=diag(-1,1,1,1), rather than Euclidean. This means there are three types of bone:

a) Spacelike; every vector (leg) on the bone is spacelike.

b) Null; every leg on the bone is a linear combination of a null leg and a spacelike leg.

c) Timelike; there are both spacelike and timelike legs on the bone. A leg $\bar{X}$ is spacelike, null or timelike according to $\langle\bar{X},\bar{X}\rangle > 0$, $\langle\bar{X},\bar{X}\rangle = 0$, $\langle\bar{X},\bar{X}\rangle < 0$ respectively. We do not consider null bones in this thesis, for some discussion of them see [97].

Suppose the bone is timelike and is aligned to lie in the z - t plane of the Minkowski co-ordinate system (t,x,y,z) of a Regge block. A vector parallel transported on a closed path encircling the bone undergoes a rotation equal to the bone's deficit angle ε in a direction perpendicular to the bone, that is, in the x - y plane. This is just the Lorentz transformation corresponding to a rotation of angle ε in the x - y plane. We conclude that the deficit angle of a timelike bone is real. Similarly we can consider a spacelike bone lying in the x - y plane. A vector parallel transported on a path encircling this bone undergoes a rotation in the z - t plane equal to the deficit angle. Again this is a Lorentz transformation, but this time it corresponds to a velocity boost in the z-direction. The vector has rotated through an imaginary angle, and thus the deficit angle of a spacelike bone is imaginary.

The above considerations motivate the following conventions adopted in this thesis (see also Appendix I):

a) The magnitude of a spacelike leg is real while that of a timelike leg is imaginary and is written as $|\langle\bar{X},\bar{X}\rangle|^{1/2} = iX$.

b) The area of a general bone formed by two legs $\bar{X}$ and $\bar{Y}$ may be written as

$$A_{[X:Y]} = \left(\langle\bar{X},\bar{X}\rangle\langle\bar{Y},\bar{Y}\rangle - \langle\bar{X},\bar{Y}\rangle^2\right)^{1/2} \qquad (3.4)$$

so that

i) a timelike bone has imaginary area and real deficit,

ii) a spacelike bone has real area and imaginary deficit.

In the usual continuum theory Einstein's equations in a vacuum can be obtained by varying (3.2) with respect to the metric components $g_{\mu\nu}$. For RC the legs of the lattice effectively define a metric since they give proper distances, and we expect that by varying (3.3) with respect to the magnitudes of the legs (l_p, p = 1, 2, 3...) we would obtain the vacuum Regge - Einstein equations. Carrying out this procedure gives, from (3.3)

$$\frac{\partial I_R}{\partial l_p} = \sum_n \frac{\partial A_n}{\partial l_p} \varepsilon_n + \sum_n A_n \frac{\partial \varepsilon_n}{\partial l_p} = 0. \qquad (3.5)$$

If there is no contribution to (3.5) from the lattice boundary then the last term vanishes (this is proved for positive definite metrics in [95] and extended to indefinite metrics in [97]), however if a leg at the boundary is held fixed the vanishing of this term may not be complete and boundary contributions of the type discussed by Hartle and Sorkin [98] need to be considered. In this work no such boundary terms arise. Then we have

$$\sum_n \frac{\partial A_n}{\partial l_p} \varepsilon_n = 0 \qquad (3.6)$$

which are the Regge - Einstein equations for vacuum spacetimes. Normally (3.6) is a coupled system of non-linear algebraic equations to be solved for the leg lengths l_p.

This completes the introduction to RC and its application to GR at the basic level. RC provides an elegant and natural discretization of spacetime. This feature makes it particularly attractive for the quantization of gravity program and recently a large number of papers [99] have appeared on the subject.

We do not discuss the application of RC to quantum gravity, neither do we consider the mathematical and topological aspects of piecewise flat manifolds [100]. Our task is to construct classical, physical spacetimes from Regge blocks. In the next section we describe some previous attempts, pointing out limitations and problems of the methods. We then go on to describe a new formulation of RC, due to Porter [101], which circumvents many of these problems. Finally, in the last chapter, a perfect fluid matter field is coupled to the Regge lattice and the resulting formalism applied to the general relativistic collapse of spherically symmetric stellar cores.

3.2 Previous Applications:

Applications, prior to [101], of RC to classical spacetimes can be divided into two groups; the Williams approach and the Sorkin approach.

The Sorkin approach [97], [102] closely follows the original idea of Regge in that the n d Regge blocks are taken to be n d simplices. An n d simplex is the n^{th} member of the sequence {line, triangle, tetrahedron...} and is characterized by the fact that it is defined by its edge lengths alone. This would seem to be a good choice; the ten legs of the 4 d simplex could be identified with the ten components of the metric tensor. Also simple formulae exist for the volume and other properties of simplices ([103] has a useful list). However Sorkin's study of $\mathbb{R}^4$ and $S^3 \times \mathbb{R}$ simplectic nets indicated problems for general topologies. For the initial value problem one should study the resulting net very carefully in order to discover which legs are constrained and which legs one is free to specify. In any case the number of initial value equations is very large, being around seventeen for each vertex. Clearly this is prohibitive even for a numerical solution. No solutions to the Regge - Einstein

equations were given by Sorkin.

In contrast the Williams approach has produced numerical results. Following a suggestion by Wheeler [7], Collins and Williams [104] modelled a dust filled, closed Friedmann universe using lattices of 5, 16 and 600 regular tetrahedra each containing an equal amount of matter. They construct, for example, the 5 tetrahedra universe as follows:

Take a regular tetrahedron of edge length l and arbitrarily call it the central one. On each face place a second identical tetrahedron. Now close the universe by identifying triangular faces which meet along a common edge length. This can be done only for lattices of 5, 16 or 600 tetrahedra.

The 4 d Regge block produced by extending the tetrahedra in time is shown in fig 3.2(a). Areas and deficits are calculated by defining in this block a cartesian co-ordinate system (x,y,z,it). Since all the blocks are equal these calculations are straightforward. For the deficit one first finds the dihedral angles θ_{ij} between adjacent 3-volumes hinging on a bone using

$$\cos\theta_{ij} = \bar{n}_i \cdot \bar{n}_j \qquad (3.7)$$

where $\bar{n}_i$, $\bar{n}_j$ are the unit normals to the i^{th} and j^{th} 3-volumes respectively. The deficit angle is then given by (3.1) with dihedral angles replacing vertex angles.

Collins and Williams considered only the variation of the timelike leg, and then took the limit of the resulting algebraic Regge - Einstein equation as this leg length approached zero. In this way they obtained a first order ordinary differential equation relating l and its time derivative $\dot{l}$ which was integrated numerically. Clearly $\dot{l}$ governs the dynamics. If U is the volume of the universe and $\dot{U}$ its time derivative then we may write

$$U = \frac{n\, l^3}{6\sqrt{2}} \qquad n = 5,\ 16,\ 600 \qquad (3.8)$$

(a)

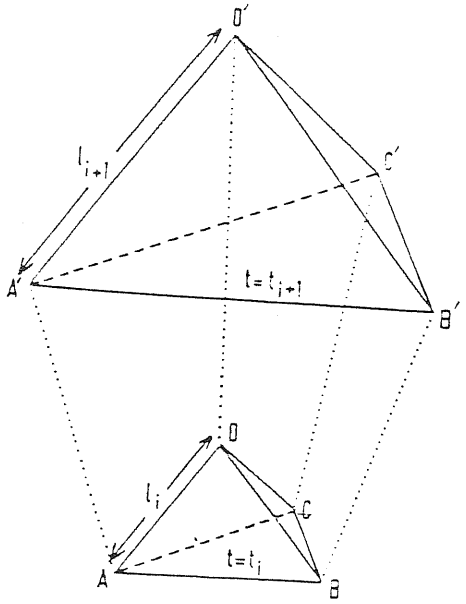

(b)

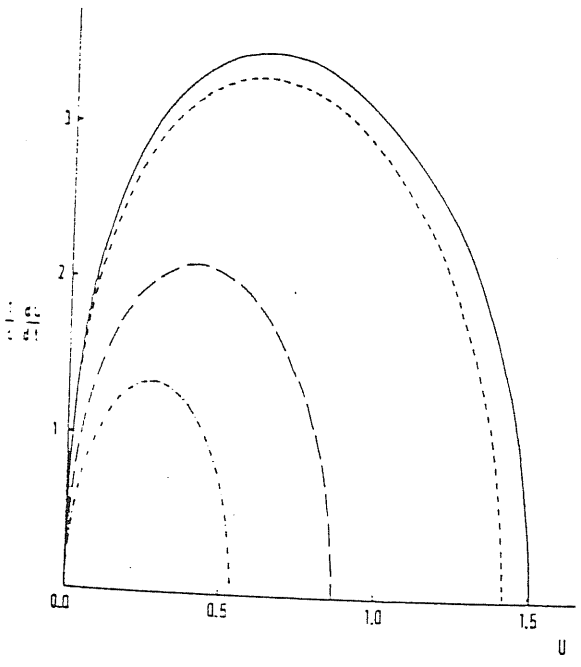

Fig. 3.2 (a) Diagram illustrating a 4-dimensional block.
(b) Rate of change of volume of the universe vs volume, analytic solution ——— , 600 tetrahedra - - - - , 16 tetrahedra — — — — , 5 tetrahedra - · - · - · - . From ref. [104].

$$\dot{U} = \frac{n l^2 \dot{l}}{2\sqrt{2}} \qquad (3.9)$$

Fig. 3.2(b) shows a plot of $\dot{U}$ verses U and compares the Regge results with the analytic solution. We see that the form of the analytic solution is followed in all cases, but only for n = 600 is there reasonable quantitative agreement.

Work along similar lines has been produced. Collins and Williams [105] give results for a 600 tetrahedra model of the Tolman universe, a closed universe containing blackbody radiation. Again there was only reasonable quantitative agreement with the analytic solution. An improvement in accuracy for the n = 600 model was obtained by Brewin [106] who by relaxing the spherical symmetry requirement sub-divided each tetrahedron into twelve smaller tetrahedra thus producing a 7200 tetrahedra universe.

Closed cosmologies which are homogeneous but anisotropic have been considered by Conners [107] and Lewis [108]. Both have used rectangular blocks rather than tetrahedra, with closure being obtained by identifying points on opposite faces of the block. We note in this case the topology is the 3-torus $T^3 = S^1 \times S^1 \times S^1$. Conner's approach differed slightly in that he used differential timelike legs from the outset rather than taking the limit at a later stage. The general qualitative behaviour of the models followed that of the analytic solutions except near the singularity where the Regge universes collapse to a non-zero minimum volume.

Other work in RC concerns the initial value problem. In this case the Regge blocks are 3 d and the 1 d edge lengths carry the curvature. For an initial spatial hypersurface of time-symmetry the relevant Regge equation is [7]

$$\frac{\sum_n l_n \varepsilon_n}{\text{'volume per vertex'}} + \text{matter terms} = 0 \qquad (3.10)$$

where l_n is the magnitude of the edge length, ε_n its associated deficit and 'volume per vertex' is the unique 3-volume associated with the vertex. (3.10) is just the Regge analogue of the time-symmetric Hamiltonian constaint equation.

Wong [109] (see also [7]) solved appropriate versions of (3.10) to costruct Schwarzschild and Reissner - Nordstrom spacetimes at the moment of time-symmetry. Of particular interest are the Regge blocks used. First the spherical surfaces were approximated by a collection of icosahedra (see fig. 3.3(a)). An icosahedron is chosen because each of its twelve vertices and thirty edge lengths are identical. The detailed breakdown of the space between successive surfaces is given in [7]. Breifly the space is divided into twenty triangular prisms with the edge length along the prism being the radial proper distance between the two surfaces. The Regge equation (3.10) then gives the dimensions of successive icosahedra in terms of the preceeding two for some given radial proper distance step. In comparison with the analytic solution (by equating 'spherical' surface areas) both spacetimes were approximated to an error of $\lesssim 10\%$.

Wong then repeated the calculations but this time he used the so called 'continuum block'. This block is of great interest to us and will be described in detail in chapter four. To construct this block a spherical surface of proper area $4\pi r^2$ is divided into surface area elements of the type shown in fig. 3.4. Elements are then joined by radial legs of equal length. In the limit of $\Delta\theta, \Delta\phi \to 0$ the spherical surfaces are approximated exactly and the Regge approximation is in the radial direction only. As we would have expected this block gave more accurate results than the icosahedra, with errors of $\lesssim 1\%$.

An axi-symmetric initial value problem was considered by Collins and Williams [110]. This application of RC is interesting because they used two types of Regge block to approximate the space. Fig. 3.5 shows details of the blocks and the axi-symmetric shells constructed from them. The use of different

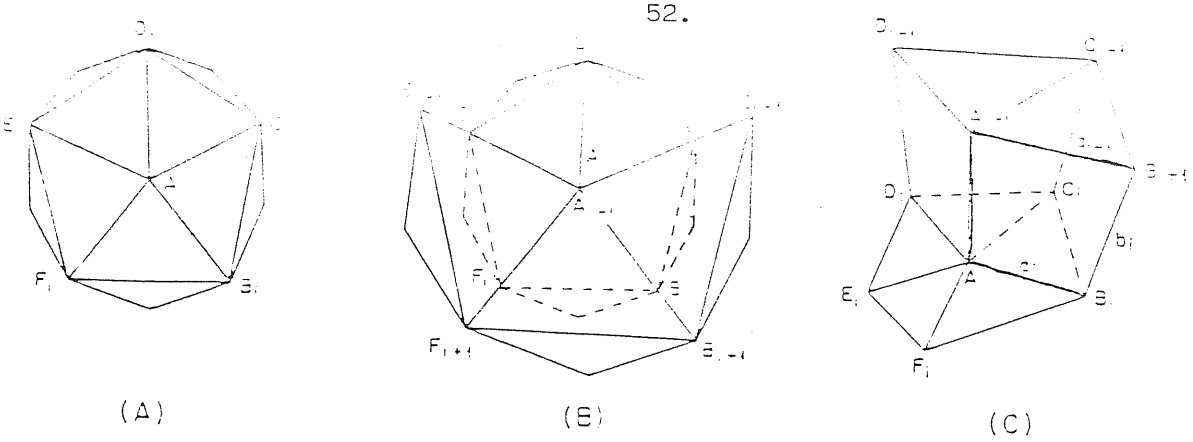

Fig. 3.3 Decomposition of 3-geometry by the icosahedral method.
From ref. [109].

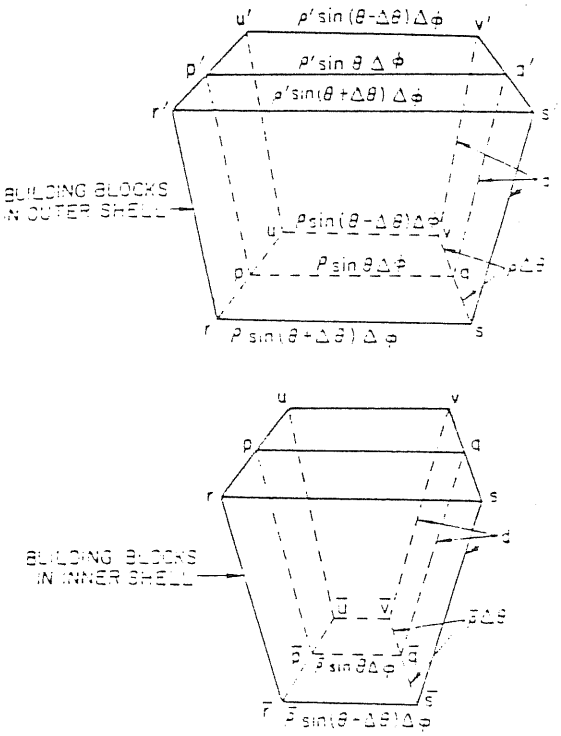

Fig. 3.4 In the continuum method the 3-dimensional space between one spherical surface and the next is broken up into building blocks such as pqrs p'q'r's'.
From ref. [109].

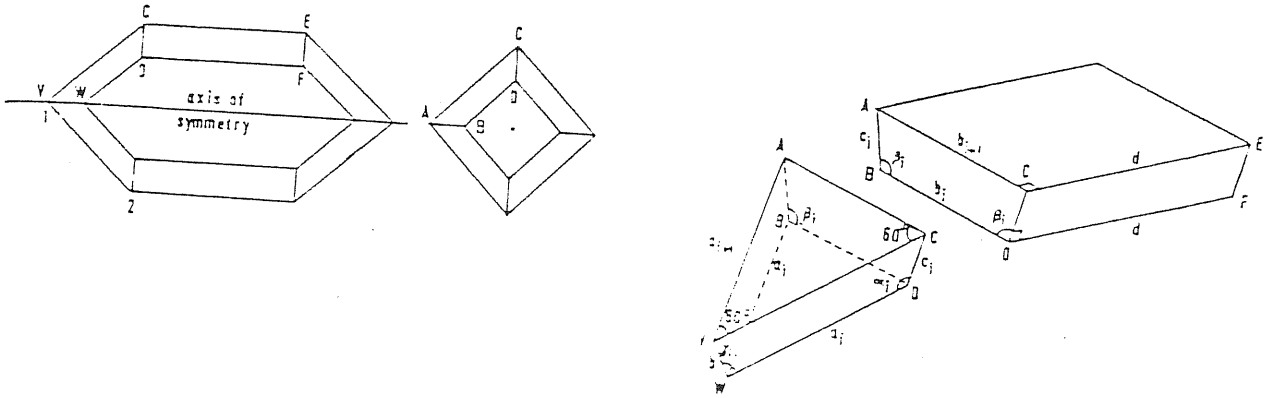

Fig. 3.5 The basic shell used for the single throat geometry and the details of the blocks used to construct this shell.
From ref. [110].

shaped blocks will be essential for approximating accurately spacetimes with little or no symmetry. In this case there will be a Regge equation for each different type of vertex; one picks a particular vertex and sums over the relevant quantities (bones in (3.3), legs in (3.10)) attached to it. Rather coarse blocks were used by Collins and Williams since they were testing the method. The solution corresponded to two asymptotically flat regions joined by a non-spherical throat. A geometry containing two throats was also considered.

Recently Williams [111] has looked again at her tetrahedra universe models. The approach has been generalized to handle homogeneous, anisotropic universes although as yet only the time-symmetric initial value problem has been solved. In this case each length of the tetrahedron may be different. Care in then required to ensure closure, and in fact only four types of closed anisotropic universe were found to exist, one with 5 tetrahedra, one with 16 and two with 600. Of these four only the two 600 tetrahedra models have a hypersurface of time-symmetry, ie. satisfy (3.10). One is similar to the Taub universe although the anisotropy behaviour differs by $\sim$20%, the other was reported to have no analytic analogue. The method does not seem to offer any advantages over the simpler rectangular blocks of Conners and Lewis.

Lastly we review some work that is not directly relevant to the theme of this thesis, ie. the construction of spacetime by computers, but is nevertheless interesting. Once a spacetime has been constructed one would like to know its properties. One approach is to study the behaviour of test particles and null geodesics in the spacetime. To this end Williams and Ellis [112], [113] have developed a formalism to trace geodesics in RC constructed spactimes. Of course in the flat Regge blocks the geodesics are straight lines, but at the boundaries between blocks they are refracted according to an extremal distance law found by considering the transformations of a co-ordinate system from block to block. The formalism was tested on a Schwarzschild spacetime of the type

constructed by Wong (using continuum blocks) and attempts were made to reproduce the classic results of GR, including perihelon precession, light bending and Thomas precession. Unfortunately in all cases they found that some thousands of Regge blocks were required for convergence to the analytic results, and even then general orbits were not well represented. This type of formalism could be very useful to us in our collapse calculations. In particular it could be used to locate apparent horizons in much the same way as Sasaki et al [49] did. However we feel that significant improvements should be made before it can be used for this purpose.

RC has modelled simple dust or radiation filled, closed, homogeneous cosmologies with moderate success. We would like to apply it to stellar collapse. This is a much more difficult problem; not only is the spacetime inhomogeneous but it also contains matter with non-zero pressure. A new approach to RC is required to deal with inhomogeneous spacetimes since the limiting procedure of the Williams approach cannot be used. This is because each vertex is now different, representing different observers over the spatial hypersurface. Porter [101] has developed this new approach and we describe it in the next section.

As regards the accuracy of RC predictions, we emphasise that the Regge - Einstein equations (3.6) are exact for the discrete topology on which they are solved and that it is this discrete topology which is the approximation. For comparison with analytic results, obtained from smooth manifolds, we should approximate the smooth topology as closely as possible. It has recently been shown [114] that the Regge action does indeed converge to the Hilbert action in the limit of block dimensions going to zero. Thus for our spherical collapse we will use the continuum block of Wong.

3.3 (3+1) Regge Calculus:

In the Hamiltonian (3+1) formulation of GR described in chapter two the timelike direction was singled out and the spacetime foliated with spatial hypersurfaces which were constant surfaces of a scalar function t related to time.

Similarly Porter singles out the timelike direction in the Regge block and foliates the spacetime with discrete spatial hypersurfaces constructed from 3 d blocks, each of which is Euclidean. However this foliation is not continuous since time is taken to be a discrete parameter. The corresponding vertices of the 3 d blocks in adjacent hypersurfaces are joined by timelike legs whose lengths are always finite; no limiting procedure is taken. Note that, unlike the Williams approach, the timelike leg lengths at each vertex may be different. Fig. 3.6 shows the general Regge block produced. Since we are to evolve the spatial leg lengths it is useful to take tetrahedra for the construction of the spatial hypersurfaces when the spacetime has no special symmetry.

This block has eight triangular areas, four of which lie in the α^{th} hypersurface and four in the $(\alpha+1)^{th}$ hypersurface, and six timelike areas (see fig. 3.6) each of which corresponds to the time evolution of a spatial leg. In addition there are twelve boost angles γ and in general one spatial leg has two associated boost angles. The faces of the block are formed by six 3 d volumes, two spatial being the upper and lower tetrahedra, and four timelike (again see fig 3.6). From simple geometric considerations we see that if the spacetime upto the α^{th} slice is specified, either from previous evolutions or the initial value problem, then a knowledge of the timelike leg lengths and the boost angles is sufficient to determine the $(\alpha+1)^{th}$ hypersurface. The system has then evolved.

The choice of the timelike leg lengths is arbitrary and corresponds in

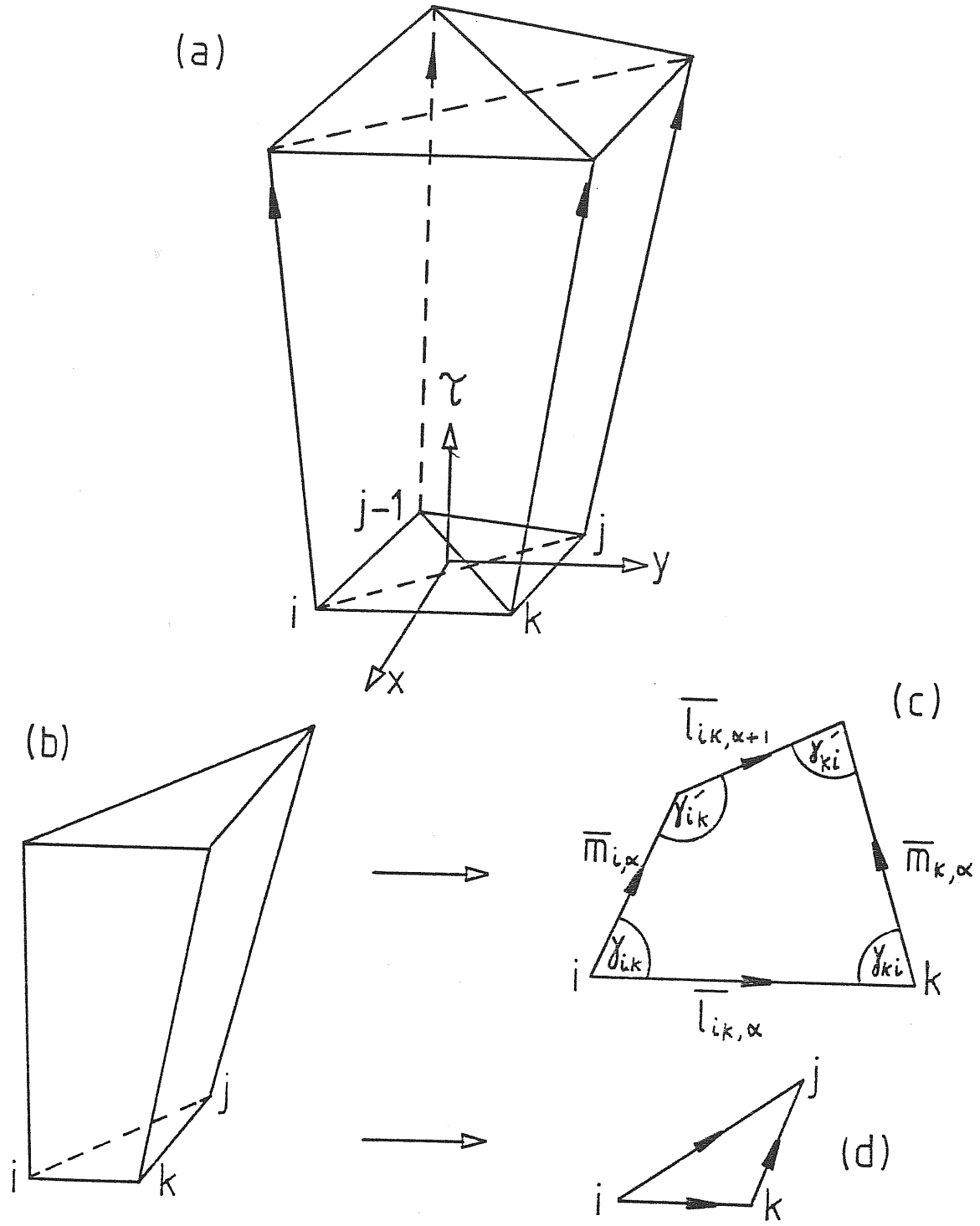

Fig. 3.6 (a) General Regge block consisting of a tetrahedron extended in time. (b) A 3-dimensional time-like face of the block. (c) A typical time-like area. (d) A spacelike area.

the continuum theory to the choice of the lapse. For the boost angles Porter has shown that the equations produced by varying the Regge action (3.3) with respect to each spatial leg length are sufficient to determine these unknowns. We do not repeat this lengthy proof but instead refer the interested reader to [101].

Intuitively such a result would be expected since in the continuum case the equations produced by varying the Hilbert action with respect to the components of the spatial metric γ_{IJ} are sufficient to evolve these components. Variation with respect to the conjugate momenta, related to the extrinsic curvature components K_{IJ}, simply gives their definition. We then have the (3+1) system of equations. This Regge formalism has many similarities with the continuum (3+1) approach. For various reasons the boost angles are adopted as the conjugate momenta to the leg lengths. We do not vary with respect to the angles, instead the legs are evolved from a knowledge of the angles using the vector sum, eg. for the timelike area of fig. 3.6,

$$\bar{l}_{ik,\alpha+1} = \bar{l}_{ik,\alpha} + \bar{m}_{k,\alpha} - \bar{m}_{i,\alpha} \qquad (3.11)$$

from which the leg length $l_{ik,\alpha+1}$ is easily found. This effectively corresponds to the continuum expression

$$K_{IJ} = -\frac{1}{2\alpha}\frac{\partial \gamma_{IJ}}{\partial t} \qquad (3.12)$$

(assuming no shift), and it is by comparison of specific instances of (3.11) and (3.12) that one is led to take the angles as the conjugate variables. This point is considered again in the next chapter.

There is a novel feature of the formalism which we now discuss. It appears we need twelve equations to solve for the twelve boost angles, but

only six spatial legs are given. Thus the variation with respect to each spatial leg should give rise to two equations. This is not unreasonable. The Regge prescription says that one should pick a particular vertex and sum over all bones attached to it. This action is then varied with respect to all legs attached to the vertex. Since each leg joins two vertices it will be varied twice. However quantities such as deficit angles etc. should be evaluated in terms of legs and boost angles etc. at the vertex in question. This produces the two equations.

We now check the compatability of the two equations with the requirement that the Regge block be flat. Consider the case when N spatial tetrahedra hinge on the leg $\bar{l}_{i\kappa,\alpha}$ (see fig. 3.7). At vertex i,α the equation obtained by variation with resect to $l_{i\kappa,\alpha}$ is

$$\frac{\partial I_R}{\partial l_{i\kappa,\alpha}}\bigg|_{i,\alpha} = \sum_{j=1}^{N} \frac{\partial A_{i\kappa j,\alpha}}{\partial l_{i\kappa,\alpha}} \varepsilon_{i\kappa j,\alpha} + \frac{\partial A_{i\kappa,\alpha-1}}{\partial l_{i\kappa,\alpha}} \varepsilon_{i\kappa,\alpha-1} + \frac{\partial A_{i\kappa,\alpha}}{\partial l_{i\kappa,\alpha}} \varepsilon_{i\kappa,\alpha} = 0 \quad (3.13)$$

while that at k,α is

$$\frac{\partial I_R}{\partial l_{i\kappa,\alpha}}\bigg|_{\kappa,\alpha} = \sum_{j=1}^{N} \frac{\partial A_{\kappa ji,\alpha}}{\partial l_{i\kappa,\alpha}} \varepsilon_{\kappa ji,\alpha} + \frac{\partial A_{\kappa i,\alpha-1}}{\partial l_{i\kappa,\alpha}} \varepsilon_{\kappa i,\alpha-1} + \frac{\partial A_{\kappa i,\alpha}}{\partial l_{i\kappa,\kappa}} \varepsilon_{\kappa i,\alpha} = 0. \quad (3.14)$$

For (3.13) and (3.14) to be compatable we require

$$\frac{\partial I_R}{\partial l_{i\kappa,\alpha}}\bigg|_{i,\alpha} - \frac{\partial I_R}{\partial l_{i\kappa,\kappa}}\bigg|_{\kappa,\alpha} = 0. \quad (3.15)$$

Consider now an observer momentarily at rest in the j^{th} tetrahedron. This 'block observer' sets up a Minkowski co-ordinate system (τ, x, y, z) such that the tetrahedron lies in a τ = constant hypersurface, and the situation is as shown previously in fig. 3.6. We note that in general the j^{th} tetrahedra of the $(\alpha-1)^{th}$ and $(\alpha+1)^{th}$ hypersurfaces will not lie in a τ = constant hypersurface.

The areas and normals may be calculated in terms of this co-ordinate system giving

$$\frac{\partial A_{i\kappa j,\alpha}}{\partial l_{i\kappa,\alpha}} = \frac{\partial A_{\kappa j i,\alpha}}{\partial l_{i\kappa,\alpha}} \tag{3.16}$$

since the triangular area $A_{i\kappa j,\alpha}$ is invariant about permutations of the vertices ijk. The typical timelike area may be written as

$$A_{i\kappa,\alpha} = \tfrac{1}{4}\left(im_{i,\alpha}\, l_{i\kappa,\alpha} \sin\gamma_{i\kappa} + im_{\kappa,\alpha}\, l_{i\kappa,\alpha} \sin\gamma_{\kappa i} + im_{i,\alpha}\, l_{i\kappa,\alpha+1} \sin\gamma'_{i\kappa} + im_{\kappa,\alpha}\, l_{i\kappa,\alpha+1} \sin\gamma'_{\kappa i}\right) \tag{3.17}$$

which is symmetric about ik, giving

$$\frac{\partial A_{i\kappa,\alpha}}{\partial l_{i\kappa,\alpha}} = \frac{\partial A_{\kappa i,\alpha}}{\partial l_{i\kappa,\alpha}}\,, \tag{3.18}$$

similarly for $A_{i\kappa,\alpha-1}$. Compatability then requires

$$\begin{aligned} \varepsilon_{i\kappa j,\alpha} &= \varepsilon_{\kappa j i,\alpha} \\ \varepsilon_{i\kappa,\alpha} &= \varepsilon_{\kappa i,\alpha} \\ \varepsilon_{i\kappa,\alpha-1} &= \varepsilon_{\kappa i,\alpha-1} \end{aligned} \tag{3.19}$$

For convenience we concentrate on the first condition. As usual the deficit angle of a bone is found by first caculating the unit normals to the 3-volumes having this bone in common, the dihedral angles between adjacent 3-volumes are then found and we find the deficit from (3.1). For $\varepsilon_{i\kappa j,\alpha}$ one such 3-volume is formed by legs $\bar{l}_{ij,\alpha}$, $\bar{l}_{i\kappa,\alpha}$ and $\bar{m}_{i,\alpha}$ at vertex i, α. We denote its unit 1-form normal by

$$\tilde{n}(\bar{l}_{i\kappa,\alpha} : \bar{l}_{ij,\alpha} : \bar{m}_{i,\alpha}) = \frac{\tilde{\Sigma}(\bar{l}_{i\kappa,\alpha} : \bar{l}_{ij,\alpha} : \bar{m}_{i,\alpha})}{|\tilde{\Sigma}|} \tag{3.20}$$

where the volume 1-form is given by

$$\Sigma_\Lambda = \varepsilon_{\Lambda\Gamma\Delta\Omega}\, l^{\Gamma}_{iK,\alpha}\, l^{\Delta}_{ij,\alpha}\, m^{\Omega}_{i,\alpha} \qquad (3.21)$$

and $\varepsilon_{\Lambda\Gamma\Delta\Omega}$ is the totally anti-symmetric Levi - Civita tensor.

The evaluation of the deficit $\varepsilon_{Kji,\alpha}$ requires the unit 1-form normal to the same timelike 3-volume but this time formed by legs $\bar{l}_{iK,\alpha}$, $\bar{l}_{Kj,\alpha}$, $\bar{m}_{K,\alpha}$ at vertex k,α. We have

$$\tilde{n}\left(\bar{l}_{iK,\alpha} : \bar{l}_{Kj,\alpha} : \bar{m}_{K,\alpha}\right) = \frac{\tilde{\Sigma}\left(\bar{l}_{iK,\alpha} : \bar{l}_{Kj,\alpha} : \bar{m}_{K,\alpha}\right)}{|\tilde{\Sigma}|} \,. \qquad (3.22)$$

If the Regge block is to be flat then its 3 d faces should also be flat, implying a unique normal for each face regardless of which legs are used to evaluate it, ie.

$$\tilde{n}\left(\bar{l}_{iK,\alpha} : \bar{l}_{ij,\alpha} : \bar{m}_{i,\alpha}\right) = \tilde{n}\left(\bar{l}_{iK,\alpha} : \bar{l}_{Kj,\alpha} : \bar{m}_{K,\alpha}\right). \qquad (3.23)$$

Applying a similar argument to the other 3 d volumes we see that the compatability requirement $\varepsilon_{iKj,\alpha} = \varepsilon_{Kji,\alpha}$ is a geometrical constraint that the Regge block should not 'twist'†. The solution of equations (3.13) and (3.14) together imply this constraint, and we may use (3.23) to acertain the accuracy to which the block remains flat during an evolution of the spacetime. Alternatively one may apply to (3.13) identities of the type (3.23) and obtain (3.14) or vice-versa.

To begin an evolution one must first construct an initial spacetime 'sandwich'. Again the continuum theory provides the guidelines. The four constraint equations may be obtained by varying the Hilbert action with respect

† In particular (3.23) constrains the block from twisting about a timelike axis. Such a degree of freedom is unphysical and corresponds to a rotation ot the triad (x,y,z) by an observer who does not Fermi - Walker propagate his tetrad frame [115].

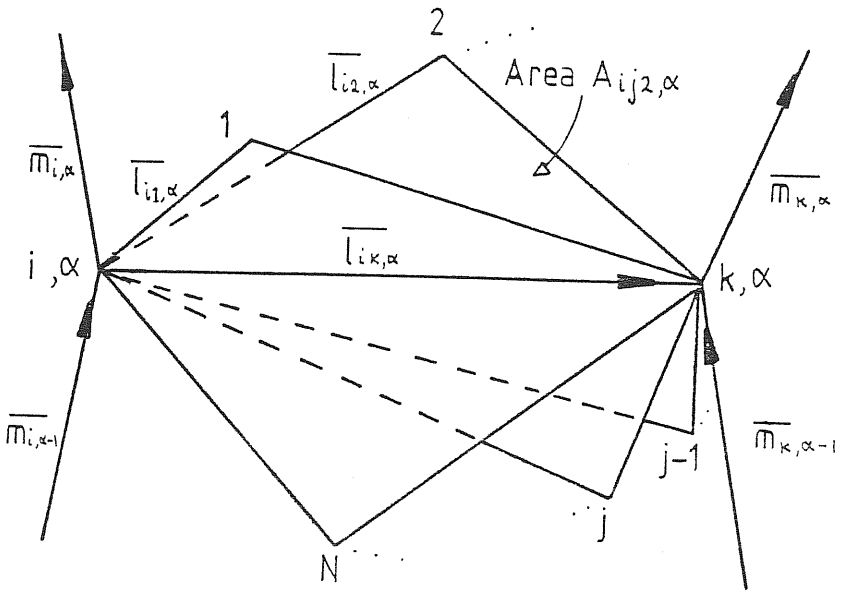

Fig. 3.7 Areas having leg $l_{iK,\alpha}$ in common.

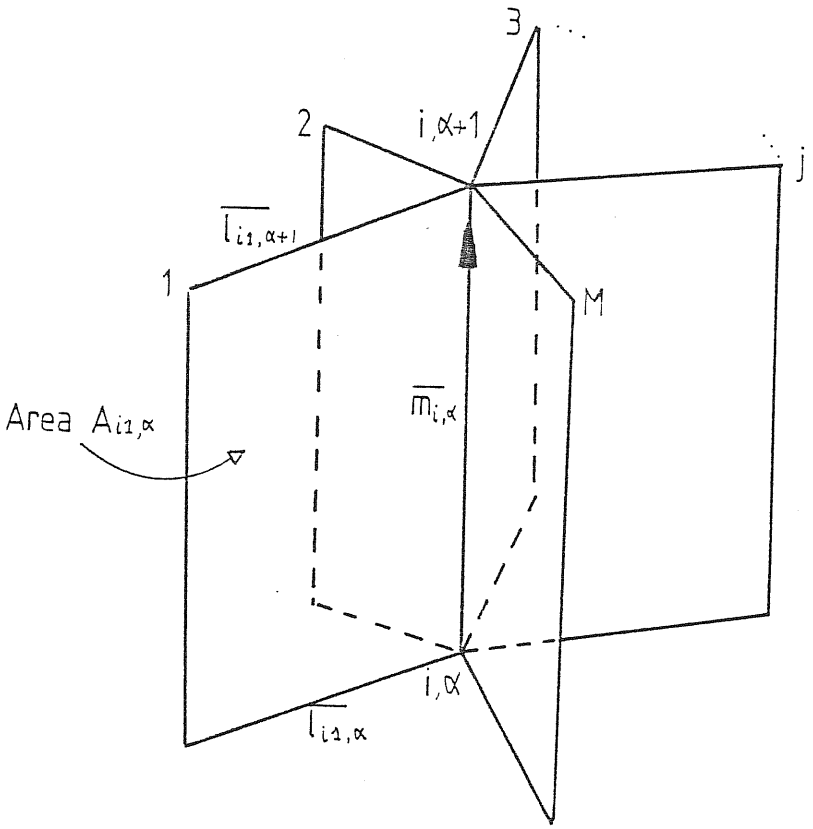

Fig. 3.8 Areas having leg $m_{i,\alpha}$ in common.

to the lapse α (Hamiltonian constraint) and the shift vector components β^I (momentum constraints). Thus we expect the variation of the Regge action with respect to the timelike leg lengths to give the analogue of the Hamiltonian constraint, and in practise this is the case. If M spatial legs meet at vertex i,α then fig. 3.8 shows the situation. Variation with respect to the magnitude of the timelike leg $\overline{m}_{i,\alpha}$ gives the constraint equation

$$\frac{\partial I_R}{\partial(im_{i,\alpha})}\bigg|_{i,\alpha} = \sum_{j=1}^{M} \frac{\partial A_{ij,\alpha}}{\partial(im_{i,\alpha})} \varepsilon_{ij,\alpha} = 0 \qquad (3.24)$$

Unlike the evolution equations, (3.13) and (3.14), this involves quantities between the α^{th} and $(\alpha+1)^{th}$ hypersurfaces only.

The shift components are not so easily found; as described later they are related to angles rather than legs. In our application of RC to stellar collapse we avoid the problem of the missing momentum constraint equations by starting from a hypersurface of time-symmetry, although a solution to the problem is currently being sought.

As referred to above we view the initial data as a spacetime sandwich since it is not yet clear how to incorporate York's conformal approach to the initial value problem into RC. There are two types of sandwich, the 'thin sandwich' where the spatial metric and its time derivative are given on an initial hypersurface, and the 'thick sandwich' where the spatial metric is given on adjacent hypersurfaces. The correspondence with (3+1) RC is clear. The thin sandwich is a specification of the spatial leg lengths and the boost angles, subject not only to the usual constraint equations but also to the no twist constraints (3.23) while the thick sandwich is a specification of the spatial leg lengths on adjacent hypersurfaces. In fact because of equations (3.11) the two are identical.

3.4 The Kinematics of Regge Spacetime:

The choice of observers who describe the numerically constructed spacetime is, as was discussed, a choice of lapse and shift. This gauge freedom is present in (3+1) RC. The timelike leg lengths determine the proper time between adjacent hypersurfaces while the freedom of the Regge block to 'lean' in three independent directions corresponds to the shift freedom. If the block does lean then the top tetrahedron of fig. 3.6 is displaced relative to the lower one, with the boost angles changing to accommodate the shift. We expect therefore that the applied shift will be related to the values of the boost angles.

In practical calculations it is more convenient to use the components of the timelike legs rather than the boost angles. The block observer of the previous section at rest in the j^{th} tetrahedron measures the components of the spatial legs at vertex i,α as

$$\begin{aligned} \bar{l}_{ik,\alpha} &= (0, l^x_{ik,\alpha}, l^y_{ik,\alpha}, l^z_{ik,\alpha}) \\ \bar{l}_{ij,\alpha} &= (0, l^x_{ij,\alpha}, l^y_{ij,\alpha}, l^z_{ij,\alpha}) \\ \bar{l}_{ij-1,\alpha} &= (0, l^x_{ij-1,\alpha}, l^y_{ij-1,\alpha}, l^z_{ij-1,\alpha}) \end{aligned} \qquad (3.25)$$

and the components of the timelike leg at i,α as

$$\bar{m}_{i,\alpha} = m_{i,\alpha}(\sinh A_{i,\alpha}, \sinh X_{i,\alpha}, \sinh Y_{i,\alpha}, \sinh Z_{i,\alpha}) \qquad (3.26)$$

say, with normalization

$$-\sinh^2 A_{i,\alpha} + \sinh^2 X_{i,\alpha} + \sinh^2 Y_{i,\alpha} + \sinh^2 Z_{i,\alpha} = -1. \qquad (3.27)$$

The boost angle γ_{ik} between legs $\bar{m}_{i,\alpha}$ and $\bar{l}_{ik,\alpha}$ is given by

$$\cos\gamma_{ik} = \frac{\langle \bar{m}_{i,\alpha} , \bar{l}_{ik,\alpha} \rangle}{i m_{i,\alpha} l_{ik,\alpha}} \tag{3.28}$$

with similar results for γ_{ij}, γ_{ij-1} giving

$$-i \begin{pmatrix} \sinh X_{i,\alpha} \\ \sinh Y_{i,\alpha} \\ \sinh Z_{i,\alpha} \end{pmatrix} = \begin{pmatrix} l^{x}_{ik,\alpha} & l^{y}_{ik,\alpha} & l^{z}_{ik,\alpha} \\ l^{x}_{ij,\alpha} & l^{y}_{ij,\alpha} & l^{z}_{ij,\alpha} \\ l^{x}_{ij-1,\alpha} & l^{y}_{ij-1,\alpha} & l^{z}_{ij-1,\alpha} \end{pmatrix}^{-1} \begin{pmatrix} \cos\gamma_{ik} \\ \cos\gamma_{ij} \\ \cos\gamma_{ij-1} \end{pmatrix} \tag{3.29}$$

and thus we may adopt the spatial components of the timelike leg as the fundamental unknowns.

The block observer is related to an Eulerian observer at i,α moving normal to the spatial hypersurfaces along the vector

$$\bar{n} = (m_{i,\alpha} , 0 , 0 , 0) \tag{3.30}$$

by the Lorentz transformation

$$\hat{m}_{i,\alpha} = \hat{\Lambda}_{r'} n^{r'} \tag{3.31}$$

ie.

$$\bar{m}_{i,\alpha} = m_{i,\alpha} (\Lambda^{0}_{0'} , \Lambda^{x}_{0'} , \Lambda^{y}_{0'} , \Lambda^{z}_{0'}) \tag{3.32}$$

and by comparison with (3.26)

$$\begin{aligned} \Lambda^{0}_{0'} &= \sinh A_{i,\alpha} \\ \Lambda^{x}_{0'} &= \sinh X_{i,\alpha} \\ \Lambda^{y}_{0'} &= \sinh Y_{i,\alpha} \\ \Lambda^{z}_{0'} &= \sinh Z_{i,\alpha} \end{aligned} \tag{3.33}$$

If a shift vector is now applied to vertex i,α the Eulerian observer is boosted to an observer moving along the vector

$$\bar{t} = (\alpha\, dt\,,\ \beta^{x} dt\,,\ \beta^{y} dt\,,\ \beta^{z} dt)\,, \tag{3.34}$$

where dt is a co-ordinate time interval and

$$-\alpha^2 dt^2 + (\beta^{x})^2 dt^2 + (\beta^{y})^2 dt^2 + (\beta^{z})^2 dt^2 = -m^2_{i,\alpha}\,, \tag{3.35}$$

and is related to the block observer by

$$\hat{m}_{i,\alpha} = \hat{\Lambda}_{r'}\, \hat{t}^{r'}. \tag{3.36}$$

For an arbitrary boost of velocity v in a direction $\bar{k} = (0,k^{x},k^{y},k^{z})$, $\langle \bar{k},\bar{k}\rangle = 1$, we have [22]

$$\begin{aligned} \Lambda^{0}_{0'} &= \gamma \\ \Lambda^{I}_{0'} &= -v\,\Lambda^{0}_{0'}\,k^{I} \\ \Lambda^{I}_{J'} &= (\Lambda^{0}_{0'} - 1)\,k^{I}k^{J} + \delta^{IJ} \end{aligned} \tag{3.37}$$

where $\gamma = (1-v^2)^{-\frac{1}{2}}$ and δ^{IJ} is the Kronecker delta. We note that the normalization condition (3.27) is a consequence of the property

$$-(\Lambda^{0}_{0'})^2 + (\Lambda^{x}_{0'})^2 + (\Lambda^{y}_{0'})^2 + (\Lambda^{z}_{0'})^2 = -1\,. \tag{3.38}$$

By substitution we may write the last equation of (3.37) as

$$\Lambda^{I}_{J'} = \frac{\Lambda^{I}_{0'}\,\Lambda^{J}_{0'}}{(\Lambda^{0}_{0'} + 1)} + \delta^{IJ}\,. \tag{3.39}$$

Further substitution of (3.39) into (3.36) gives, using (3.33)

$$m^0_{i,\alpha} = \alpha\, dt \sinh A_{i,\alpha} + \beta^x dt \sinh X_{i,\alpha} + \beta^y dt \sinh Y_{i,\alpha} + \beta^z dt \sinh Z_{i,\alpha}$$

$$m^x_{i,\alpha} = \alpha\, dt \sinh X_{i,\alpha} + \beta^x dt \left(1 + \frac{\sinh^2 X_{i,\alpha}}{1+\sinh A_{i,\alpha}}\right) + \beta^y dt \frac{\sinh X_{i,\alpha} \sinh Y_{i,\alpha}}{1+\sinh A_{i,\alpha}} \quad (3.40)$$

$$+ \beta^z dt \frac{\sinh X_{i,\alpha} \sinh Z_{i,\alpha}}{1+\sinh A_{i,\alpha}}$$

with similar expressions for $m^y_{i,\alpha}$, $m^z_{i,\alpha}$, and these are the components of the timelike leg $m_{i,\alpha}$ as measured by the block observer with a shift applied to vertex i, α .

As in the continuum case the shift vector may be chosen to simplify the Regge - Einstein equations by setting, for example, a component of $\overline{m}_{i,\alpha}$ equal to zero, or we can use it to make the co-ordinates follow matter.

4. SPHERICALLY SYMMETRIC COLLAPSE

4.1 Discretization of the Spacetime:

The formulation of RC described in section 3.3 has been extensively tested for spherically symmetric vacuum and dust filled spacetimes. Porter derived the spherical Regge -Einstein equations using both the icosahedron and continuum block approximations. He then constructed the Schwarzschild solution and the dust filled Tolman - Bondi universe [116]. Various time slicings were used for the former, some making the solution appear dynamical. Good agreement with the analytic solutions was obtained in all cases (although there was always some error growth at the centre). This showed that the formalism could handle inhomogeneous spacetimes as required, and was able to accurately reproduce analytic solutions of Einstein's equations.

Porter's work also showed that the continuum block provides a much smoother approximation to the spherical topology than the icosahedron. This is in agreement with the findings of Wong mentioned earlier. We will use the continuum block throughout this chapter.

The continuum spherically symmetric 3 - geometry in a particular spatial hypersurface t_α is approximated by a collection of spherical surfaces each of which is identified by its proper area, $A_{i,\alpha} = 4\pi r_{i,\alpha}^2$ with $A_{1,\alpha} = 0 \ \forall\alpha$ and $i = 1, 2, 3....$. Each spherical surface is then subdivided into area elements by dividing the polar angle $0 \leq \theta \leq \pi$ and the azimuthal angle $0 \leq \phi \leq 2\pi$ into equal intervals $\Delta\theta, \Delta\phi$ repectively. The corresponding area elements of successive surfaces are joined by radial legs of constant θ, ϕ, and thus we obtain, for example, the spatial block lying between surfaces $r_{i,\alpha}$ and $r_{i+1,\alpha}$ shown in fig. 4.1. The block edges $r_{i,\alpha}\Delta\theta$ and $r_{i,\alpha}\sin\theta\Delta\phi$ are chords of circles whose proper circumferences are $2\pi r_{i,\alpha}$ and $2\pi r_{i,\alpha}\sin\theta$ respectively,

and in the limit $\Delta\theta, \Delta\phi \to 0$ we have $r_{i,\alpha} \to$ Schwarzschild r co-ordinate at verex i,α .

The block is extended in time by attaching timelike legs to each vertex, and then in the resulting 4 d Regge block we establish a Minkowski co-ordinate system (τ,x,y,z) such that the 3 d block lies in a τ = costant hypersurface. Fig. 4.2 shows some of the timelike areas produced.

In this co-ordinate system we may write the legs attached to the vertex marked * in fig. 4.1 as

$$\overline{r_{i,\alpha} \sin\theta \Delta\phi} = (0, 0, r_{i,\alpha} \sin\theta \Delta\phi, 0)$$

$$\overline{r_{i,\alpha} \Delta\theta} = (0, r_{i,\alpha} s, \tfrac{1}{2} r_{i,\alpha} \Delta(\sin\theta) \Delta\phi, 0)$$

$$\overline{d_{i,\alpha}} = (0, -\frac{\Delta r_{i+1,\alpha} \Delta\Omega}{2s}, \frac{\Delta r_{i+1,\alpha}}{2} \sin\theta \Delta\phi, \kappa d_{i,\alpha}) \qquad (4.1)$$

$$\overline{m_{i,\alpha}} = m_{i,\alpha} (\sinh A^u_{i,\alpha}, -s \sinh Y_{i,\alpha}, \sin\theta \Delta\phi \sinh Y_{i,\alpha}, \sinh V^u_{i,\alpha})$$

with normalization

$$-\sinh^2 A^u_{i,\alpha} + (s^2 + \sin^2\theta \Delta\phi^2) \sinh^2 Y_{i,\alpha} + \sinh^2 V^u_{i,\alpha} = -1 \qquad (4.2)$$

where

$$s = \Delta\theta (1 - \tfrac{1}{4} \cos^2\theta \Delta\phi^2)^{\frac{1}{2}}$$

$$\Delta(\sin\theta) = \sin(\theta + \Delta\theta) - \sin\theta \approx \Delta\theta \cos\theta - \frac{\Delta\theta^2}{2} \sin\theta$$

for $\Delta\theta$ small

$$\Delta\Omega = \Delta\theta^2 + \tfrac{1}{2} \sin\theta \cos\theta \Delta\theta \Delta\phi^2 \qquad (4.3)$$

$$\Delta r_{i+1,\alpha} = r_{i+1,\alpha} - r_{i,\alpha}$$

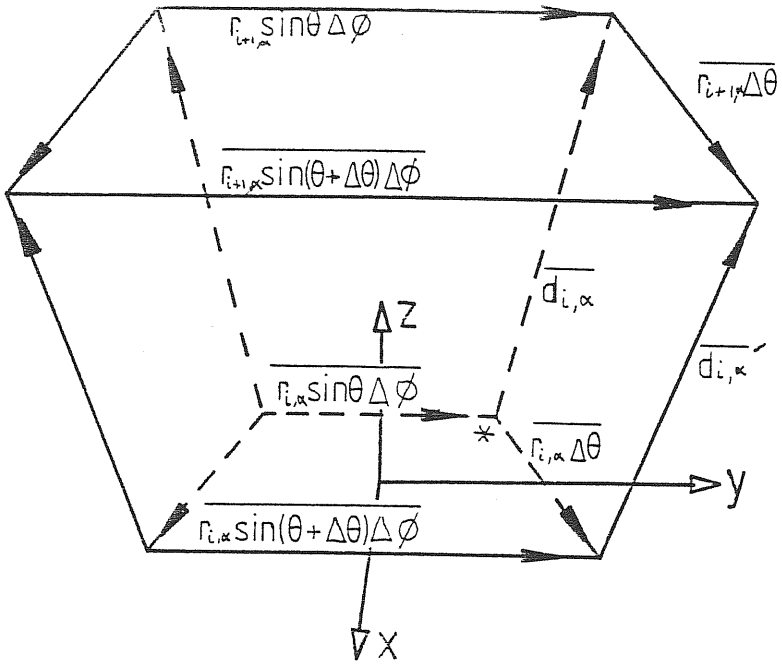

Fig. 4.1 Spatial block used for the discretization of spherically symmetric space time.

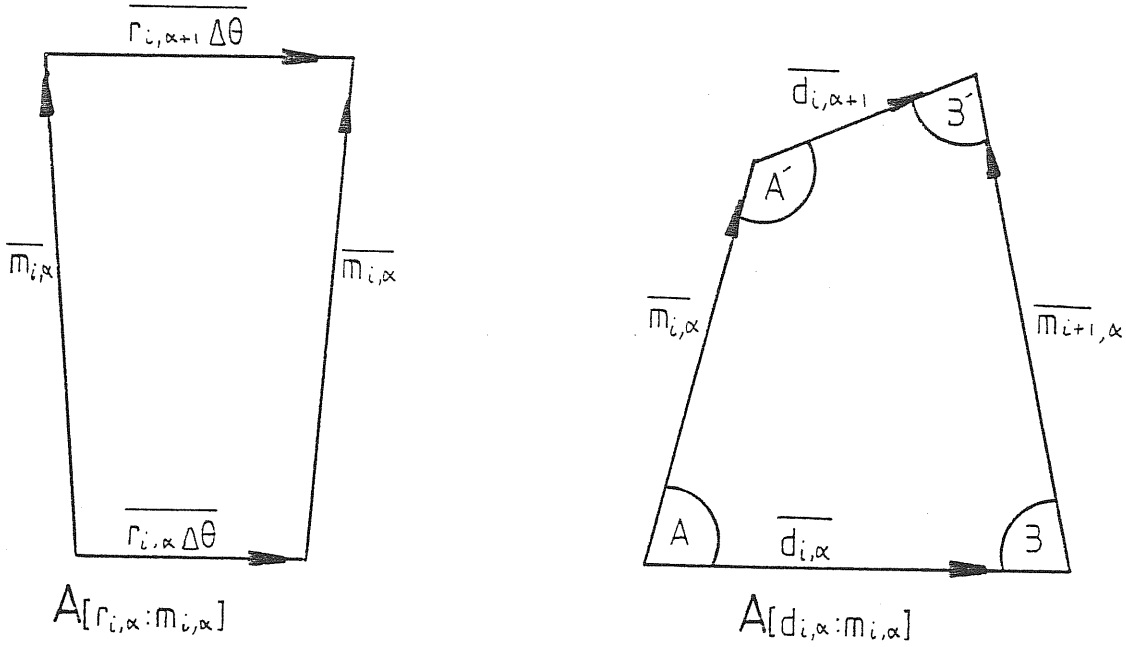

Fig. 4.2 Some of the timelike areas produced by extending the spatial block in time.

and k is a parameter such that

$$\lim_{\Delta\theta,\Delta\phi\to 0} k = 1 \tag{4.4}$$

and in practise we take k = 1 aways. In terms of the co-ordinate system in the block lying between surfaces $r_{i-1,\alpha}$ and $r_{i,\alpha}$ the above timelike leg is written as

$$\overline{m_{i,\alpha}} = m_{i,\alpha}\left(\sinh A^{L}_{i,\alpha}, -\frac{\Delta\Omega}{s}\sinh Y_{i,\alpha}, \sin\theta\Delta\phi\sinh Y_{i,\alpha}, \sinh V^{L}_{i,\alpha}\right). \tag{4.5}$$

In our continuum approximation considerable simplification is obtained by ignoring quantities of order $O(\Delta\theta^3)$ etc. and higher while still maintaining a second order accuracy.

As an example we calculate the timelike area $A_{[d_{i,\alpha}:m_{i,\alpha}]}$ shown in fig. 4.2 and its associated deficit $\varepsilon_{[d_{i,\alpha}:m_{i,\alpha}]}$. From (3.17) we may write

$$A_{[d_{i,\alpha}:m_{i,\alpha}]} = \tfrac{1}{4}\left(im_{i,\alpha}\, d_{i,\alpha}\sin A + im_{i+1,\alpha}\, d_{i,\alpha}\sin B + im_{i,\alpha}\, d_{i,\alpha+1}\sin A' + im_{i+1,\alpha}\, d_{i,\alpha+1}\sin B'\right). \tag{4.6}$$

Inspection of the timelike area $A_{[d_{i,\alpha}:m_{i,\alpha}]}$ in fig. 4.2 gives

$$\overline{d_{i,\alpha+1}} = \overline{d_{i,\alpha}} + \overline{m_{i+1,\alpha}} - \overline{m_{i,\alpha}} \tag{4.7}$$

so that

$$\begin{aligned} d_{i,\alpha+1} = \Big(& m_{i+1,\alpha}\sinh A^{L}_{i+1,\alpha} - m_{i,\alpha}\sinh A^{u}_{i,\alpha}, \\ & -m_{i+1,\alpha}\sinh Y_{i+1,\alpha}\frac{\Delta\Omega}{s} - \frac{\Delta r_{i+1,\alpha}}{2}\frac{\Delta\Omega}{s} + m_{i,\alpha}\, s\sinh Y_{i,\alpha}, \\ & \left[m_{i+1,\alpha}\sinh Y_{i+1,\alpha} + \frac{\Delta r_{i+1,\alpha}}{2} - m_{i,\alpha}\sinh Y_{i,\alpha}\right]\sin\theta\Delta\phi, \\ & m_{i+1,\alpha}\sinh V^{L}_{i+1,\alpha} + k\, d_{i,\alpha} - m_{i,\alpha}\sinh V^{u}_{i,\alpha}\Big). \end{aligned} \tag{4.8}$$

Using (4.1), (4.5) and (4.8) we find

$$\cos A = \frac{\langle \bar{m}_{i,\alpha} , \bar{d}_{i,\alpha} \rangle}{i m_{i,\alpha} d_{i,\alpha}} \approx -i \sinh V^{u}_{i,\alpha}$$

$$\cos B = -\frac{\langle \bar{m}_{i+1,\alpha} , \bar{d}_{i,\alpha} \rangle}{i m_{i+1,\alpha} d_{i,\alpha}} \approx i \sinh V^{L}_{i+1,\alpha} \qquad (4.9)$$

$$\cos A' = -\frac{\langle \bar{m}_{i,\alpha} , \bar{d}_{i,\alpha+1} \rangle}{i m_{i,\alpha} d_{i,\alpha+1}} \approx i \bar{\mu}^{u}_{i,\alpha+1}$$

$$\cos B' = \frac{\langle \bar{m}_{i+1,\alpha} , \bar{d}_{i,\alpha+1} \rangle}{i m_{i+1,\alpha} d_{i,\alpha+1}} \approx -i \bar{\mu}^{L}_{i+1,\alpha+1}$$

giving

$$A_{[d_{i,\alpha} : m_{i,\alpha}]} = \tfrac{1}{4} \left(i m_{i,\alpha} d_{i,\alpha} \cosh V^{u}_{i,\alpha} + i m_{i+1,\alpha} d_{i,\alpha} \cosh V^{L}_{i+1,\alpha} \right. \qquad (4.10)$$

$$\left. + i m_{i,\alpha} d_{i,\alpha+1} \cosh \bar{V}^{u}_{i,\alpha+1} + i m_{i+1,\alpha} d_{i,\alpha+1} \cosh \bar{V}^{L}_{i+1,\alpha+1} \right)$$

where we have introduced the definitions

$$\bar{\mu}^{u}_{i,\alpha+1} = -\frac{1}{d_{i,\alpha+1}} \left[m_{i+1,\alpha} L_{i,\alpha} - d_{i,\alpha} \sinh V^{u}_{i,\alpha} - m_{i,\alpha} \right]$$

$$\bar{\mu}^{L}_{i+1,\alpha+1} = -\frac{1}{d_{i,\alpha+1}} \left[m_{i,\alpha} L_{i,\alpha} + d_{i,\alpha} \sinh V^{L}_{i+1,\alpha} - m_{i+1,\alpha} \right]$$

$$L_{i,\alpha} = \cosh V^{L}_{i+1,\alpha} \cosh V^{u}_{i,\alpha} - \sinh V^{L}_{i+1,\alpha} \sinh V^{u}_{i,\alpha} \qquad (4.11)$$

$$\cosh \bar{V}^{u}_{i,\alpha+1} = \left[1 + \left(\bar{\mu}^{u}_{i,\alpha+1} \right)^2 \right]^{1/2}$$

$$\cosh \bar{V}^{L}_{i+1,\alpha+1} = \left[1 + \left(\bar{\mu}^{L}_{i+1,\alpha+1} \right)^2 \right]^{1/2} .$$

The calculation of the deficit is a little more involved. Fig. 4.3 shows the four 3 d volumes meeting on the area $A_{[d_{i,\alpha}:m_{i,\alpha}]}$ (one dimension suppressed for clarity). From the geometry of the situation we see that $\psi_1 = \psi_2$ and $\psi_3 = \psi_4$ where ψ_1, ψ_2 etc. are the dihedral angles between adjacent 3-volumes. The deficit is then

$$\varepsilon_{[d_{i,\alpha}:m_{i,\alpha}]} = 2\pi - 2\psi_1 - 2\psi_3 \,. \tag{4.12}$$

The volume 1-form of the 3-volume defined by legs $\overline{m_{i,\alpha}}$, $\overline{d_{i,\alpha}}$ and $\overline{r_{i,\alpha}\sin\theta\,\Delta\phi}$ at vertex i,α is

$$\Sigma_\Lambda = \varepsilon_{\Lambda\Gamma\Delta\Omega}\, m^{\Gamma}_{i,\alpha}\, d^{\Delta}_{i,\alpha}\, r^{\Omega}_{i,\alpha} \sin\theta\,\Delta\phi \tag{4.13}$$

which when divided by the (approximate) volume of the parallelpiped gives the 1-form normal

$$\tilde{n}\left(\overline{m_{i,\alpha}} : \overline{d_{i,\alpha}} : \overline{r_{i,\alpha}\sin\theta\,\Delta\phi}\right) = \frac{1}{\sinh^2 A^u_{i,\alpha}} \left(s \sinh\gamma_{i,\alpha} - \frac{\Delta\Omega}{s}\,\frac{\Delta r_{i+1,\alpha}}{2\,d_{i,\alpha}} \sinh V^u_{i,\alpha},\right.$$

$$\left. \sinh A^u_{i,\alpha},\ 0,\ \frac{\Delta\Omega}{s}\,\frac{\Delta r_{i+1,\alpha}}{2\,d_{i,\alpha}} \sinh A^u_{i,\alpha} \right). \tag{4.14}$$

The 1-form normal of the adjacent 3-volume defined by legs $\overline{m_{i,\alpha}}$, $\overline{d_{i,\alpha}}$, $\overline{r_{i,\alpha}\Delta\theta}$ at i,α is found, in the same way, to be

$$\tilde{n}\left(\overline{m_{i,\alpha}} : \overline{d_{i,\alpha}} : \overline{r_{i,\alpha}\Delta\theta}\right) = \frac{1}{\sinh^2 A^u_{i,\alpha}} \left(\sin\theta\Delta\phi\left[\sinh\gamma_{i,\alpha} - \frac{\Delta r_{i+1,\alpha}}{2\,d_{i,\alpha}} \sinh V^u_{i,\alpha}\right],\right.$$

$$\left. \frac{\Delta(\sin\theta)\Delta\phi}{2s} \sinh A^u_{i,\alpha},\ -\sinh A^u_{i,\alpha},\ \sin\theta\,\Delta\phi\,\frac{\Delta r_{i+1,\alpha}}{2\,d_{i,\alpha}} \sinh A^u_{i,\alpha} \right). \tag{4.15}$$

The dihedral angle ψ_1 is obtained from

$$\cos\psi_1 = \left\langle \tilde{n}\left(\overline{m_{i,\alpha}} : \overline{d_{i,\alpha}} : \overline{r_{i,\alpha}\sin\theta\,\Delta\phi}\right),\ \tilde{n}\left(\overline{m_{i,\alpha}} : \overline{d_{i,\alpha}} : \overline{r_{i,\alpha}\Delta\theta}\right)\right\rangle \tag{4.16}$$

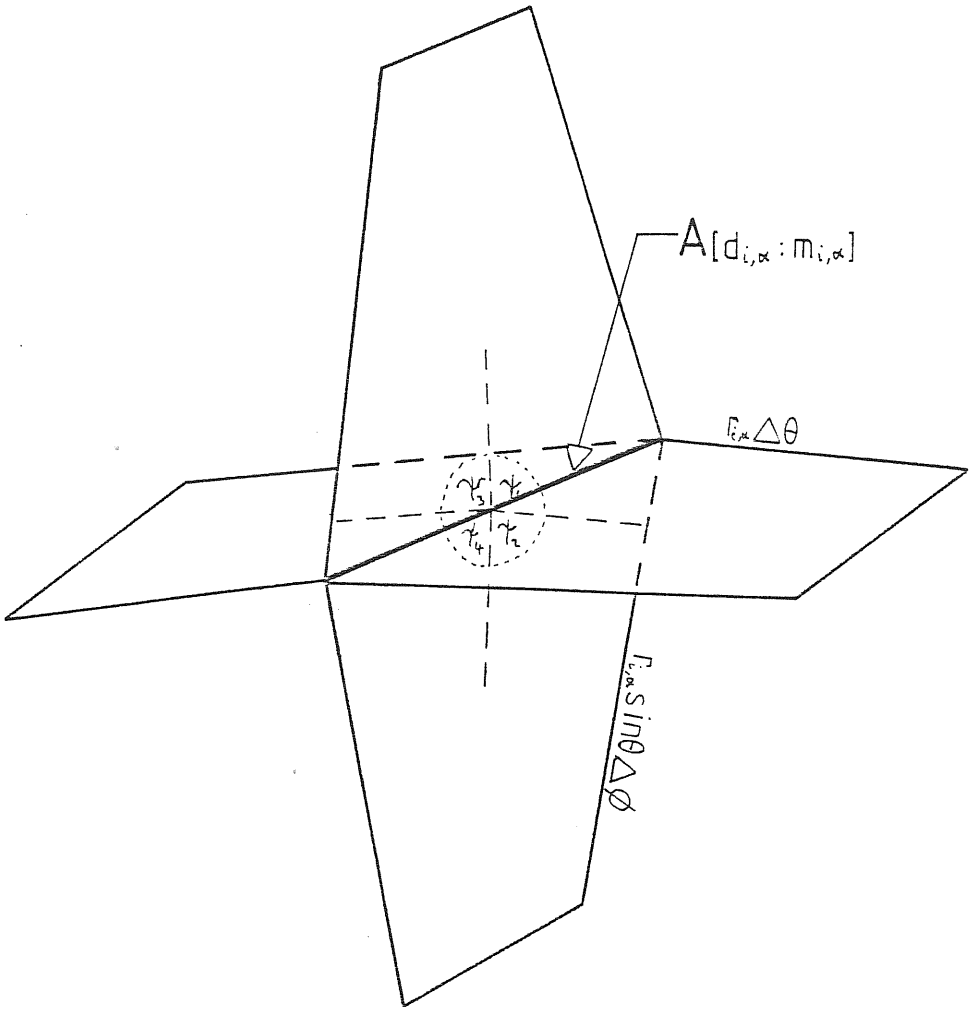

Fig. 4.3 Schematic diagram showing the four 3-dimensional volumes meeting on the area $A_{[d_{i,\alpha}:m_{i,\alpha}]}$. The deficit is found from the difference of 2π and the dihedral angles γ_1, γ_2, γ_3 and γ_4. The dimension along the timelike leg is suppressed for clarity.

whence

$$\cos\psi_1 = \frac{1}{\sinh^2 A^u_{i,\alpha}} \left\{ \tfrac{1}{2}\cos\theta \sinh^2 A^u_{i,\alpha}\,\Delta\phi + \sin\theta\Delta\theta\Delta\phi \left[\left(\frac{\Delta r_{i+1,\alpha}}{2d_{i,\alpha}}\right)^2 \right.\right. \tag{4.17}$$

$$\left.\left. + \frac{\Delta r_{i+1,\alpha}}{d_{i,\alpha}} \sinh V^u_{i,\alpha} \sinh \gamma_{i,\alpha} - \sinh^2 \gamma_{i,\alpha} - \tfrac{1}{4}\sinh^2 A^u_{i,\alpha} \right] \right\}$$

with a similar expression for ψ_3.

We may use expansions for the inverse trigonometric functions since the arguments are small, thus we find finally

$$\varepsilon_{[m_{i,\alpha};\, d_{i,\alpha}]} = -\frac{\sin\theta\Delta\theta\Delta\phi}{\cosh^2 V^u_{i,\alpha}} \left[\left(\frac{\Delta r_{i+1,\alpha}}{d_{i,\alpha}}\right)^2 - \left(1 - 4\frac{\Delta r_{i+1,\alpha}}{d_{i,\alpha}}\right.\right. \tag{4.18}$$

$$\left.\left. \times \sinh V^u_{i,\alpha} \sinh \gamma_{i,\alpha} + 4\sinh^2 \gamma_{i,\alpha} + \sinh^2 V^u_{i,\alpha} \right) \right].$$

When calculated at vertex i+1,α the deficit is

$$\varepsilon_{[m_{i,\alpha};\, d_{i,\alpha}]} = -\frac{\sin\theta\Delta\theta\Delta\phi}{\cosh^2 V^L_{i+1,\alpha}} \left[\left(\frac{\Delta r_{i+1,\alpha}}{d_{i,\alpha}}\right)^2 - \left(1 - 4\frac{\Delta r_{i+1,\alpha}}{d_{i,\alpha}}\right.\right. \tag{4.19}$$

$$\left.\left. \times \sinh V^L_{i+1,\alpha} \sinh \gamma_{i+1,\alpha} + 4\sinh^2 \gamma_{i+1,\alpha} + \sinh^2 V^L_{i+1,\alpha} \right) \right]$$

and the 'no twist' constraint is

$$\sinh\gamma_{i,\alpha} - \frac{\Delta r_{i+1,\alpha}}{2d_{i,\alpha}} \sinh V^u_{i,\alpha} = \frac{\cosh V^u_{i,\alpha}}{\cosh V^L_{i+1,\alpha}} \left(\sinh\gamma_{i+1,\alpha} - \frac{\Delta r_{i+1,\alpha}}{2d_{i,\alpha}} \sinh V^L_{i+1,\alpha} \right) \tag{4.20}$$

from a comparison of the zero components of the 1-form normals.

For convenience we list all area variations and deficit angles in Appendix II.

4.2 Coupling Matter to the Regge Lattice:

There are several ways in which one might include the effects of matter in RC spacetimes. Normally the properties of a source are described by the stress-energy tensor $T^{\mu\nu}$ and thus we could, for example, add appropriate stress-energy terms to the right hand side of the Regge - Einstein equations. An alternative approach is to use a matter Lagrangian $\mathcal{L}_m$ and vary the total action

$$I_T = \int (R + \mathcal{L}_m)\sqrt{-g}\, d^4x \,. \tag{4.21}$$

The second of these appraoches is preferable since the scalar $\mathcal{L}_m\sqrt{-g}$ is easier to translate into Regge quantities than the individual $T^{\mu\nu}$ components. Also one would like to keep the variational characteristics of the methodology.

We require, then, an action principle for a relativistic perfect fluid. Several exists in the literature [77], [117], [118], however following Porter we choose the Schutz variational principle [117] with total action

$$I_T = \int (R + 16\pi p)\sqrt{-g}\, d^4x \,. \tag{4.22}$$

This is chosen for several reasons. Firstly the Lagrangian $\mathcal{L}_m = 16\pi p$ is simple, being just the pressure of the fluid. Secondly, as will be detailed below, the fluid 4-velocity may be written in terms of six scalar potentials. The use of scalars in RC is particularly advantageous since they are unchanged by Lorentz transformations from block to block. We can then place the scalars on the vertices of the lattice.

Schutz writes the 4-velocity of the fluid as

$$U_\mu = \frac{1}{w}\left(\phi_{,\mu} + \alpha\beta_{,\mu} + \theta S_{,\mu}\right) \qquad (4.23)$$

where w, ϕ, α, β, θ and S are the six scalar potentials, some of which have a physical meaning, eg. w = specific relativistic enthalpy, S = specific entropy. Variation of the total action (4.22) with respect to the independent variables ϕ, α, β, θ, S produces an evolution equation for each potential along with the baryon conservation equation when combined with the 4-velocity normalization. Schutz has shown that the system is equivalent to the ordinary fluid equations based on the divergence of the stress-energy tensor. By varying (4.22) with respect to the metric components $g^{\mu\nu}$ we obtain the usual Einstein - Hydro equations. Note that the pressure p = p(w,S) is a function of all the independent variables via (4.23).

We may simplify (4.23) for our purposes. In stellar collapse using a perfect fluid one assumes isentropic flow ($S,_\mu = 0$). Also Schutz has shown that gauge freedom exists in his velocity potential representation. On the initial spatial hypersurface one is free to chose any one of ϕ, α, β or θ arbitrarily. We use this freedom to choose $\alpha = 0$ which has the evolution equation $U^\mu \alpha_{,\mu} = 0$, so we expect α to remain zero along fluid flow lines. Then (4.23) is reduced to

$$U_\mu = \frac{\phi_{,\mu}}{w} \,. \qquad (4.24)$$

The equations governing the fluid flow in the continuum theory are obtained from (4.22), (4.24) and the 4-velocity normalization. These are to be rewritten in a discrete form.

Write, for the spherical lattice,

$$I_M = 16\pi \int_V \rho\sqrt{-g}\, d^4x = 16\pi \sum_{\substack{\text{Regge}\\ \text{blocks}}} \int_{\substack{\text{Regge}\\ \text{block}}} \rho\sqrt{-g}\, d^4x = 16\pi \sin\theta \Delta\theta \Delta\phi \sum_{\substack{\text{Regge}\\ \text{blocks}}} \int_{t_\alpha}^{t_{\alpha+1}} \int_{R_i}^{R_{i+1}} \rho r^2 \sqrt{-g^{(2)}}\, dR\, dt \,. \tag{4.25}$$

The double integral is approximated over the rectangular region of the (t,R) plane $t_\alpha \leq t \leq t_{\alpha+1}$, $R_i \leq R \leq R_{i+1}$ by the trapezoidal rule. Provided the blocks are small we expect sufficient accuracy. Then

$$\begin{aligned} I_{MD} = 4\pi \sin\theta \Delta\theta \Delta\phi \sum_\alpha \sum_i \Big[& i m_{i,\alpha} \cosh V^u_{i,\alpha}\, \rho_{i,\alpha}\, r^2_{i,\alpha}\, d_{i,\alpha} \\ & + i m_{i,\alpha} \cosh \bar{V}^u_{i,\alpha+1}\, \rho_{i,\alpha+1}\, r^2_{i,\alpha+1}\, d_{i,\alpha+1} + i m_{i+1,\alpha} \cosh V^L_{i+1,\alpha}\, \rho_{i+1,\alpha}\, r^2_{i+1,\alpha}\, d_{i,\alpha} \\ & + i m_{i+1,\alpha} \cosh \bar{V}^L_{i+1,\alpha+1}\, \rho_{i+1,\alpha+1}\, r^2_{i+1,\alpha+1}\, d_{i,\alpha+1} \Big] \end{aligned} \tag{4.26}$$

where we have used

$$\begin{aligned} d_i &\approx (R_{i+1} - R_i)\sqrt{g_{RR}}_{\,i} \approx (R_{i+1} - R_i)\sqrt{g_{RR}}_{\,i+1} \\ i m_{i,\alpha} \cosh V^u_{i,\alpha} &\approx (t_{\alpha+1} - t_\alpha)\sqrt{g_{oo}}_{\,i,\alpha} \\ i m_{i,\alpha} \cosh \bar{V}^u_{i,\alpha} &\approx (t_{\alpha+1} - t_\alpha)\sqrt{g_{oo}}_{\,i,\alpha+1} \\ i m_{i+1,\alpha} \cosh V^L_{i+1,\alpha} &\approx (t_{\alpha+1} - t_\alpha)\sqrt{g_{oo}}_{\,i+1,\alpha} \\ i m_{i+1,\alpha} \cosh \bar{V}^L_{i+1,\alpha} &\approx (t_{\alpha+1} - t_\alpha)\sqrt{g_{oo}}_{\,i+1,\alpha+1} \,. \end{aligned} \tag{4.27}$$

Again we expect this approximation to be adequate if the Regge block is small since then the metric components will be nearly constant across the block.

For the moment we will work with the simple diagonal metric in spherical

symmetry,

$$ds^2 = -\alpha^2 dt^2 + g_{RR}(t,R)dR^2 + r^2(t,R)d\Omega^2. \quad (4.28)$$

Using equation (4.24) and the ϕ evolution equation $U^\Gamma \phi_{,\Gamma} = -w$ we can write the 4-velocity normalization as

$$g^{\Lambda\Gamma}\phi_{,\Lambda}\phi_{,\Gamma} = -w^2. \quad (4.29)$$

Noting that $U_\theta = U_\phi = 0$ in spherical collapse, for the diagonal metric (4.28) we have

$$\frac{\phi_{,0}^2}{g_{00}} + \frac{\phi_{,R}^2}{g_{RR}} = -w^2 . \quad (4.30)$$

The form of the equations obtained by variation of the discrete total action depends crucially on the way this equation is differenced. Unfortunately the differencing is ambiguous, one must compromise between stability and accuracy with some experimentation required. The collapse problem is hyperbolic in nature and so there will be characteristic curves moving from the surface to the centre and from the centre to the surface at the local sound speed. We would like to collect information from both sets of characteristics, ie. from points on either side of the vertex i,α in the spatial hypersurface. We will write (4.30) in the discrete form,

$$w_{i,\alpha}^2 = -\frac{(\phi_{i,\alpha+1} - \phi_{i,\alpha})^2}{(im_{i,\alpha})^2 \cosh^2 V_{i,\alpha}^u} - \frac{1}{2}\left[\frac{(\phi_{i+1,\alpha} - \phi_{i,\alpha})^2}{d_{i,\alpha}^2} + \frac{(\phi_{i,\alpha} - \phi_{i-1,\alpha})^2}{d_{i-1,\alpha}^2}\right] \quad (4.31)$$

where we have spatially averaged the quantity $\frac{\phi_{,R}^2}{g_{RR}}$ and have again used the identifications (4.27). An equally good form of (4.30) is

$$W_{i,\alpha}^2 = -\frac{(\phi_{i,\alpha+1}-\phi_{i,\alpha})^2}{(im_{i,\alpha})^2\cosh^2 V_{i,\alpha}^u} - \frac{(\phi_{i+1,\alpha}-\phi_{i,\alpha})(\phi_{i,\alpha}-\phi_{i-1,\alpha})}{d_{i,\alpha}\,d_{i-1,\alpha}} . \tag{4.32}$$

Some experimentation will be required to choose the most suitable expression. The discrete total action

$$I_{TD} = 2\sum_{\substack{\text{bones}\\ n}} A_n \mathcal{E}_n + I_{MD} \tag{4.33}$$

is now varied with respect to the leg lengths $im_{i,\alpha}$, $d_{i,\alpha}$ and $r_{i,\alpha}\sin\theta\,\Delta\phi$, and the scalar potential $\phi_{i,\alpha}$. We consider each variation in turn.

a) $im_{i,\alpha}$ variation.

As discussed above this yields the constraint equation,

$$\begin{aligned} &2\frac{\partial A_{[\theta_{i,\alpha}:m_{i,\alpha}]}}{\partial(im_{i,\alpha})}\mathcal{E}_{[\theta_{i,\alpha}:m_{i,\alpha}]} + 2\frac{\partial A_{[\phi_{i,\alpha}:m_{i,\alpha}]}}{\partial(im_{i,\alpha})}\mathcal{E}_{[\phi_{i,\alpha}:m_{i,\alpha}]} \\ &+\frac{\partial A_{[d_{i,\alpha}:m_{i,\alpha}]}}{\partial(im_{i,\alpha})}\mathcal{E}_{[d_{i,\alpha}:m_{i,\alpha}]} + \frac{\partial A_{[d_{i-1,\alpha}:m_{i,\alpha}]}}{\partial(im_{i,\alpha})}\mathcal{E}_{[d_{i-1,\alpha}:m_{i,\alpha}]} \\ &+\frac{1}{2}\frac{\partial I_{MD}}{\partial(im_{i,\alpha})} = 0 \end{aligned} \tag{4.34}$$

The factors in front of the area variations come from simply counting the number of similar bones having the leg $im_{i,\alpha}$ in common. Substituting for the area and deficit values we obtain

$$4(r_{i,\alpha}+m_{i,\alpha}\sinh Y_{i,\alpha})\left[\frac{\Delta r_{i,\alpha}+2d_{i-1,\alpha}\sinh Y_{i,\alpha}\sinh V^{L}_{i,\alpha}}{d_{i-1,\alpha}\cosh V^{L}_{i,\alpha}}-\frac{\Delta r_{i+1,\alpha}+2d_{i,\alpha}\sinh Y_{i,\alpha}\sinh V^{u}_{i,\alpha}}{d_{i,\alpha}\cosh V^{u}_{i,\alpha}}\right.$$

$$-\frac{(d_{i,\alpha}\cosh V^{u}_{i,\alpha}+d_{i,\alpha+1}\cosh \bar{V}^{u}_{i,\alpha+1})}{2\cosh^2 V^{u}_{i,\alpha}}\left[\left(\frac{\Delta r_{i+1,\alpha}}{d_{i,\alpha}}\right)^2-\{\cosh^2 V^{u}_{i,\alpha}\right.$$

$$\left.\left.+4\sinh Y_{i,\alpha}(\sinh Y_{i,\alpha}-\frac{\Delta r_{i+1,\alpha}}{d_{i,\alpha}}\sinh V^{u}_{i,\alpha})\}\right]\right.$$

$$-\frac{(d_{i-1,\alpha}\cosh V^{L}_{i,\alpha}+d_{i-1,\alpha+1}\cosh \bar{V}^{L}_{i,\alpha+1})}{2\cosh^2 V^{L}_{i,\alpha}}\left[\left(\frac{\Delta r_{i,\alpha}}{d_{i-1,\alpha}}\right)^2-\{\cosh^2 V^{L}_{i,\alpha}\right.$$

$$\left.\left.+4\sinh Y_{i,\alpha}(\sinh Y_{i,\alpha}-\frac{\Delta r_{i,\alpha}}{d_{i-1,\alpha}}\sinh V^{L}_{i,\alpha})\}\right]\right.$$

$$-4\pi\left[\{p_{i,\alpha}+\frac{1}{2}\left(\frac{P_{i,\alpha}+P_{i,\alpha}}{w^2_{i,\alpha}}\right)\left(\frac{(\phi_{i+1,\alpha}-\phi_{i,\alpha})^2}{d^2_{i,\alpha}}+\frac{(\phi_{i,\alpha}-\phi_{i-1,\alpha})^2}{d^2_{i-1,\alpha}}\right)\}\times\right.$$

$$r^2_{i,\alpha}\left(d_{i,\alpha}\cosh V^{u}_{i,\alpha}+d_{i-1,\alpha}\cosh V^{L}_{i,\alpha}+\frac{m_{i,\alpha-1}}{m_{i,\alpha}}d_{i,\alpha}\cosh \bar{V}^{u}_{i,\alpha}+\frac{m_{i,\alpha-1}}{m_{i,\alpha}}d_{i-1,\alpha}\cosh \bar{V}^{L}_{i,\alpha}\right)$$

$$+\left(\frac{m_{i,\alpha-1}}{m_{i,\alpha}}P_{i,\alpha}r^2_{i,\alpha}d_{i,\alpha}\cosh \bar{V}^{u}_{i,\alpha}-P_{i,\alpha+1}r^2_{i,\alpha+1}d_{i,\alpha+1}\cosh \bar{V}^{u}_{i,\alpha+1}\right)$$

$$\left.+\left(\frac{m_{i,\alpha-1}}{m_{i,\alpha}}P_{i,\alpha}r^2_{i,\alpha}d_{i-1,\alpha}\cosh \bar{V}^{L}_{i,\alpha}-P_{i,\alpha+1}r^2_{i,\alpha+1}d_{i-1,\alpha+1}\cosh \bar{V}^{L}_{i,\alpha+1}\right)\right]=0$$

(4.35)

b) $d_{i,\alpha}$ variation.

We have

$$2\frac{\partial A_{[d_{i,\alpha}:\phi_{i,\alpha}]}}{\partial d_{i,\alpha}}\varepsilon_{[d_{i,\alpha}:\phi_{i,\alpha}]}+2\frac{\partial A_{[d_{i,\alpha}:\theta_{i,\alpha}]}}{\partial d_{i,\alpha}}\varepsilon_{[d_{i,\alpha}:\theta_{i,\alpha}]}$$

$$+\frac{\partial A_{[d_{i,\alpha}:m_{i,\alpha}]}}{\partial d_{i,\alpha}}\varepsilon_{[d_{i,\alpha}:m_{i,\alpha}]}+\frac{\partial A_{[d_{i,\alpha}:m_{i,\alpha-1}]}}{\partial d_{i,\alpha}}\varepsilon_{[d_{i,\alpha}:m_{i,\alpha-1}]} \qquad (4.36)$$

$$+\tfrac{1}{2}\frac{\partial I_{MD}}{\partial d_{i,\alpha}}=0$$

which when evaluated at vertex i,α is

$$4(r_{i,\alpha}+r_{i+1,\alpha})\left[\frac{2d_{i,\alpha}\sinh\gamma_{i,\alpha}-\Delta r_{i+1,\alpha}\sinh V^{u}_{i,\alpha}}{2d_{i,\alpha}\cosh V^{u}_{i,\alpha}}+\bar{\sigma}^{u}_{i,\alpha}\right]$$

$$-\frac{(m_{i,\alpha}\cosh V^{u}_{i,\alpha}+m_{i+1,\alpha}\cosh V^{L}_{i+1,\alpha})}{2\cosh^2 V^{u}_{i,\alpha}}\left[\left(\frac{\Delta r_{i+1,\alpha}}{d_{i,\alpha}}\right)^2-(1-\right.$$

$$\left.\frac{4\Delta r_{i+1,\alpha}}{d_{i,\alpha}}\sinh\gamma_{i,\alpha}\sinh V^{u}_{i,\alpha}+4\sinh^2\gamma_{i,\alpha}+\sinh^2 V^{u}_{i,\alpha})\right]$$

$$-\frac{(m_{i,\alpha-1}\cosh\bar{V}^{u}_{i,\alpha}+m_{i+1,\alpha+1}\cosh\bar{V}^{L}_{i+1,\alpha})}{2\cosh^2 V^{u}_{i,\alpha-1}}\left[\left(\frac{\Delta r_{i+1,\alpha-1}}{d_{i,\alpha-1}}\right)^2-(1-\right.$$

$$\left.\frac{4\Delta r_{i+1,\alpha-1}}{d_{i,\alpha-1}}\sinh\gamma_{i,\alpha-1}\sinh V^{u}_{i,\alpha-1}+4\sinh^2\gamma_{i,\alpha-1}+\sinh^2 V^{u}_{i,\alpha-1})\right]$$

$$+4\pi\left[p_{i,\alpha}r^2_{i,\alpha}(m_{i,\alpha}\cosh V^{u}_{i,\alpha}+m_{i,\alpha-1}\cosh\bar{V}^{u}_{i,\alpha})\right.$$

$$+p_{i+1,\alpha}r^2_{i+1,\alpha}(m_{i+1,\alpha}\cosh V^{L}_{i+1,\alpha}+m_{i+1,\alpha-1}\cosh\bar{V}^{L}_{i+1,\alpha})+$$

$$\frac{1}{2}\left(\frac{\rho_{i,\alpha}+\rho_{i,\alpha}}{w^2_{i,\alpha}}\right)\frac{(\phi_{i+1,\alpha}-\phi_{i,\alpha})^2}{d^2_{i,\alpha}}\,r^2_{i,\alpha}\left(m_{i,\alpha}\cosh V^u_{i,\alpha}+m_{i,\alpha-1}\cosh\bar{V}^u_{i,\alpha}\right.$$

$$\left.+\frac{d_{i-1,\alpha}}{d_{i,\alpha}}m_{i,\alpha}\cosh V^L_{i,\alpha}+\frac{d_{i-1,\alpha}}{d_{i,\alpha}}m_{i,\alpha-1}\cosh\bar{V}^L_{i,\alpha}\right)$$

$$+\frac{1}{2}\left(\frac{\rho_{i+1,\alpha}+\rho_{i+1,\alpha}}{w^2_{i+1,\alpha}}\right)\frac{(\phi_{i+1,\alpha}-\phi_{i,\alpha})^2}{d^2_{i,\alpha}}\,r^2_{i+1,\alpha}\left(\frac{d_{i+1,\alpha}}{d_{i,\alpha}}m_{i+1,\alpha}\cosh V^u_{i+1,\alpha}\right.$$

$$\left.+\frac{d_{i+1,\alpha}}{d_{i,\alpha}}m_{i+1,\alpha-1}\cosh\bar{V}^u_{i+1,\alpha}+m_{i+1,\alpha}\cosh V^L_{i+1,\alpha}+m_{i+1,\alpha-1}\cosh\bar{V}^L_{i,\alpha}\right)\Bigg]=0$$

(4.37)

while at vertex i+1,α it is

$$4(r_{i+1,\alpha}-r_{i,\alpha})\left[\frac{2d_{i,\alpha}\sinh\gamma_{i+1,\alpha}-\Delta r_{i+1,\alpha}\sinh V^L_{i+1,\alpha}}{2d_{i,\alpha}\cosh V^L_{i+1,\alpha}}+\bar{\sigma}^L_{i+1,\alpha}\right]$$

$$-\frac{(m_{i,\alpha}\cosh V^u_{i,\alpha}+m_{i+1,\alpha}\cosh V^L_{i+1,\alpha})}{2d^2_{i,\alpha}\cosh^2 V^L_{i+1,\alpha}}\left[\left(\frac{\Delta r_{i+1,\alpha}}{d_{i,\alpha}}\right)^2-(1-\right.$$

$$\left.4\frac{\Delta r_{i+1,\alpha}}{d_{i,\alpha}}\sinh\gamma_{i+1,\alpha}\sinh V^L_{i+1,\alpha}+4\sinh^2\gamma_{i+1,\alpha}+\sinh^2 V^L_{i+1,\alpha}\right)\Bigg]$$

$$-\frac{(m_{i,\alpha-1}\cosh\bar{V}^u_{i,\alpha}+m_{i+1,\alpha-1}\cosh\bar{V}^L_{i+1,\alpha})}{2d^2_{i,\alpha-1}\cosh^2 V^L_{i+1,\alpha-1}}\left[\left(\frac{\Delta r_{i+1,\alpha-1}}{d_{i,\alpha-1}}\right)^2-(1-\right.$$

$$\left.4\frac{\Delta r_{i+1,\alpha-1}}{d_{i,\alpha-1}}\sinh\gamma_{i+1,\alpha-1}\sinh V^L_{i+1,\alpha-1}+4\sinh^2\gamma_{i+1,\alpha-1}+\sinh^2 V^L_{i+1,\alpha-1}\right)\Bigg]$$

$$+4\pi\Bigg[\rho_{i,\alpha}r^2_{i,\alpha}\left(m_{i,\alpha}\cosh V^u_{i,\alpha}+m_{i,\alpha-1}\cosh\bar{V}^u_{i,\alpha}\right)$$

$$+\rho_{i+1,\alpha}r^2_{i+1,\alpha}\left(m_{i+1,\alpha}\cosh V^L_{i+1,\alpha}+m_{i+1,\alpha-1}\cosh\bar{V}^L_{i+1,\alpha}\right)$$

$$+\frac{1}{2}\left(\frac{\rho_{i,\alpha}+\rho_{i,\alpha}}{w^2_{i,\alpha}}\right)\frac{(\phi_{i+1,\alpha}-\phi_{i,\alpha})^2}{d^2_{i,\alpha}}\,r^2_{i,\alpha}\left(m_{i,\alpha}\cosh V^u_{i,\alpha}+m_{i,\alpha-1}\cosh\bar{V}^u_{i,\alpha}+\right.$$

$$\frac{d_{i-1,\alpha}}{d_{i,\alpha}} m_{i,\alpha} \cosh V^{L}_{i,\alpha} + \frac{d_{i-1,\alpha}}{d_{i,\alpha}} m_{i,\alpha-1} \cosh \bar{V}^{L}_{i,\alpha} \Big)$$

$$+ \frac{1}{2} \left(\frac{P_{i+1,\alpha} + P_{i+1,\alpha}}{w^2_{i+1,\alpha}} \right) \frac{(\phi_{i+1,\alpha} - \phi_{i,\alpha})^2}{d^2_{i,\alpha}} r^2_{i+1,\alpha} \left(\frac{d_{i+1,\alpha}}{d_{i,\alpha}} m_{i+1,\alpha} \cosh V^{u}_{i+1,\alpha} \right.$$

$$\left. + \frac{d_{i+1,\alpha}}{d_{i,\alpha}} m_{i+1,\alpha-1} \cosh \bar{V}^{u}_{i+1,\alpha} + m_{i+1,\alpha} \cosh V^{L}_{i+1,\alpha} + m_{i+1,\alpha-1} \cosh \bar{V}^{L}_{i,\alpha} \right) \Big] = 0 \quad (4.38)$$

The definitions of the quantities $\bar{\sigma}^{u}_{i,\alpha}$ and $\bar{\sigma}^{L}_{i+1,\alpha}$ are given in Appendix II.

c) $r_{i,\alpha} \sin\theta \Delta\phi$ variation.

This gives the equation

$$2 \frac{\partial A_{[\theta_{i,\alpha} : \phi_{i,\alpha}]}}{\partial (r_{i,\alpha} \sin\theta \Delta\phi)} \mathcal{E}_{[\theta_{i,\alpha} : \phi_{i,\alpha}]} + \frac{\partial A_{[d_{i,\alpha} : \phi_{i,\alpha}]}}{\partial (r_{i,\alpha} \sin\theta \Delta\phi)} \mathcal{E}_{[d_{i,\alpha} : \phi_{i,\alpha}]}$$

$$+ \frac{\partial A_{[d_{i-1,\alpha} : \phi_{i,\alpha}]}}{\partial (r_{i,\alpha} \sin\theta \Delta\phi)} \mathcal{E}_{[d_{i-1,\alpha} : \phi_{i,\alpha}]} + \frac{\partial A_{[\phi_{i,\alpha} : m_{i,\alpha}]}}{\partial (r_{i,\alpha} \sin\theta \Delta\phi)} \mathcal{E}_{[\phi_{i,\alpha} : m_{i,\alpha}]} \quad (4.39)$$

$$+ \frac{\partial A_{[\phi_{i,\alpha} : m_{i,\alpha-1}]}}{\partial (r_{i,\alpha} \sin\theta \Delta\phi)} \mathcal{E}_{[\phi_{i,\alpha} : m_{i,\alpha-1}]} + \frac{1}{2} \frac{\partial I_{MD}}{\partial (r_{i,\alpha} \sin\theta \Delta\phi)} = 0$$

which in full is

$$2 r_{i,\alpha} (-\sinh V^{u}_{i,\alpha} + \sinh V^{L}_{i,\alpha} + \bar{\mu}^{u}_{i,\alpha} + \bar{\mu}^{L}_{i,\alpha})$$

$$+ 2 d_{i,\alpha} \left[\frac{2 d_{i,\alpha} \sinh Y_{i,\alpha} - \Delta r_{i+1,\alpha} \sinh V^{u}_{i,\alpha}}{2 d_{i,\alpha} \cosh V^{u}_{i,\alpha}} + \bar{\sigma}^{u}_{i,\alpha} \right]$$

$$+ 2 d_{i-1,\alpha} \left[\frac{2 d_{i-1,\alpha} \sinh Y_{i,\alpha} - \Delta r_{i,\alpha} \sinh V^{L}_{i,\alpha}}{2 d_{i-1,\alpha} \cosh V^{L}_{i,\alpha}} + \bar{\sigma}^{L}_{i,\alpha} \right] +$$

$$m_{i,\alpha}\left[\frac{\Delta r_{i,\alpha}+2d_{i-1,\alpha}\sinh\gamma_{i,\alpha}\sinh V^{L}_{i,\alpha}}{d_{i-1,\alpha}\cosh V^{L}_{i,\alpha}}-\frac{\Delta r_{i+1,\alpha}+2d_{i,\alpha}\sinh\gamma_{i,\alpha}\sinh V^{u}_{i,\alpha}}{d_{i,\alpha}\cosh V^{u}_{i,\alpha}}\right]$$

$$+m_{i,\alpha-1}\left[\frac{\Delta r_{i,\alpha-1}+2d_{i-1,\alpha-1}\sinh\gamma_{i,\alpha-1}\sinh V^{L}_{i,\alpha-1}}{d_{i-1,\alpha-1}\cosh V^{L}_{i,\alpha-1}}-\frac{\Delta r_{i+1,\alpha-1}+2d_{i,\alpha-1}\sinh\gamma_{i,\alpha-1}\sinh V^{u}_{i,\alpha-1}}{d_{i,\alpha-1}\cosh V^{u}_{i,\alpha-1}}\right]$$

$$+4\pi\left[p_{i,\alpha}r_{i,\alpha}m_{i,\alpha}\left(d_{i,\alpha}\cosh V^{u}_{i,\alpha}+d_{i-1,\alpha}\cosh V^{L}_{i,\alpha}\right)\right.$$

$$\left.+p_{i,\alpha}r_{i,\alpha}m_{i,\alpha-1}\left(d_{i,\alpha}\cosh\bar{V}^{u}_{i,\alpha}+d_{i-1,\alpha}\cosh\bar{V}^{L}_{i,\alpha}\right)\right]=0. \tag{4.40}$$

Because of spherical symmetry an identical equation is obtained from the $r_{i,\alpha}\Delta\theta$ variation.

d) $\phi_{i,\alpha}$ variation.

From Schutz [117] this yields the baryon conservation equation,

$$-D\left[\left(\frac{\mathcal{P}_{i,\alpha}+p_{i,\alpha}}{w^{2}_{i,\alpha}}\right)\frac{(\phi_{i,\alpha+1}-\phi_{i,\alpha})}{m_{i,\alpha}\cosh V^{u}_{i,\alpha}}r^{2}_{i,\alpha}\left(d_{i,\alpha}+\frac{m_{i,\alpha-1}\cosh\bar{V}^{u}_{i,\alpha}}{m_{i,\alpha}\cosh V^{u}_{i,\alpha}}d_{i,\alpha}\right.\right.$$

$$\left.\left.+\frac{\cosh V^{L}_{i,\alpha}}{\cosh V^{u}_{i,\alpha}}d_{i-1,\alpha}+\frac{m_{i,\alpha-1}\cosh\bar{V}^{L}_{i,\alpha}}{m_{i,\alpha}\cosh V^{u}_{i,\alpha}}d_{i-1,\alpha}\right)\right]$$

$$+\frac{(\phi_{i+1,\alpha}-\phi_{i,\alpha})}{d^{2}_{i,\alpha}}\mu\left[\left(\frac{\mathcal{P}_{i+1,\alpha}+p_{i+1,\alpha}}{w^{2}_{i+1,\alpha}}\right)r^{2}_{i+1,\alpha}\left(m_{i+1,\alpha}\cosh V^{u}_{i+1,\alpha}d_{i+1,\alpha}\right.\right.$$

$$+m_{i+1,\alpha-1}\cosh\bar{V}^{u}_{i+1,\alpha}d_{i+1,\alpha}+m_{i+1,\alpha}\cosh V^{L}_{i+1,\alpha}d_{i,\alpha}$$

$$\left.\left.+m_{i+1,\alpha-1}\cosh\bar{V}^{L}_{i+1,\alpha}d_{i,\alpha}\right)\right]-$$

$$\frac{(\phi_{i,\alpha}-\phi_{i-1,\alpha})}{d^2_{i-1,\alpha}}\mu\left[\left(\frac{P_{i,\alpha}+P_{i,\alpha}}{W^2_{i,\alpha}}\right)\Gamma^2_{i,\alpha}\left(m_{i,\alpha}\cosh V^u_{i,\alpha}\,d_{i,\alpha}\right.\right.$$

$$+ m_{i,\alpha-1}\cosh \bar{V}^u_{i,\alpha}\,d_{i,\alpha} + m_{i,\alpha}\cosh V^L_{i,\alpha}\,d_{i-1,\alpha}$$

$$\left.\left.+ m_{i,\alpha-1}\cosh \bar{V}^L_{i,\alpha}\,d_{i-1,\alpha}\right)\right] = 0 \tag{4.41}$$

where the difference operators D and μ are defined by

$$D f_{i,\alpha} = f_{i,\alpha} - f_{i,\alpha-1}$$

$$\mu f_{i,\alpha} = \tfrac{1}{2}\left(f_{i,\alpha} + f_{i-1,\alpha}\right). \tag{4.42}$$

In all of the above we have obtained the pressure variations by writing, eg.

$$\frac{\partial P_{i,\alpha}}{\partial(im_{i,\alpha})} = \frac{dP_{i,\alpha}}{dW_{i,\alpha}}\frac{\partial W_{i,\alpha}}{\partial(im_{i,\alpha})} \tag{4.43}$$

similarly for $\Gamma_{i,\alpha}$, $d_{i,\alpha}$ and $\phi_{i,\alpha}$. The quantity $\frac{\partial W_{i,\alpha}}{\partial(im_{i,\alpha})}$ is obtained from equation (4.31) while $\frac{dP_{i,\alpha}}{dW_{i,\alpha}}$ is given by the first law of thermodynamics specialized to isontropic flow;

$$\frac{dP}{dW} = \frac{(\rho+P)}{W}. \tag{4.44}$$

Equations (4.37), (4.38), (4.40) and (4.41) are to be solved iteratively for the unknowns $\sinh Y_{i,\alpha}$, $\sinh V^u_{i,\alpha}$, $\sinh V^L_{i,\alpha}$ and $W_{i,\alpha}$. Then $\phi_{i,\alpha}$ is evolved explicitly via equation (4.31) and the spatial legs are evolved using

$$r_{i,\alpha+1} = r_{i,\alpha} + 2 m_{i,\alpha} \sinh Y_{i,\alpha} \tag{4.45}$$

and

$$d_{i,\alpha+1} = \left[2 m_{i,\alpha} m_{i+1,\alpha} L_{i,\alpha} - m_{i,\alpha}^2 - m_{i+1,\alpha}^2 \right.$$

$$\left. + 2 d_{i,\alpha} \left(m_{i+1,\alpha} \sinh V^L_{i+1,\alpha} - m_{i,\alpha} \sinh V^U_{i,\alpha} \right) + d_{i,\alpha}^2 \right]^{\frac{1}{2}} \tag{4.46}$$

which are obtained from inspection of fig. 4.2 and equations (4.7), (4.8).

The relationship between the Regge evolution variables and the continuum extrinsic curvature is manifest most clearly in equation (4.45). We have

$$\begin{aligned} &\text{continuum} \qquad K_{\phi\phi} = -\frac{1}{2\alpha} \frac{\partial r^2}{\partial t} = -\frac{r}{\alpha} \frac{\partial r}{\partial t} \\ &\text{Regge} \qquad \sinh Y_{i,\alpha} = \frac{r_{i,\alpha+1} - r_{i,\alpha}}{2 m_{i,\alpha}} \end{aligned} \tag{4.47}$$

so that $K_{\phi\phi} \sim - 2 r_{i,\alpha} \sinh Y_{i,\alpha}$.

If there is a non-zero shift vector equation (4.31) becomes

$$w_{i,\alpha}^2 = - \frac{(\phi_{i,\alpha+1} - \phi_{i,\alpha})^2}{(i m_{i,\alpha})^2 \cosh^2 V^U_{i,\alpha}} + \beta^R dt \frac{(\phi_{i,\alpha+1} - \phi_{i,\alpha})}{(i m_{i,\alpha})^2 \cosh^2 V^U_{i,\alpha}} \left[\frac{(\phi_{i+1,\alpha} - \phi_{i,\alpha})}{d_{i,\alpha}} \right.$$

$$\left. + \frac{(\phi_{i,\alpha} - \phi_{i-1,\alpha})}{d_{i-1,\alpha}} \right] - \frac{1}{2} \left(1 + \frac{(\beta^R dt)^2}{(i m_{i,\alpha})^2 \cosh^2 V^U_{i,\alpha}} \right) \left[\frac{(\phi_{i+1,\alpha} - \phi_{i,\alpha})^2}{d_{i,\alpha}^2} + \frac{(\phi_{i,\alpha} - \phi_{i-1,\alpha})^2}{d_{i-1,\alpha}^2} \right] \tag{4.48}$$

where $\beta^R dt$ is a shift in the co-ordinate R direction. This may be used in conjunction with the transformations (3.40) to rewrite the spherical Regge - Einstein equations with shift.

4.3 The Regge - TOV Equations:

The interval describing static, spherically symmetric spacetime in continuum GR is

$$ds^2 = -\alpha^2 dt^2 + g_{rr}\, dr^2 + r^2 d\Omega^2 \tag{4.49}$$

where α and g_{rr} are functions of Schwarzschild r only. One may use (4.49) with Einstein's equations coupled to a perfect fluid to produce the Tolman - Oppenheimer - Volkov equations describing static, spherically symmetric fluid bodies [22]. These bodies provide a starting point for stellar collapse calculations. The aim of this section is to reduce the Regge - Einstein equations shown previously to the static case.

Clearly for static spacetime we require

$$\left.\begin{aligned} W_{i,\alpha+1} &= W_{i,\alpha} \\ r_{i,\alpha+1} &= r_{i,\alpha} \\ d_{i,\alpha+1} &= d_{i,\alpha} \\ m_{i,\alpha+1} &= m_{i,\alpha} \end{aligned}\right\} \forall \alpha \tag{4.50}$$

which from equations (4.45) and (4.46) leads to

$$\left.\begin{aligned} \sinh Y_{i,\alpha} &= 0 \\ \sinh V^{u}_{i,\alpha} &= \sinh V^{L}_{i+1,\alpha} = \frac{m_{i+1,\alpha} - m_{i,\alpha}}{2 d_{i,\alpha}} \end{aligned}\right\} \forall \alpha \tag{4.51}$$

where we have used the no twist constraint (4.20) for the latter. Only the time component of the fluid 4-velocity is non-zero so equation (4.31) becomes

$$W_{i,\alpha} = \frac{(\phi_{i,\alpha+1} - \phi_{i,\alpha})}{m_{i,\alpha} \cosh V^{u}_{i,\alpha}} \,. \tag{4.52}$$

For infinitesimal timelike legs $(m_{i+1,\alpha} - m_{i,\alpha}) << d_{i,\alpha}$ and we may write $m_{i,\alpha} \approx \alpha_{i,\alpha} dt$ where dt is an infinitesimal co-ordinate time interval. Then

$$\cosh V^{u}_{i,\alpha} = \cosh V^{L}_{i+1,\alpha} \approx [1 + O(dt^2)]^{1/2} \approx 1 \qquad (4.53)$$

and we rewrite (4.52) as

$$W_{i,\alpha} = \left(\frac{\phi_{,0}}{\alpha}\right)_{i,\alpha} . \qquad (4.54)$$

Applying conditions (4.50) - (4.54) to equations (4.35), (4.37), (4.38), (4.40) and (4.41) we obtain

$$4r_i\left[\frac{\Delta r_i}{d_{i-1}} - \frac{\Delta r_{i+1}}{d_i}\right] + d_{i-1}\left[1 - \left(\frac{\Delta r_i}{d_{i-1}}\right)^2\right] + d_i\left[1 - \left(\frac{\Delta r_{i+1}}{d_i}\right)^2\right] - 8\pi\rho_i r_i^2 (d_i + d_{i-1}) = 0 \qquad (4.55)$$

$$-(r_{i+1} + r_i)\frac{\Delta\alpha_{i+1}}{d_i} + (r_i + r_{i-1})\frac{\Delta\alpha_i}{d_{i-1}} + 2\alpha_i\left[\frac{\Delta r_i}{d_{i-1}} - \frac{\Delta r_{i+1}}{d_i}\right] + 8\pi\rho_i r_i \alpha_i (d_i + d_{i-1}) = 0 \qquad (4.56)$$

$$-2(r_i + r_{i+1})\frac{\Delta r_{i+1}}{d_i^2}\Delta\alpha_{i+1} + (\alpha_i + \alpha_{i+1})\left[1 - \left(\frac{\Delta r_{i+1}}{d_i}\right)^2\right] + 8\pi(\rho_i r_i^2 \alpha_i + \rho_{i+1} r_{i+1}^2 \alpha_{i+1}) = 0 \qquad (4.57)$$

$$(\phi_{,0})_{i,\alpha} = (\phi_{,0})_{i,\alpha-1} = \text{constant} \qquad (4.58)$$

which are similar to those first derived by Porter in [101]. Note that (4.37) and (4.38) reduced to the same equation (4.57).

We now consider the boundary conditions. Fig. 4.4 shows the type of 3 d spatial blocks where we have $r_1 = 0$. The contribution of one central Regge block to the matter action is

$$I_{MCEN} = 16\pi \int_{\substack{all\\time}} \int_{r_1=0}^{r_2} \int_{\theta}^{\theta+\Delta\theta} \int_{\phi}^{\phi+\Delta\phi} p\sqrt{-g}\; d^4x \tag{4.59}$$

which may be approximated as

$$I_{MCEN} = \tfrac{4}{3} \sin\theta\Delta\theta\Delta\phi \sum_{\alpha} [\, p_{1,\alpha}\, d_{1,\alpha}\, r_{2,\alpha}^2\, im_{1,\alpha} \cosh V^u_{1,\alpha}$$

$$+ p_2\, d_{1,\alpha}\, r_{2,\alpha}^2\, im_{2,\alpha} \cosh V^L_{2,\alpha} + p_{1,\alpha+1}\, d_{1,\alpha+1}\, r^2_{2,\alpha+1}\, im_{1,\alpha} \cosh \bar{V}^u_{1,\alpha+1}$$

$$+ p_{2,\alpha+1}\, d_{1,\alpha+1}\, r^2_{2,\alpha+1}\, im_{2,\alpha} \cosh \bar{V}^L_{2,\alpha+1}\,] \tag{4.60}$$

where we have spatially averaged the quantity $p\sqrt{-g_{oo}}$ over the proper 3-volume $V = \frac{1}{3} r^2_{2,\alpha} \sin\theta\Delta\theta\Delta\phi\; d_{i,\alpha}$.

The action (4.60) is used for the centre boundary conditions of the collapsing star. The variations with respect to the legs $im_{1,\alpha}$ and $d_{1,\alpha}$ and the potential $\phi_{1,\alpha}$ will be described in the next section. Here we merely assume the results obtained by taking these variations followed by reduction to static spacetime.

Using $r_{-i} = -r_i$, $d_{-i} = d_i$ and $\alpha_{-i} = \alpha_i$, due to symmetry about the centre, in equations (4.55) and (4.57), and replacing the matter terms with the centre matter terms obtained from (4.60) we find

$$r_2 = \frac{d_1}{\left(1 + \frac{8\pi}{3} p_1 d_1^2\right)^{\frac{1}{2}}} \tag{4.61}$$

$$\alpha_2 = \frac{\left(1 + \frac{r_2^2}{d_1^2} + \frac{8\pi}{3} p_1 r_2^2\right) \alpha_1}{\left(3\frac{r_2^2}{d_1^2} - 1 - \frac{8\pi}{3} p_2 r_2^2\right)} \,. \tag{4.62}$$

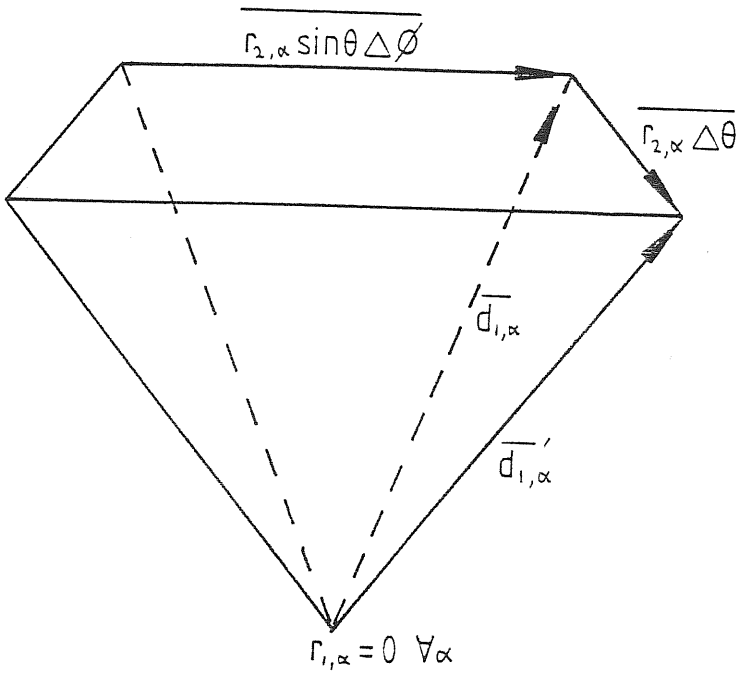

Fig. 4.4 A central spatial block.

The total mass M of the body is normally obtained by evaluating the integral

$$M = 4\pi \int_0^{r_s} \rho r^2 dr \tag{4.63}$$

where r_s is the surface radius. We approximate this as

$$M = \frac{2\pi}{3} r_2^3 (\rho_1 + \rho_2) + 2\pi \sum_{i=2}^{s-1} (\rho_i r_i^2 + \rho_{i+1} r_{i+1}^2) \Delta r_{i+1} . \tag{4.64}$$

An equation of state is now required. For simplicity we use a polytropic equation of state,

$$p = K \rho_0^{\Gamma}$$

$$\rho_0 \pi = \frac{p}{\Gamma - 1} \tag{4.65}$$

where we take adiabatic index $\Gamma = \frac{5}{3}$ and K = constant. Such an equation of state describes, to sufficient accuracy, the degenerate cores of highly evolved stars (see [119]). In terms of relativistic enthalpy we rewrite (4.65) as

$$p = K_0 (w-1)^{\frac{\Gamma}{\Gamma-1}}$$

(4.66)

$$\rho = p\left(\frac{w + \Gamma - 1}{(\Gamma-1)(w-1)}\right)$$

where

$$K_0 = \left(\frac{1}{k}\right)^{\frac{1}{\Gamma-1}} \left(\frac{\Gamma-1}{\Gamma}\right)^{\frac{\Gamma}{\Gamma-1}} \tag{4.67}$$

is simply a scaling constant. For the present we follow Mann [86] and Porter [101] and choose $K_0 = 1.07499 \times 10^{-12}$. This will enable us to compare results directly.

The system of equations is solved as follows: One chooses the central enthalpy w_{CEN} and an initial proper step length d_1. Clearly we are free to choose the d_i's since this determines the degree of discretization. Equation (4.61) is soved for r_2 and then (4.54) and (4.62) are solved for α_2 and w_2 by Newtonian iteration. With these values we then solve (4.55) and (4.56) for the unknowns r_{i+1} and α_{i+1} from the centre out. The MINPACK routine HYBRD1 which minimises a system of non-linear algebraic equations is used for this purpose. The enthalpy w_{i+1} is found from equation (4.54) once α_{i+1} has been obtained. The surface is reached when $w_{i+1} = 1$ since this corresponds to a vacuum. For $w_{i+1} < 1$ we estimate the position of the surface by linear interpolation between vertices i and i+1. We then take two steps back to vertex i-1 and bisect the interval between this vertex and the approximate surface. After solving again for vertex i the surface is found by fixed point iteration. This procedure ensures that the proper distance step to the surface is not unduly small relative to the previous step. Rapidly varying step lengths can cause problems when the system is evolved.

The arbitrary time scaling can be fixed by choosing $\phi_{,0}$ = constant = central enthalpy w_{CEN} such that $\alpha = 1$ at the centre. This means co-ordinate time and proper time are synchronized at the centre.

Figs. 4.5 - 4.7 show some representative stellar models produced. The first has $w_{CEN} = 1.14$ and is stable to radial perturbations. The second has $w_{CEN} = 1.178$. This is at the peak of the stability curve where the eigenvalue for radial perturbations is zero, and thus it is marginally stable. Such a star can provide a useful test for any collapse code. Numerical instabilities are not damped as with physically stable initial data, and they may push this star into the unstable regime causing it to collapse. The last star has $w_{CEN} = 25$ and represents a highly condensed configuration unstable to radial perturbations. This is expected to undergo collapse to a black hole on a

dynamical timescale.

Figs. 4.8 and 4.9 show mass verses central enthalpy and mass verses radius curves from which the radial stability properties of the stars can be determined (see the discussion in [8]). The characteristic maximum stable masses and the spiral are clearly seen.

There were no problems with numerical instabilities and for all values of central enthalpy the equations converged satisfactory. For $w_{CEN} \gtrsim 120$ the fixed point iteration sometimes failed to find the surface. As w_{CEN} increases the enthalpy profile approaches a delta function in nature which makes the surface difficult to find. The computer time needed to solve the equations is negligible being around 5×10^{-3} secs. per vertex, and since we are using a package routine this represents an upper limit.

Any numerical results should be thoroughly examined and tested before they are to be believed. To this end we perform two tests on the results obtained. First we compare radii and masses with those of identical models produced by Mann using the finite element method. Fig. 4.10 shows the comparisons. The results are seen to be very similar in all cases. They are significantly more accurate than previous models produced by Porter.

As a second test we look at the convergence of the solutions as the number of blocks used is increased. This should also give us some idea of the local truncation error of the RC scheme. Fig. 4.11 shows the results for $w_{CEN} = 1.178$. Clearly the total mass and radius are converging to a value near $M = 7.302 \times 10^{4}$ cm and $R = 8.204 \times 10^{5}$ cm respectively. This is within 0.05% and 0.01% of Mann's results.

In conclusion we can say that RC is capable of producing relativistic, static stellar models with an accuracy comparable to other numerical methods.

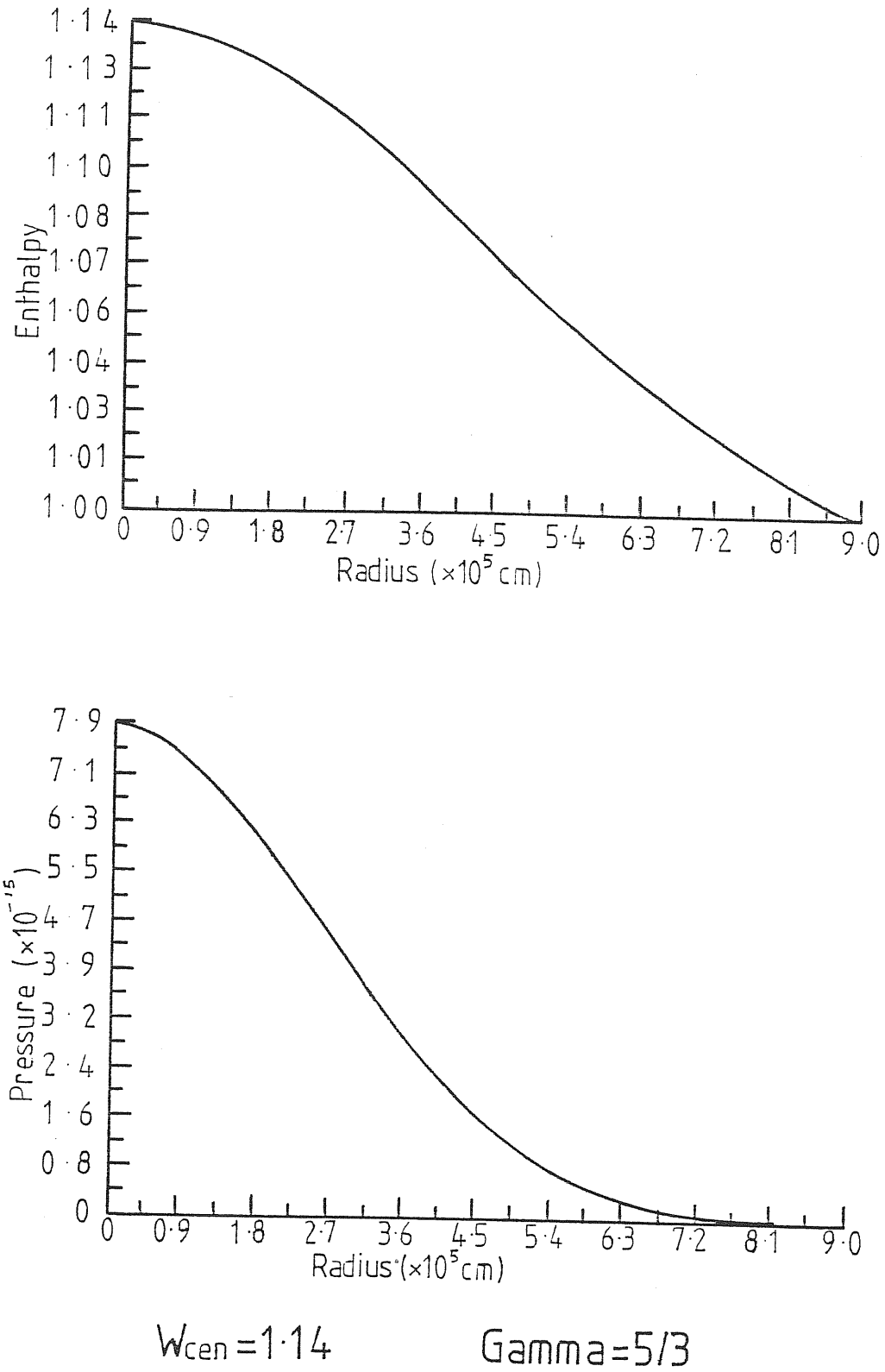

Fig. 4.5 Solution of Regge - TOV equations for central density = 1.14 using a polytropic equation of state.

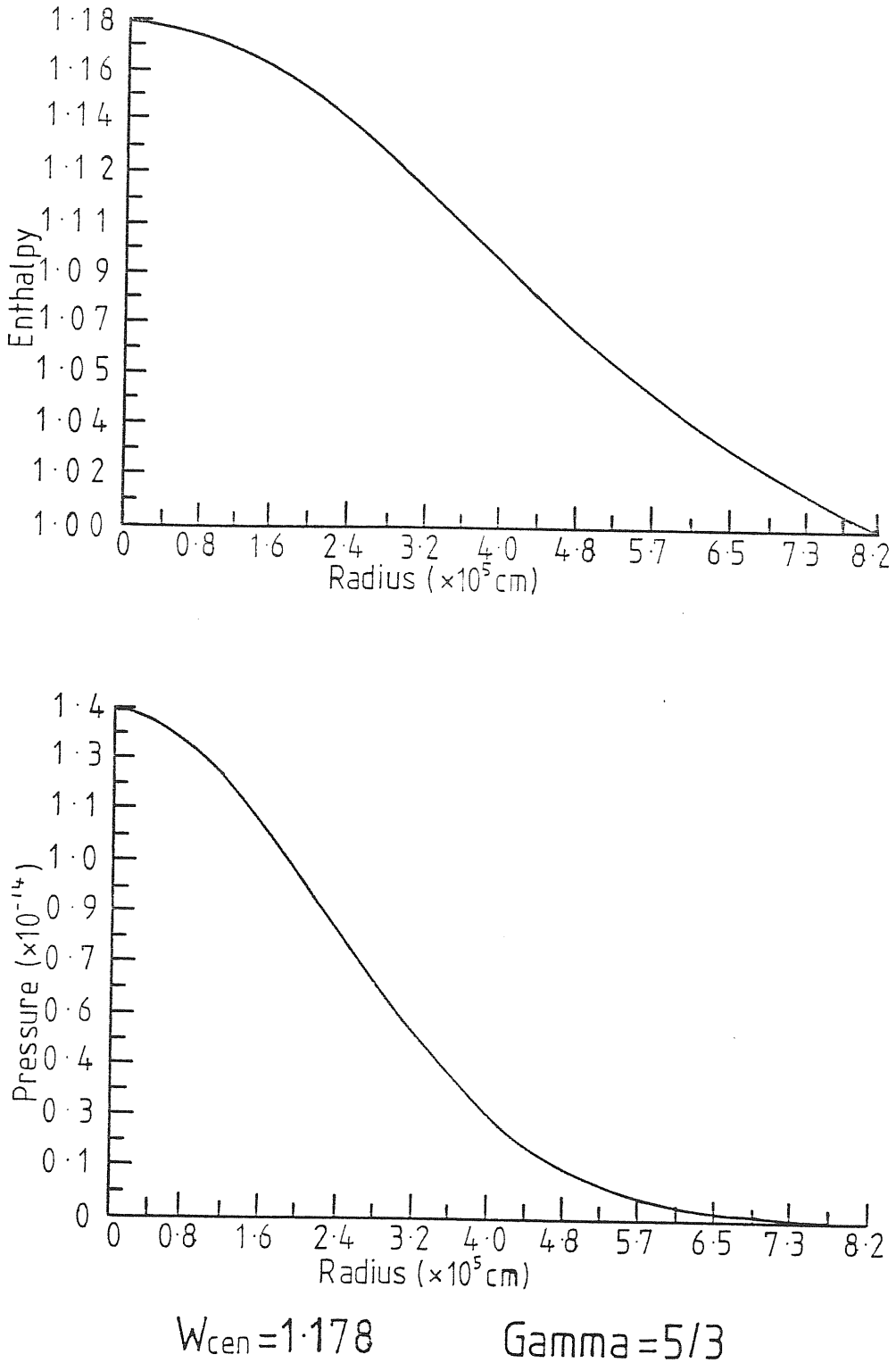

Fig. 4.6 Solution Of Regge - TOV equations for central density = 1.178 using a polytropic equation of state.

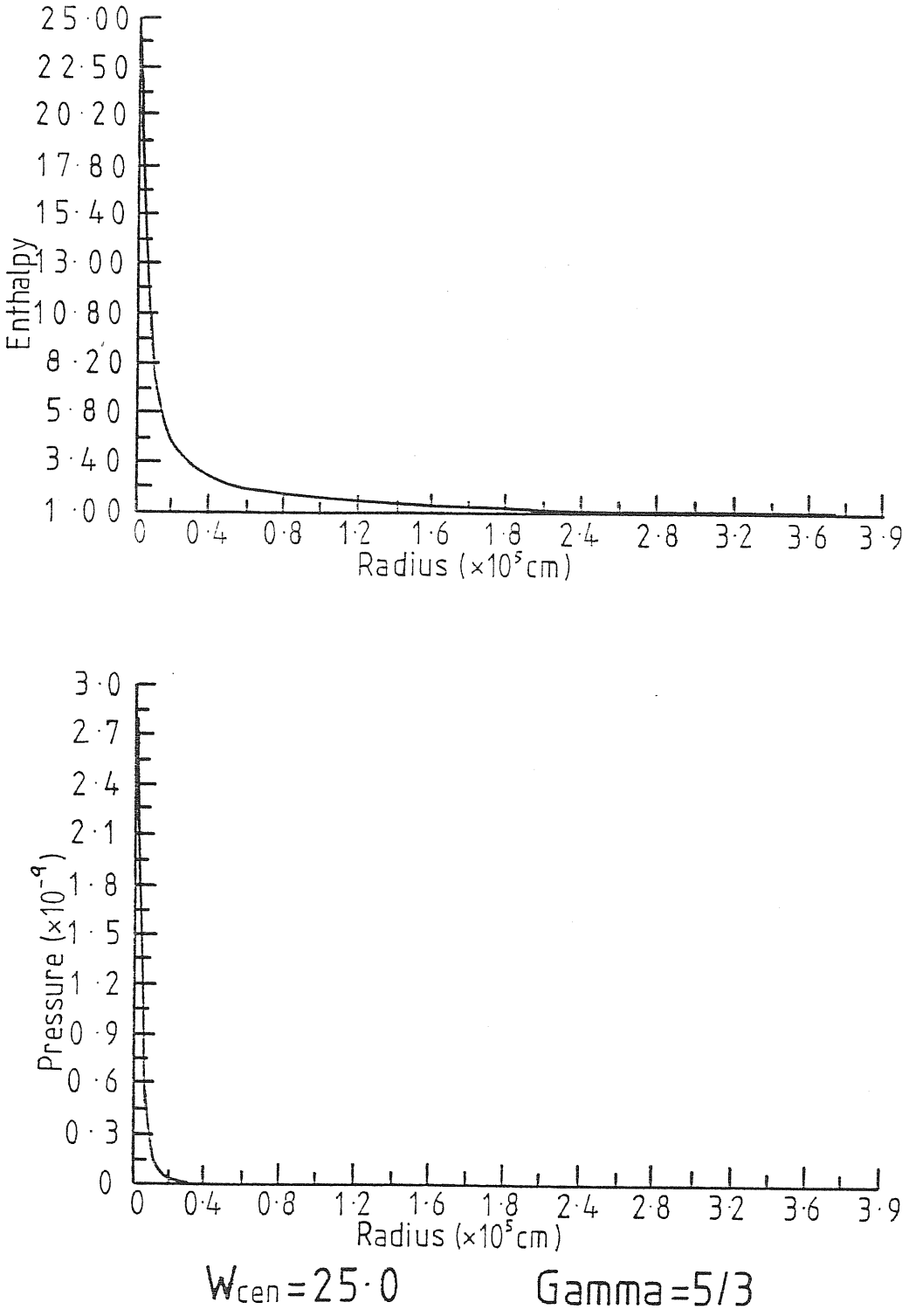

Fig. 4.7 Solution of Regge - TOV equations for central density = 25 using a polytropic equation of state.

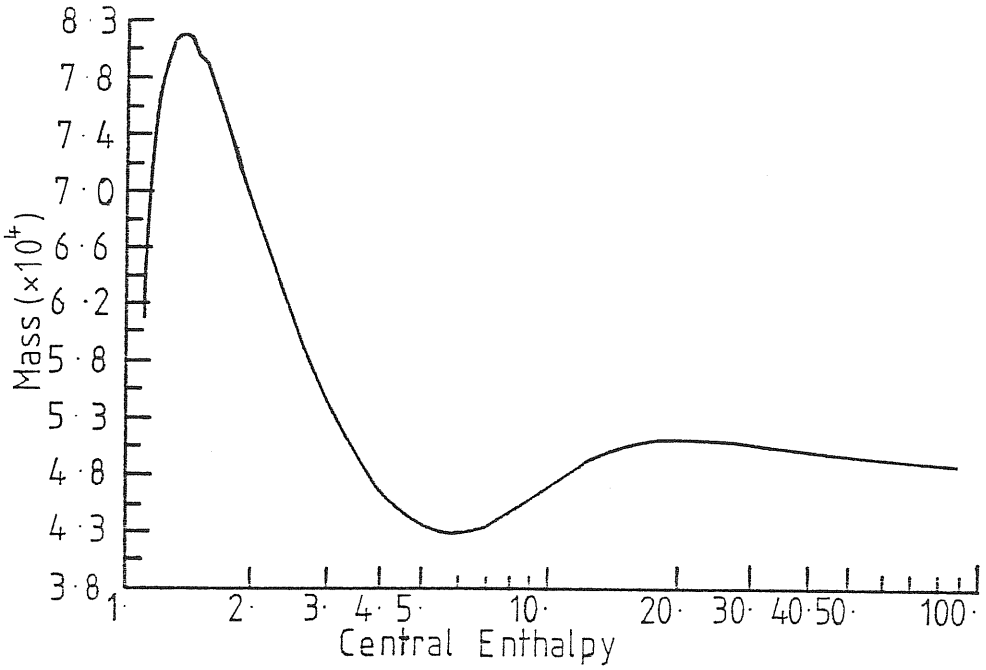

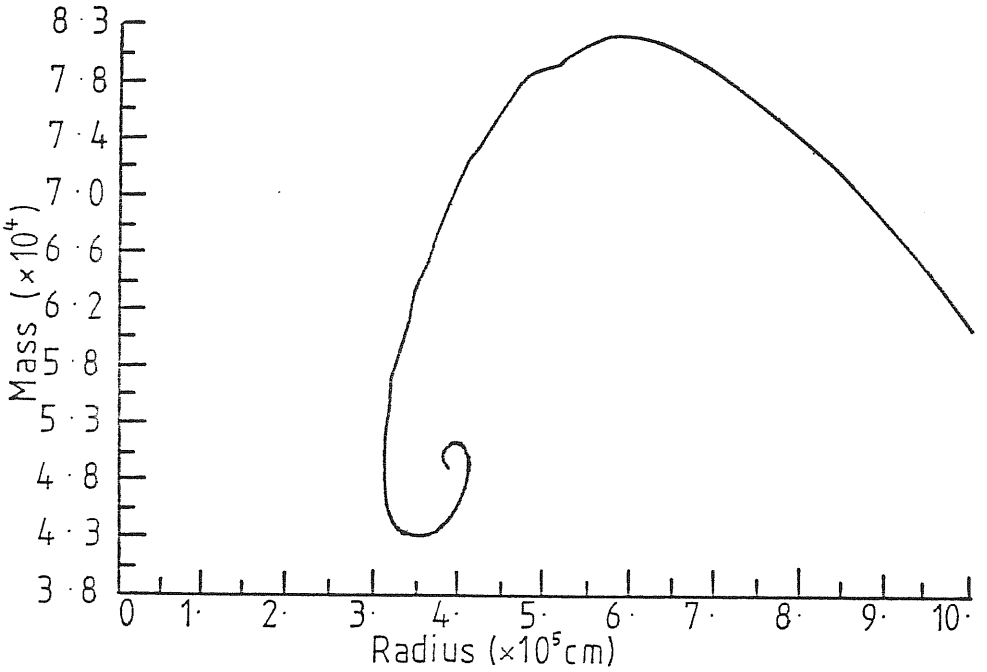

Gamma=5/3

Figs. 4.8 and 4.9 showing mass vs central enthalpy and mass vs radius for a sequence of equilibrium Regge - TOV polytropes. Adiabatic index $\Gamma = 5/3$.

Comparison of the Regge - TOV Models with those of Mann using the Finite Element Method (FEM).

		FEM		Regge		Difference	
$\frac{R}{M}$	Central Enthalpy	Mass ($x10^4$ cm)	Radius ($x10^5$ cm)	Mass ($x10^4$ cm)	Radius ($x10^5$ cm)	Mass %	Radius %
13	1.14	6.7682	8.9752	6.77749	8.96872	0.137	0.07
11	1.178	7.29848	8.205	7.30766	8.19976	0.125	0.06
8	25	4.9365	3.96965	4.93921	3.96737	0.05	0.06

Fig. 4.10 Table of comparison. Polytropic equations of state with $\gamma = 5/3$ is used. The average number of blocks in the Regge Models is 60.

Variation of Mass and Radius with the Number of Blocks used $w_{CEN} = 1.178$.

Number of Blocks	Mass ($\times 10^4$ cm)	Radius ($\times 10^5$ cm)	Difference in Mass %	Difference in Radius %
4	6.49208	8.40673	11.04	2.46
8	7.13317	8.13003	2.26	0.914
15	7.29099	8.16527	0.103	0.484
33	7.31846	8.18920	0.274	0.193
63	7.30766	8.19976	0.125	0.064
139	7.30258	8.20363	0.056	0.017

Fig. 4.11 Test of convergence of Regge - TOV soution for $w_{CEN} = 1.178$. Comparison is with an equivalent model of Mann using the finite element method.

4.4 Spherically Symmetric Collapse:

Here we describe briefly some of the progress made in modelling spherical collapse using RC. The stellar models produced in the previous section form the basis of the initial data. For test purposes we will evolve the static data of the $w_{CEN} = 1.14$ star which is known to be physically stable. In a collapse calculation one normally modifies the static data in some way to ensure collapse. None of the methods used are particularly realistic and since this is not a problem confined to RC collapse we do not discuss it here. [36] gives some account of the methods. Possibly the easiest option is to evolve an unstable star such as the $w_{CEN} = 25$ model, however an obvious objection is that such a star would not occur in nature.

We assume zero shift vector and an interval of the form

$$ds^2 = -\alpha^2 dt^2 + g_{rr} dr^2 + r^2 d\Omega^2 \qquad (4.68)$$

where α and g_{rr} are functions of t and r. Thus r is our radial co-ordinate. This describes an essentially Eulerian gauge.

At this point we normalized the stellar models, using K_o, such that the central density equals one for any central enthalpy. The masses, radii and pressures scale accordingly. This makes the results from computer runs easier to interpret and the numbers span a smaller numerical range.

Boundary conditions at the centre of the star are dicussed first. The contribution to the matter action of a central Regge block is equation (4.60). We vary this with respect to $im_{,\alpha}$, $d_{1,\alpha}$ and $\phi_{1,\alpha}$. From these variations and the spherical symmetry conditions at the centre

$$\left.\begin{aligned} r_{1,\alpha} &= 0 \\ \sinh \gamma_{1,\alpha} &= 0 \\ r_{-i,\alpha} &= -r_{i,\alpha} \\ d_{-i,\alpha} &= d_{i,\alpha} \\ im_{-i,\alpha} &= im_{i,\alpha} \\ \phi_{1,\alpha} &= \phi_{2,\alpha} \end{aligned}\right\} \forall \alpha \qquad (4.69)$$

where the last condition is obtained from the requirement that the fluid velocity be zero across the centre, we find

a) $im_{i,\alpha}$ variation

$$(d_{1,\alpha}\cosh V^u_{1,\alpha} + d_{1,\alpha+1}\cosh \bar{V}^u_{1,\alpha+1})\left[\frac{r^2_{2,\alpha}}{d^2_{1,\alpha}\cosh^2 V^u_{1,\alpha}} - 1\right]$$

$$+ \frac{4\pi}{3}\left\{\rho_{i,\alpha} r^2_{2,\alpha} d_{1,\alpha}\left(\cosh V^u_{1,\alpha} + \frac{m_{1,\alpha-1}}{m_{1,\alpha}}\cosh \bar{V}^u_{1,\alpha}\right)\right.$$

$$\left. + \left(\rho_{1,\alpha} r^2_{2,\alpha}\frac{m_{1,\alpha-1}}{m_{1,\alpha}}\cosh \bar{V}^u_{1,\alpha} - \rho_{1,\alpha+1} r^2_{2,\alpha+1} d_{1,\alpha+1}\cosh \bar{V}^u_{1,\alpha+1}\right)\right\} = 0 \qquad (4.70)$$

giving the constraint equation at the centre,

b) $d_{1,\alpha}$ variation

$$4 r_{2,\alpha}\left[-\frac{r_{2,\alpha}\sinh V^u_{1,\alpha}}{2 d_{1,\alpha}\cosh V^u_{1,\alpha}} + \bar{\sigma}^u_{1,\alpha}\right] - \tfrac{1}{2}\left(m_{1,\alpha}\cosh V^u_{1,\alpha} + m_{2,\alpha}\cosh V^L_{2,\alpha}\right)$$

$$\times\left[\left(\frac{r_{2,\alpha}}{d_{1,\alpha}\cosh V^u_{1,\alpha}}\right)^2 - 1\right] - \tfrac{1}{2}\left(m_{1,\alpha-1}\cosh \bar{V}^u_{1,\alpha} + m_{2,\alpha-1}\cosh \bar{V}^L_{2,\alpha}\right)$$

$$\times\left[\left(\frac{r_{2,\alpha-1}}{d_{1,\alpha-1}\cosh V^u_{1,\alpha-1}}\right)^2 - 1\right] + \frac{4\pi}{3}\left\{\rho_{1,\alpha} r^2_{2,\alpha}\left(m_{1,\alpha}\cosh V^u_{1,\alpha} + m_{1,\alpha-1}\cosh \bar{V}^u_{1,\alpha}\right)\right.$$

$$\left. + \rho_{2,\alpha} r^2_{2,\alpha}\left(m_{2,\alpha}\cosh V^L_{2,\alpha} + m_{2,\alpha-1}\cosh \bar{V}^L_{2,\alpha}\right)\right\} = 0 \qquad (4.71)$$

c) $\phi_{i,\alpha}$ variation

$$D\left(\frac{P_{1,\alpha}+P_{1,\alpha}}{W^2_{1,\alpha}}\right)\frac{(\phi_{1,\alpha+1}-\phi_{1,\alpha})}{m^2_{1,\alpha}\cosh^2 V^u_{1,\alpha}}\,r^2_{2,\alpha}\,d_{1,\alpha}\,(m_{1,\alpha}\cosh V^u_{1,\alpha}+m_{1,\alpha-1}\cosh \bar{V}^u_{1,\alpha})=0. \tag{4.72}$$

For the surface of the star we take advantage of Birkhoff's theorem and fit Schwarzschild spacetime by writing the proper distance step as

$$d_{s,\alpha}\simeq\left(1-\frac{2M_{,\alpha}}{r_{s,\alpha}}\right)^{-1/2}\Delta r_{s+1,\alpha} \tag{4.73}$$

where i = s is the surface vertex and $M_{,\alpha}$ is the total mass of the star on time slice t_α. An extra block is placed outside the star and we then take the limit as its spatial dimensions go to zero, ie. $d_{s,\alpha}\to 0$. Clearly equation (4.73) holds since $r_{s+1,\alpha}\to r_{s,\alpha}$. Also $\cosh V^L_{s+1,\alpha}\to\cosh V^u_{s,\alpha}$.

The procedure for the solution of the equations is then as follows: With inital data set up on the first slice we build a time-symmetric sandwich. Time-symmetric spacetime is momentarily static and so we use the same conditions as in that case. Obviously they hold only over an infinitesimal time interval.

A time slicing condition is required to specify the timelike legs $m_{i,\alpha}$. For the evolution of the w_{COLN} = 1.14 static data we choose the natural Schwarzschild like slicing

$$m_{i,\alpha}=\alpha_i\,\Delta t\quad\forall\alpha \tag{4.74}$$

where $-\alpha_i^2$ is the g_{00} component of the static spacetime metric (see fig. 4.12). The timelike killing vector field then maps the spacetime onto itself so that it should remain static. This is a good test of the numerical code. Δt is a co-ordinate time step.

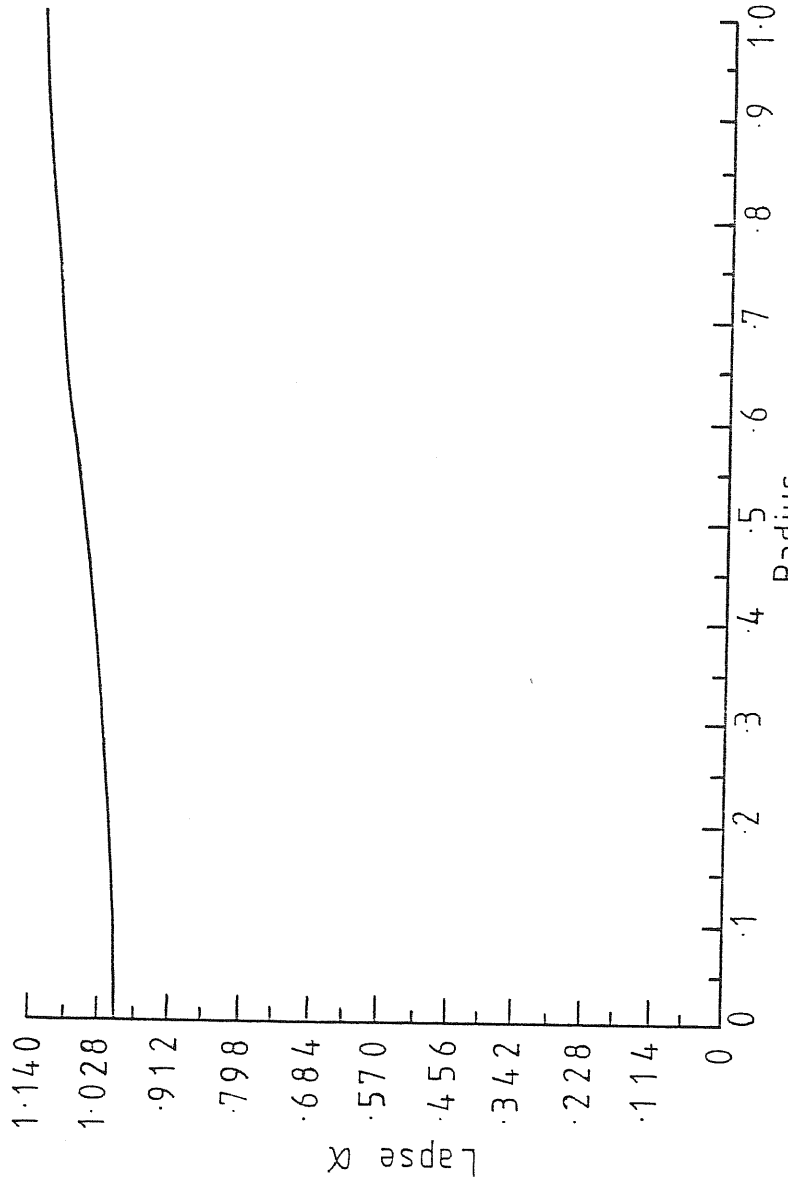

Fig. 4.12 Metric function $\alpha = \sqrt{g_{00}}$ vs radius/surface radius for the static spacetime of a $w_{EN} = 1.14$ polytropic sphere.

Equations (4.37), (4.38) and (4.41) are solved iteratively for $\sinh V^{u}_{i,\alpha}$, $\sinh V^{L}_{i,\alpha}$ and $w_{i,\alpha}$ again using the routine HYBRD1. Several sweeps of the net using a Gauss - Seidel type iteration are required for convergence. Convergence is monitored via the norms of the residuals of the unknown quantities. Once the unknowns have been found the spatial legs $d_{i,\alpha}$ and the velocity potentials $\phi_{i,\alpha}$ are evolved explicitly using equations (4.46) and (4.31) respectively. The constraint equation (4.35) can be used to check the accuracy of the solution.

Unfortunately an oscillation develops in the velocity potential at the centre at an early stage and rapidly grows so the the program crashes around co-ordinate time t = 5M. The numerical values of the velocity potential indicate local radial velocities approaching the speed of light. The oscillation is rapidly damped in the outer regions of the star which remain static to good accuracy. Total mass is conserved ($\sim 10^{-5}$ % change). For this case of $\sinh Y_{i,\alpha} = 0 \ \forall_{i,\alpha}$ the no twist constraint is satisfied all along the slice at all times.

The reason for the central oscillation is not known at present. It is probably true that RC contains very little implicit artificial viscosity (unlike eg. the Lax - Wendroff difference scheme). We are currently working on a solution to this problem.

There are several other problems to solve before a full collapse calculation may be considered. While the Eulerian Schwarzschild grid is adequate for the test evolution of static data a collapsing star would rapidly fall towards the centre with a subsequent loss of accuracy due to the coarser and coarser discretization. We propose two solutions to the problem.

a) One may use a shift vector to make some radial co-ordinate (vertex number, say) follow the matter velocity, ie. make $\phi_{i+1,\alpha} = \phi_{i,\alpha} \ \forall_{i,\alpha}$, giving a Lagrangian type grid. Schwarzschild r will then be a function of vertex number and time.

b) As an alterntive we may use the Schwarzschild grid with a grid velocity v_g, that is, move the vertices at $r_{i,\alpha}$ relative to the continuous co-ordinate r. This corresponds to moving the spherical shells of section 4.1 in and out. When differencing time derivatives such as $\phi_{,0}$ we must remember to include a convective term due to the motion of the grid [66], [120],

$$\phi_{,0} = \frac{(\phi_{i,\alpha+1} - \phi_{i,\alpha})}{\Delta t} + \frac{1}{2} V_g \left[\frac{(\phi_{i+1,\alpha} - \phi_{i,\alpha})}{\Delta r_{i+1,\alpha}} + \frac{(\phi_{i,\alpha} - \phi_{i-1,\alpha})}{\Delta r_{i,\alpha}} \right] \quad (4.75)$$

so for example equation (4.31) becomes

$$W^2_{i,\alpha} = - \frac{(\phi_{i,\alpha+1} - \phi_{i,\alpha})^2}{(im_{i,\alpha})^2 \cosh^2 V^u_{i,\alpha}} - 2 \sinh Y_{i,\alpha} \frac{(\phi_{i,\alpha+1} - \phi_{i,\alpha})}{i(im_{i,\alpha}) \cosh^2 V^u_{i,\alpha}}$$

$$\times \left[\frac{(\phi_{i+1,\alpha} - \phi_{i,\alpha})}{\Delta r_{i+1,\alpha}} + \frac{(\phi_{i,\alpha} - \phi_{i-1,\alpha})}{\Delta r_{i,\alpha}} \right]$$

$$+ 2 \frac{\sinh^2 Y_{i,\alpha}}{\cosh^2 V^u_{i,\alpha}} \left[\frac{(\phi_{i+1,\alpha} - \phi_{i,\alpha})^2}{\Delta r^2_{i+1,\alpha}} + \frac{(\phi_{i,\alpha} - \phi_{i-1,\alpha})^2}{\Delta r^2_{i,\alpha}} \right]$$

$$- \frac{1}{2} \left[\frac{(\phi_{i+1,\alpha} - \phi_{i,\alpha})^2}{d^2_{i,\alpha}} + \frac{(\phi_{i,\alpha} - \phi_{i-1,\alpha})^2}{d^2_{i-1,\alpha}} \right] \quad (4.76)$$

where the grid velocity is governed by a choice of $\sinh Y_{i,\alpha}$. For the evolution of the static data we set $\sinh Y_{i,\alpha} = 0$ for all time corresponding to zero grid velocity.

A second problem concerns the handling of shocks. Being a discrete method RC will be unable to deal with steep gradients. As discussed in chapter

two, one normally uses a diffusive term in the form of a bulk viscosity added to the pressure. However we use relativistic enthalpy as the basic thermodynamic variable and have assumed dS = 0 in the derivation of the Regge - Einstein equations. Some modification of the velocity potential formulation for a perfect fluid to include the effects of a viscosity is required.

One feature of RC which offers advantages in shock handling over standard numerical methods is the fact that it is based on a variational principle. The variation of the action with respect to $\Gamma_{i,\alpha}$ is a variation with respect to vertex positions on which the thermodynamic variables and velocity potentials are defined. By solving equation (4.40) iteratively along with equations (4.37), (4.38) and (4.41) a value of $\sinh Y_{i,\alpha}$ (grid velocity) is obtained which moves the vertices to where they are needed most. This is similar to the moving finite element method of Gelinas, Doss and Miller [121] which is spectacularly successful in handling single and multiple steep gradients. Some care is required since all regions of the star need to be adequately covered to maintain accuracy. Also we should not let vertices cross or even too close.

4.5 Conclusions and Discussion:

The Regge Calculus provides a formulation of General Relativity which differs fundamentally from the continuum theory. Its use in numerical relativity is motivated by the way in which a natural discretization of the space-time may be obtained.

In practise, for simple geometries, discretization of the ADM (3+1) equations via the highly developed finite difference methods is vastly superior. However the increase in complexity is considerable when the number of dimensions is higher than one. Regge Calculus on the other hand starts from 3 d and is

reduced to 1 or 2 d by symmetry arguments. We expect then that for the construction of spacetimes with little or no symmetry Regge Calculus will be a tractable alternative for the numerical relativist.

There is much work which needs to be done before this goal is achieved. The Regge -Einstein equations are implicit in nature and require iterative methods to solve them. This is costly in terms of computer time. Our spherical collapse code currently has a speed of 0.033 secs. per vertex per evolution on a GOULD 32/97 computer. This is very slow, but we emphasise that it represents an upper limit since at this stage a package is employed. An efficient implicit equation solver needs to be developed. A second problem, as mentioned previously, is the handling of shocks.

The advantages which may be obtained in higher dimensions justifies the development of the method and its application to test problems such as spherical collapse. In any case it is worthwhile having fundamentally different formulations of General Relativity for numerical work which may be compared to ascertain the reliability of results.

REFERENCES

[1] Smarr L. (ed) "Sources of Gravitational Radiation" (Cambridge University Press, 1979).

[2] Nathalie D. and Piran T. (eds) "Gravitational Radiation, Les Houches 1982" (North Holland, 1983).

[3] Bancel D. and Signore M. (eds) "Problems of Collapse and Numerical Relativity" (Reidel, 1984).

[4] Moncreif V., Cunningham C. and Price R. "Radiation from Slightly Non-spherical Models of Gravitaional Collapse" in ref. [1].

[5] Price R. "Non-spherical Perturbations of Relativistic Gravitational Collapse, I: Scalar and Gravitational Perturbations" Phys. Rev. D5, 2419, (1972).

[6] Ruffini R. "Gravitational Radiation from a Mass Projected into a Schwarzschild Black Hole" Phys. Rev. D7, 972 (1973).

[7] Wheeler J.A. "Geometrodynamics and the Issue of the Final State" in "Relativity Groups and Topology" Eds. de Witt C. and de Witt B. (Gordon and Breach, 1964).

[8] Harrison B.K., Thorne K.S., Wakano M. and Wheeler J.A. "Gravitation Theory and Gravitational Collapse" (University of Chicago Press, 1965).

[9] Miller J.C. and Sciama D.W. "Gravitational Collapse to the Black Hole State" in "General Relativity and Gravitation. One Hundred Years after the Birth of Albert Einstein" Ed. Held (Plenum Press, 1980).

[10] Van Riper K.A. and Lattimer J.M. "Stellar Core Collapse. I. Infall Epoch" Ap. J. 249, 270, (1981).

[11] Rees M.J. and Stoneham R.T. "Supernovae: A Survey of Current Research" (Reidel, 1982).

[12] Landau L.D. Phys. Zs. Sowjetunion 1, 285, (1932).

[13] Chandrasekhar S. "The Highly Collapsed Configurations of a Stellar Mass. (Second Paper)." MNRAS 95, 207, (1935).

[14] Greenstein J.L., Boksenberg A., Carswell R. and Shortridge K. "The Rotation and Gravitational Redshift of White Dwarfs" Ap. J. 212, 186, (1977).

[15] Woolsey S.E. and Weaver T.A. "Type II Supernovae" in ref. [3].

[16] Wilson J.R. "Stellar Collapse and Supernovae" in ref. [1].

[17] Shapiro S.L. and Teukolsky S.A. "Black Holes, White Dwarfs and Neuton Stars" (Wiley - Interscience, 1983).

[18] de Felice F. and Yunqiang Yu "Stellar Rotation and Gravitational Collapse: The $\frac{a}{m}$ Issue." J. Phys. A. Math. Gen. 15, 3341, (1982).

[19] Van Riper "Stellar Core Collapse: II. Inner Core Bounce and Shock Propagation" Ap. J. 257, 793, (1982).

[20] Hillebrandt W. and Müller E. "Computer Simulations of Stellar Collapse and Shock Wave Propagation" Astron. Astrophys. 103, 147,(1981).

[21] Hillebrandt W., Nomoto K. and Wolff R.G. "Supernova Explosions of Massive Stars. The Mass Range 8 to $10M_{\odot}$" Astron. Astrophys. 133, 175, (1984).

[22] Misner C.W., Thorne K. and Wheeler J.A. "Gravitation" (Freeman, 1973).

[23] Oppenheimer J.R. and Snyder H. "On Continued Gravitational Contraction" Phys. Rev. 56, 455, (1939).

[24] Liang E. "Some Exact Models of Inhomogeneous Dust Collapse" Phys. Rev. D10, 447, (1974).

[25] May M.M. and White R.H. "Hydrodynamic Calculations of General Relativistic Collapse" Phys. Rev. 141, 1232, (1966).

[26] May M.M. and White R.H. "Stellar Dynamics and Gravitational Collapse" in "Methods in Computational Physics" Eds. Alder B., Fernback S. and Rotenberg M., Vol.7, (Academic Press, 1967).

[27] Tolman R.C. "Relativity, Thermodynamics and Cosmology" (Clarendon Press, 1937).

[28] von Neumann J. and Richtmeyer R.D. "A Method for the Numerical Calculation of Hydrodynamical Shocks" J. Appl. Phys. 21, 232, (1950).

[29] Misner C.W. and Sharp D.H. "Relativistic Equations for Adiabatic, Spherically Symmetric Gravitational Collapse" Phys. Rev. 136, B571, (1964).

[30] Hernandez W.C. and Misner C.W. "Observer Time as a Co-ordinate in Relativistic Spherical Hydrodynamics" Ap. J. 143, 452, (1966).

[31] Miller J.C. "Computer Calculations of the Gravitational Collapse of Stars in a Full General Relativistic Treatment" D.Phil Thesis, University of Oxford, (1974).

[32] Smarr L. and Wilson J. "A Numerical Method for Relativistic Hydrodynamics" in ref [1].

[33] Shapiro S.L. and Teukolsky S.A. "Gravitational Collapse of Supermassive Stars to Black Holes: Numerical Solution of the Einstein Equations" Ap. J. Lett. 234, L177,(1979).

[34] Shapiro S.L. and Teukolsky S.A. "Gravitational Collapse to Neutron Stars and Black Holes: Computer Generation of Spherical Spacetimes" Ap. J. 235, 199, (1980).

[35] Evans C.R., Smarr L. and Wilson J.R. "Numerical Relativistic Gravitational Collapse with Spatial Time Slices" preprint (1984).

[36] Smith A.L.H. "Numerical Calculations on the Collapse of Relativistic Fluid Polytropes" D.Phil Thesis, University of Oxford, (1983).

[37] Piran T. and Stark R.F. "Gravitational Radiation, Gravitational Collapse and Numerical Relativity" 12th Texas Symposium on General Relativity (1984).

[38] Nakamura T. " General Relativistic Collapse of Rotating Stars" in ref. [2].

[39] Nakamura T., Maeda K., Miyama S. and Sasaki M. "General Relativistic Collapse of an Axially Symmetric Star. I. The Formulation and the Initial Value Equations" Prog. Theo. Phys. 63, 1229, (1980).

[40] Nakamura T. "Numerical Relativity" preprint (1982).

[41] Nakamura T. "General Relativistic Collapse of Axially Symmetric Stars Leading to the Formation of Black Holes." Prog. Theo. Phys. 65, 1876, (1981).

[42] Nakamura T. and Sato H. "General Relativistic Collapse of Non-rotating, Axi-symmetric Stars" Prog. Theo. Phys. 67, 1396, (1982).

[43] Sasaki M. "[(2+1)+1] Formalism of General Relativity" in ref. [3].

[44] Maeda K., Sasaki M., Nakamura T. and Miyama S. "A New Formalism of the Einstein Equations for Relativistic Rotating Systems." Prog. Theo. Phys. 63, 719, (1980).

[45] Maeda K. and Oohara K. "General Relativistic Gravitational Collapse of Rotating Stars with Magnetic Fields" Prog. Theo. Phys. 68, 567, (1982).

[46] Tassoul J.L. "Theory of Rotating Stars." (Princeton University Press, 1978).

[47] Miller J.C. and de Felice F. "Gravitational Collapse and Rotation. I. Mass Shedding and Reduction of the $\frac{a}{m}$ Ratio" preprint, (1985).

[48] de Felice F., Miller J.C. and Yunqiang Yu "Gravitational Collapse and Rotation: Gravitational Radiation and Reduction of the $\frac{a}{m}$ Ratio" preprint, (1985).

[49] Saski M., Maeda K., Miyama S; and Nakamura T. "A Method of Determining Apparent Horizons in [(2+1)+1] Formalism of the Einstein Equations" Prog. Theo. Phys. 63, 1051, (1980).

[50] Oohara K., Nakamura T. and Kojima Y. "Apparent Horizons of Time Symmetric Initial Value for Three Black Holes." Phys. Lett. 107A, 452, (1985).

[51] Stark R.F. and Piran T. "Gravitational Wave Emission from Rotating Gravitational Collapse" preprint (1985).

[52] Thorne K.S. "Gravitational Radiation: An Introductory Review" in ref. [2].

[53] Arnowitt R., Deser S. and Misner C. "The Dynamics of General Relativity" in "Gravitation: An Introduction to Current Research" ed. Witten L. (Wiley, 1962).

[54] York J.W. "The Initial Value Problem" in ref. [2].

[55] de Felice F. "Time - Like Tetrads" preprint (1984).

[56] Sachs R.K. "Gravitational Radiation" in "Relativity, Groups and Topology" ed. de Witt B. (Gordon and Breach, 1964).

[57] Geroch R. "A Method of Generating Solutions of Einstein's Equations" J.Math.Phys. 12, 918 (1971).

[58] Detweiler S.L. "Black Holes and Gravitational Waves: Perturbation Analysis" in ref. [1].

[59] Smarr L. and York J. "Kinematical Conditions in the Construction of Spacetime" Phys. Rev. D17, 2529, (1978).

[60] Lichnerowicz A. "L'integration des équations de la gravitation relativiste et le problème des n corps" J. Math. Pures et Appl. 23, 37, (1944).

[61] York J. "Kinematics and Dynamics of General Relativity" in ref.[1].

[62] Estabrook F., Wahlquist H., Christensen S., de Witt B., Smarr L. and Tsiang E. "Maximally Slicing a Black Hole" Phys. Rev. D7, 2814, (1973).

[63] Centrella J. and Wilson J. "Planar Numerical Cosmology" Ap. J. 273, 428, (1983).

[64] Centrella J. and Wilson J. "Planar Numerical Cosmology II" Ap. J. Suppl. 54, 229, (1984).

[65] Bardeen J., and Piran T. "General Relativistic Axi-symmetric Rotating Systems: Co-ordinates and Equations" Phys. Rep. 96, 205, (1983).

[66] Piran T. "Methods of Numerical Relativity" in ref. [2].

[67] Bardeen J. "Gauge and Radiation Conditions in Numerical Relativity" in ref. [2].

[68] Taub A. "Relativistic Fluid Mechanics" Ann. Rev. Fluid Mech. 10, 301, (1978).

[69] Smarr L. and York J. "Radiation Gauge in General Relativity" Phys. Rev. D17, 1945, (1978).

[70] Eardley D.M. and Smarr L. "Time Functions in Numerical Relativity I, Marginally Bound Dust Collapse" Phys. Rev. D19, 2239, (1980).

[71] d'Inverno R.A. "(2+2) Formalism in General Relativity" in ref. [3].

[72] Geroch R. "Domain of Dependence" J. Math. Phys. 11, 437, (1970).

[73] Wald R. "General Relativity" (University of Chicago Press, 1984).

[74] York J. "Conformally Invariant Orthogonal Decomposition of Symmetric Tensors on Reimannian Manifolds and the Initial Value Problem of General Relativity" J. Math. Phys. 14, 456, (1973).

[75] Isenberg J., O Murchadha N. and York J. "The Initial Value Problem of General Relativity" Phys. Rev. D13, 1532, (1976).

[76] Isenberg J. and Nester J. "Extension of the York Field Decomposition to Gravitationally Coupled Fields" Ann. of Phys. 108, 368, (1977).

[77] Hawking S. and Ellis G. "The Large Scale Structure of Spacetime" (Cambridge University Press, 1973).

[78] York J. and Piran T. "The Initial Value Problem and Beyond" in "Space-time and Geometry" eds. Matzner R. and Shepley L. (University of Texas, 1982).

[79] O Murchadha N. and York J. "Existence and Uniqueness of Solutions to the Hamiltonian Constraint of General Relativity on Compact Manifolds" J. Math. Phys. 14, 1551, (1973).

[80] O Murchadha N. and York J. "Initial Value Problem of General Relativity. I. General Formulation and Physical Interpretation" Phys. Rev. D10, 428, (1974).

[81] Potter D. "Computational Physics" (Wiley, 1973).

[82] Richtmyer R. and Morton K. "Difference Methods for Initial Value Problems" (Wiley, 1967).

[83] Ames W.F. "Numerical Methods for Partial Differential Equations" (Academic Press, 1977).

[84] Smarr L. "Basic Concepts in Finite Differencing" in ref. [1].

[85] Roache P.J. "Computational Fluid Dynamics" (Hermosa, 1972).

[86] Mann P.J. "The Search for Stable Finite Element Methods for Simple Relativistic Systems" Comp. Phys. Comm. 30, 127, (1983).

[87] Mann P.J. "Some Mixed Finite Element - Finite Difference Methods for Spherically Symmetric Relativistic Collapse" J. Comp. Phys. 58, 377, (1985).

[88] Mitchell A. and Wait R. "The Finite Element Method in Partial Differential Equations" (Wiley, 1977).

[89] Zienkiewicz O.C. "The Finite Element Method" (McGraw - Hill, 1977).

[90] McKee C.R. and Stirling A.C. "Relativistic Shock Hydrodynamics" Ap. J. 181, 903, (1973).

[91] Boris A.P. and Book D.L. "Flux Corrected Transport. I. SHASTA, A Fluid Transport Algorithm That Works" J. Comp. Phys. 11, 38 (1973).

[92] Book D.L. Boris J.P. and Hain K. " Flux Corrected Transport II: Generalizations of the Method" J. Comp. Phys. 18, 248, (1975).

[93] Gilden D.L. "Thermal Instability in Molecular Clouds" Ap.J. 283, 679, (1984).

[94] Gilden D.L. and Shapiro S.L. "Gravitational Radiation from Colliding Compact Stars: Hydrodynamical Calculations in Two Dimensions" Ap.J. 287, 728, (1984).

[95] Regge T. "General Relativity without Co-ordinates" Il. Nuovo Cimento 19, 558, (1961).

[96] Friedberg R. and Lee T.D. "Derivation of Regge's Action from Einstein's Theory of General Relativity" preprint, (1984).

[97] Sorkin R. "Time Evolution Problem in Regge Calculus" Phys. Rev. D12, 385, (1975).

[98] Hartle J.B. and Sorkin R. "Boundary Terms in the Action for the Regge Calculus" GRG 13, 541, (1981).

[99] Rocek M; and Williams R. "Quantum Regge Calculus" Phys. Lett. 104B, 31, (1981).

Rocek M; and Williams R. "The Quantization of Regge Calculus" Z.Phys. C21, 371, (1984).

Warner N.P. "The Application of Regge Calculus to Quantum Gravity and Quantum Field Theory in a Curved Background" Proc. R. Soc. Lond. A383, 359, (1982).

Jevicki A. and Ninomiya M. " Lattice Gravity and Strings" preprint, (1984).

Hamber H. and Williams R. "Higher Derivative Quantum Gravity on a Simplicial Lattice" preprint, (1984).

[100] Cheeger J., Müller W. and Schrader R. "On the Curvature of Piecewise Flat Spaces" Comm. Math. Phys. 92, 405, (1984).

[101] Porter J. "Numerical Study of Non-homogeneous Spacetimes Using Regge Calculus" D.Phil Thesis, University of Oxford, (1982).

[102] Sorkin R. "The Electromagnetic Field on a Simplicial Net" J. Math. Phys. 16, 2432, (1975).

[103] Hartle J.B. "Simplicial Minisuperspace I. General Discussion" preprint, (1984).

[104] Collins P. and Williams R; "Dynamics of the Freidmann Universe Using Regge Calculus" Phys. Rev. D7, 965, (1973).

[105] Collins P. and Williams R. "Regge Calculus Model for the Tolman Universe" Phys. Rev. D10, 3537, (1974).

[106] Brewin L. "Computer Generated Solutions Using Regge Calculus" in GR10.

[107] Conners P.A. "Computations in Relativistic Astrophysics" D.Phil. Thesis, University of Oxford, (1978).

[108] Lewis S.M. "Two Cosmological Solutions of Regge Calculus" Phys. Rev. D25, 25, (1982).

[109] Wong C.Y. "Application of Regge Calculus to Schwarzschild and Reissner - Nordstorm Geometrics at the Moment of Time-symmetry" J.Math. Phys. 12, 70, (1971).

[110] Collins P. and Williams R. "Application of Regge Calculus to the Axially Symmetric Initial Value Problem in GR" Phys. Rev. D5, 1908, (1972).

[111] Williams R. "The Time-symmetric Initial Value Problem for a Homogeneous Anisotopic Empty Closed Universe, Using Regge Calculus" preprint (1984).

[112] Williams R. and Ellis G. "Regge Calculus and Observations.I. Formalism and Application to Radial Motion and Circular Orbits" GRG 13, 361, (1981).

[113] WIlliams R. and Ellis G. "Regge Calculus and Observations.II. Further Applications" GRG 16, 1003, (1984).

[114] Feinberg G., Friedberg R., Lee T. and Ren H. "Lattice Gravity Near the Continuum Limit" preprint, (1984).

[115] Synge J. "Relativity: The General Theory" (North Holland, 1960).

[116] Bondi H. "Spherically Symmetric Models in General Relativity" MNRAS 107, 410, (1947).

[117] Schutz B. "Perfect Fluids in General Relativity: Velocity Potentials and a Variational Principle" Phys. Rev. D2, 2762, (1970).

[118] Taub A. "General Relativistic Variational Principle for Perfect Fluids" Phys. Rev. 94, 1468, (1954).

[119] Shapiro S. and Teukolsky S. "Black Holes, White Dwarfs and Neutron Stars" (Wiley, 1983).

[120] Piran T. "Lagrangian Relativistic Hydrodynamics with Eulerian Co-ordinates" in "Essays in General Relativity" ed. Tipler F. (Academic Press, 1980).

[121] GelinasR., Doss S. and Miller K. "The Moving Finite Element Method: Applications to General Partial Differential Equations with Multiple Large Gradients" J.Comp. Phys. 40, 202; (1981).

APPENDIX I

A.1 Notation and Conventions for Chapters Three and Four:

Geometrized units are used (c = G = 1) except where stated otherwise.

Tensor Indicies;

Capital Greek (eg. Δ , Γ) take values 0, 1, 2, 3.

Capital Latin (eg. I, J) take values 1, 2, 3.

Difference Indicies;

Small Greek (eg. α , β) label spatial hypersurfaces and take values α = 1, 2, 3..... with α = 1 being the initial hypersurface.

Small Latin (eg. i, j) denote the spatial vertices to which a variable is attached and take the values i = 1, 2, 3....

The Minkowski metric $\eta_{\Gamma\Delta}$ = diag. (-1, 1, 1, 1).

$\varepsilon_{\Delta\Gamma\Lambda\Omega}$ is the totally anti-symmetric Levi - Civita tensor such that $\varepsilon_{0123} = +1$.

A vector is denoted by $\bar{x}$ and a 1-form by $\tilde{x}$.

The inner product is denoted by $\langle\ ,\ \rangle$.

$A_{[x_{i,\alpha}\,:\,y_{i,\alpha}]}$ denotes the area of a bone containing the legs $\bar{X}_{i,\alpha}$, $\bar{Y}_{i,\alpha}$. Square brackets do not denote anti-symmetrization.

$\varepsilon_{[x_{i,\alpha}\,:\,y_{i,\alpha}]}$ denotes the deficit angle associated with the above bone.

The magnitude of a timelike quantity is imaginary while that of a spacelike quantity is real.

The general metric tensor $g_{\Gamma\Delta}$ has signature (-, +, +, +).

APPENDIX II

A.2 Area Variations and Deficits:

a) $im_{i,\alpha}$ variation,

$$\frac{\partial A_{[\theta_{i,\alpha}:m_{i,\alpha}]}}{\partial(im_{i,\alpha})} = \frac{1}{2}\left(r_{i,\alpha} + m_{i,\alpha}\sinh Y_{i,\alpha}\right)\Delta\theta$$

$$\frac{\partial A_{[\phi_{i,\alpha}:m_{i,\alpha}]}}{\partial(im_{i,\alpha})} = \frac{1}{2}\left(r_{i,\alpha} + m_{i,\alpha}\sinh Y_{i,\alpha}\right)\sin\theta\,\Delta\phi$$

$$\frac{\partial A_{[d_{i,\alpha}:m_{i,\alpha}]}}{\partial(im_{i,\alpha})} = \frac{1}{4}\left(d_{i,\alpha}\cosh V^{u}_{i,\alpha} + d_{i,\alpha+1}\cosh \bar{V}^{u}_{i,\alpha+1}\right)$$

$$\frac{\partial A_{[d_{i-1,\alpha}:m_{i,\alpha}]}}{\partial(im_{i,\alpha})} = \frac{1}{4}\left(d_{i-1,\alpha}\cosh V^{L}_{i,\alpha} + d_{i-1,\alpha+1}\cosh \bar{V}^{L}_{i,\alpha+1}\right).$$

b) $r_{i,\alpha}\sin\theta\Delta\phi$ variation,

$$\frac{\partial A_{[\theta_{i,\alpha}:\phi_{i,\alpha}]}}{\partial(r_{i,\alpha}\sin\theta\Delta\phi)} = \frac{1}{2}r_{i,\alpha}\Delta\theta$$

$$\frac{\partial A_{[d_{i,\alpha}:\phi_{i,\alpha}]}}{\partial(r_{i,\alpha}\sin\theta\Delta\phi)} = \frac{1}{2}d_{i,\alpha}$$

$$\frac{\partial A_{[d_{i-1,\alpha}:\phi_{i,\alpha}]}}{\partial(r_{i,\alpha}\sin\theta\,\Delta\phi)} = \tfrac{1}{2}\,d_{i-1,\alpha}$$

$$\frac{\partial A_{[\phi_{i,\alpha}:m_{i,\alpha}]}}{\partial(r_{i,\alpha}\sin\theta\,\Delta\phi)} = \tfrac{1}{2}\,i m_{i,\alpha}$$

$$\frac{\partial A_{[\phi_{i,\alpha}:m_{i,\alpha-1}]}}{\partial(r_{i,\alpha}\sin\theta\,\Delta\phi)} = \tfrac{1}{2}\,i m_{i,\alpha-1}$$

c) $d_{i,\alpha}$ variation,

$$\frac{\partial A_{[d_{i,\alpha}:\phi_{i,\alpha}]}}{\partial d_{i,\alpha}} = \tfrac{1}{4}(r_{i,\alpha}+r_{i+1,\alpha})\sin\theta\,\Delta\phi$$

$$\frac{\partial A_{[d_{i,\alpha}:\theta_{i,\alpha}]}}{\partial d_{i,\alpha}} = \tfrac{1}{4}(r_{i,\alpha}+r_{i+1,\alpha})\,\Delta\theta$$

$$\frac{\partial A_{[d_{i,\alpha}:m_{i,\alpha}]}}{\partial d_{i,\alpha}} = \tfrac{1}{4}(i m_{i,\alpha}\cosh V^{u}_{i,\alpha} + i m_{i+1,\alpha}\cosh V^{L}_{i+1,\alpha})$$

$$\frac{\partial A_{[d_{i,\alpha}:m_{i,\alpha-1}]}}{\partial d_{i,\alpha}} = \tfrac{1}{4}(i m_{i,\alpha-1}\cosh \bar{V}^{u}_{i,\alpha} + m_{i+1,\alpha-1}\cosh \bar{V}^{L}_{i+1,\alpha}).$$

d) deficit angles at vertex i,α ,

$$\mathcal{E}_{[\theta_{i,\alpha}:m_{i,\alpha}]} = \left[\frac{\Delta r_{i,\alpha} + 2\, d_{i-1,\alpha} \sinh\gamma_{i,\alpha} \sinh V^{L}_{i,\alpha}}{d_{i-1,\alpha} \cosh V^{L}_{i,\alpha}} \right.$$

$$\left. - \frac{\Delta r_{i+1,\alpha} + 2\, d_{i,\alpha} \sinh\gamma_{i,\alpha} \sinh V^{u}_{i,\alpha}}{d_{i,\alpha} \cosh V^{u}_{i,\alpha}} \right] \sin\theta\, \Delta\phi .$$

$$\mathcal{E}_{[\phi_{i,\alpha}:m_{i,\alpha}]} = \mathcal{E}_{[\theta_{i,\alpha}:m_{i,\alpha}]} \frac{\Delta\theta}{\sin\theta\, \Delta\phi} .$$

$$\mathcal{E}_{[d_{i,\alpha}:m_{i,\alpha}]} = - \frac{\Delta r^{2}_{i+1,\alpha}}{d^{2}_{i,\alpha}} \left[1 - \frac{d^{2}_{i,\alpha}}{\Delta r^{2}_{i+1,\alpha}} \left(1 - 4 \frac{\Delta r_{i+1,\alpha}}{d_{i,\alpha}} \sinh\gamma_{i,\alpha} \sinh V^{u}_{i,\alpha} \right.\right.$$

$$\left.\left. + 4 \sinh^{2}\gamma_{i,\alpha} + \sinh^{2} V^{u}_{i,\alpha} \right) \right] \frac{\sin\theta\, \Delta\theta\, \Delta\phi}{\cosh^{2} V^{u}_{i,\alpha}} .$$

$$\mathcal{E}_{[d_{i-1,\alpha}:m_{i,\alpha}]} = - \frac{\Delta r^{2}_{i,\alpha}}{d^{2}_{i,\alpha}} \left[1 - \frac{d^{2}_{i-1,\alpha}}{\Delta r^{2}_{i,\alpha}} \left(1 - 4 \frac{\Delta r_{i,\alpha}}{d_{i-1,\alpha}} \sinh\gamma_{i,\alpha} \sinh V^{L}_{i,\alpha} \right.\right.$$

$$\left.\left. + 4 \sinh^{2}\gamma_{i,\alpha} + \sinh^{2} V^{L}_{i,\alpha} \right) \right] \frac{\sin\theta\, \Delta\theta\, \Delta\phi}{\cosh^{2} V^{L}_{i,\alpha}} .$$

$$\mathcal{E}_{[\theta_{i,\alpha}:\phi_{i,\alpha}]} = i \left(- \sinh V^{u}_{i,\alpha} + \sinh V^{L}_{i,\alpha} + \bar{\mu}^{u}_{i,\alpha} + \bar{\mu}^{L}_{i,\alpha} \right) .$$

$$\mathcal{E}_{[d_{i,\alpha}:\phi_{i,\alpha}]} = 2i\left[\frac{2d_{i,\alpha}\sinh\gamma_{i,\alpha} - \Delta r_{i+1,\alpha}\sinh V^{u}_{i,\alpha}}{2d_{i,\alpha}\cosh V^{u}_{i,\alpha}} + \bar{\sigma}^{u}_{i,\alpha}\right]\Delta\theta.$$

$$\mathcal{E}_{[d_{i-1,\alpha}:\phi_{i,\alpha}]} = 2i\left[\frac{2d_{i-1,\alpha}\sinh\gamma_{i,\alpha} - \Delta r_{i,\alpha}\sinh V^{L}_{i,\alpha}}{2d_{i-1,\alpha}\cosh V^{L}_{i,\alpha}} + \bar{\sigma}^{L}_{i,\alpha}\right]\Delta\theta.$$

$$\mathcal{E}_{[d_{i,\alpha}:\theta_{i,\alpha}]} = \mathcal{E}_{[d_{i,\alpha}:\phi_{i,\alpha}]}\frac{\sin\theta\,\Delta\phi}{\Delta\theta}.$$

e) deficit angles at vertex i+1, α ,

$$\mathcal{E}_{[d_{i,\alpha}:m_{i,\alpha}]} = -\frac{\Delta r^{2}_{i+1,\alpha}}{d^{2}_{i,\alpha}}\left[1 - \frac{d^{2}_{i,\alpha}}{\Delta r^{2}_{i+1,\alpha}}\left(1 - 4\frac{\Delta r_{i+1,\alpha}}{d_{i,\alpha}}\sinh\gamma_{i+1,\alpha}\sinh V^{L}_{i+1,\alpha}\right.\right.$$

$$\left.\left. + 4\sinh^{2}\gamma_{i+1,\alpha} + \sinh^{2}V^{L}_{i+1,\alpha}\right)\right]\frac{\sin\theta\,\Delta\theta\Delta\phi}{\cosh^{2}V^{L}_{i+1,\alpha}}.$$

$$\mathcal{E}_{[d_{i,\alpha}:\phi_{i,\alpha}]} = 2i\left[\frac{d_{i,\alpha}\sinh\gamma_{i+1,\alpha} - \Delta r_{i+1,\alpha}\sinh V^{L}_{i+1,\alpha}}{2d_{i,\alpha}\cosh V^{L}_{i+1,\alpha}} + \bar{\sigma}^{L}_{i+1,\alpha}\right]\Delta\theta.$$

$$\mathcal{E}_{[d_{i,\alpha}:\theta_{i,\alpha}]} = \mathcal{E}_{[d_{i,\alpha}:\phi_{i,\alpha}]}\frac{\sin\theta\,\Delta\phi}{\Delta\theta}.$$

f) definitions,

$$\bar{\sigma}^{u}_{i,\alpha} = \frac{\Delta r_{i+1,\alpha-1}}{2 d_{i,\alpha-1} \cosh V^{u}_{i,\alpha-1}} \left[\bar{\mu}^{u}_{i,\alpha} - \frac{2 \sinh Y_{i,\alpha-1}}{\Delta r_{i+1,\alpha-1}} R_{i,\alpha-1} \right].$$

$$\bar{\sigma}^{L}_{i,\alpha} = \frac{\Delta r_{i,\alpha-1}}{2 d_{i-1,\alpha-1} \cosh V^{L}_{i,\alpha-1}} \left[-\bar{\mu}^{L}_{i,\alpha} - \frac{2 \sinh Y_{i,\alpha-1}}{\Delta r_{i,\alpha-1}} R_{i-1,\alpha-1} \right].$$

$$\bar{\mu}^{u}_{i,\alpha} = -\frac{1}{d_{i,\alpha}} \left[m_{i+1,\alpha-1} L_{i,\alpha-1} - d_{i,\alpha-1} \sinh V^{u}_{i,\alpha-1} - m_{i,\alpha-1} \right].$$

$$\bar{\mu}^{L}_{i,\alpha} = -\frac{1}{d_{i-1,\alpha}} \left[m_{i-1,\alpha-1} L_{i-1,\alpha-1} + d_{i-1,\alpha-1} \sinh V^{L}_{i,\alpha-1} - m_{i,\alpha-1} \right].$$

$$R_{i,\alpha-1} = m_{i+1,\alpha-1} \sinh V^{L}_{i+1,\alpha-1} + d_{i,\alpha-1} - m_{i,\alpha-1} \sinh V^{u}_{i,\alpha-1}.$$

$$L_{i,\alpha} = \cosh V^{L}_{i+1,\alpha} \cosh V^{u}_{i,\alpha} - \sinh V^{L}_{i+1,\alpha} \sinh V^{u}_{i,\alpha}.$$